

Montana State University

Task Report 1-Literature Review

**A Feasibility Study of Road Culvert / Bridge Deck Deicing Using
Geothermal Energy**

By:

Mehran Pourakbar, PhD Student

Mohammad Khosravi, Assistant Professor

Kathryn Plymesser, Assistant Professor

Steve Perkins, Professor

Prepared for:

Montana Department of Transportation

January 2021

TABLE OF CONTENTS

LIST OF FIGURES	iii
LIST OF TABLES	vii
CHAPTER 1: INTRODUCTION	1
Problem Statement.....	1
Overview and Outline.....	2
CHAPTER 2: SURVEY RESULTS.....	4
Current Practice in Montana.....	5
Road Maintenance	5
Cost of Material	6
Culvert Maintenance.....	8
Request for Weather and Crash Dataset	8
Car Crashes in Montana.....	8
Weather in Montana.....	9
CHAPTER 3: SHALLOW GEOTHERMAL ENERGY: OVERVIEW.....	15
Primary Unit	17
Construction Technique.....	18
Heat exchanger pipes.....	19
Circulating Fluid.....	21
Heat Pump System.....	22
Power Source	23
Secondary Unit	26
CHAPTER 4: USE OF GEOTHERMAL ENERGY FOR ROAD CULVERT/BRIDGE DECK DEICING: CASE/FIELD STUDIES	28
Case Study 1: Jiangyin, China	28
Case Study 2: Jiangyin, China	30
Case Study 3: Central Switzerland	33
Case Study 4: City of Klamath Falls, Oregon.....	34
Case Study 5: Mountain Road in Japan	34
Case Study 6: Fukui City, Japan.....	36
Case Study 7: North Fork of Silver Creek, Oregon.....	37
Case Study 8: Amarillo, Texas	37
CHAPTER 5: LABORATORY STUDIES OF BRIDGE DECK DEICING SYSTEMS	39
Pipe Spacing in the Secondary Unit.....	39
Borehole Depth in Primary Unit.....	41

Preheating the deck.....	43
External Heating Systems.....	44
Inlet Flow Rate and Temperature.....	45
Soil Thermal Properties.....	46
Effect of Bio-Cementation on Thermal Properties of Soil.....	47
CHAPTER 6: NUMERICAL MODELING STUDIES ON THE EFFICIENCY OF SHALLOW GEOHERMAL ENERGY SYSTEMS.....	50
Bridge Deck Deicing System.....	50
Inlet Fluid Temperature and Flow Rate.....	50
Pipe Spacing and Embedded Depth.....	55
Weather Condition (Snowfall Rate, Wind Speed, and Ambient Temperature).....	59
Optimization of Heat Extraction/Injection in Primary Unit.....	62
CONCLUSION.....	68
REFERENCES.....	70
APPENDIX A: SURVEY OF ROAD MAINTENANCE ACTIVITIES WITHIN MONTANA STATE.....	77
APPENDIX B: SURVEY OF CULVERT MAINTENANCE ACTIVITIES WITHIN MONTANA STATE	80
APPENDIX C: REQUIRED INFORMATION.....	82

LIST OF FIGURES

Figure 1. Culvert deicing using hot, glycol filled hoses in Saskatchewan, (www.canadianundergroundinfrastructure.com)	1
Figure 2. Schematic of Ground Source Heat Pump (GSHP) for bridge deck deicing (redrawn after (Bowers & Olgun, 2014)).....	2
Figure 3. Road surface conditions of (a) Thompson Fall Section (b) Plains Section (Goodwin, 2003).....	7
Figure 4. Locations of MDT RWIS Sites (Map Source: https://roadreport.mdt.mt.gov/)	9
Figure 5. Monthly average weather data for 2015-2020: (a) ambient temperature, (b) relative humidity (c) wind speed, and (d) precipitation.....	10
Figure 6. Average daily temperature during coldest month, February 2019, in (a) Northern (b) Western (c) Southern (d) Eastern, and (e) Central Montana.....	11
Figure 7. Average daily temperature during warmest month, July 2018, in (a) North (b) West (c) South (d) East (e) Center of Montana.....	12
Figure 8. Percentage of global capacity used by various forms of direct geothermal energy in 2015 (Lund & Boyd, 2016)	15
Figure 9. GSHP system (Han & Yu, 2017)	16
Figure 10. Closed loop GSHP using for (a) cooling (b) heating of secondary unit (Kavanaugh, 2006)	16
Figure 11. (a) Open-loop system (b) closed-loop system	17
Figure 12. Various attachment arrangements of heat exchanger pipes on the reinforcement cage (Sani et al., 2019)	19
Figure 13. (a) U-shaped pipes inside an energy pile reinforcing cage (b) instrumented energy pile (Faizal et al., 2019)	20
Figure 14. Different configurations of energy loops within a GEP (Sani et al., 2019).....	20
Figure 15. The reinforcement cage of tested energy piles (a) spiral shaped (b) double U-shaped (Zarrella et al., 2013)	21
Figure 16. Process of the overall heating only in heat pump system.....	23
Figure 17. Simplified schematic of a solar assisted ground-source heat pump system (a. parallel, b. series) (Shahed & Harrison, 2009).....	23
Figure 18. Schematic view of ground-coupled heat pump combined with thermal solar collectors (Trillat-Berdal et al., 2006).....	24
Figure 19. Front and back of a PVT panel (Bakker et al., 2005)	24
Figure 20. Schematic view of tested hybrid system (Bakker et al., 2005).....	25
Figure 21. Schematic of the modified system proposed by Bernier and Shirazi (2007).....	25
Figure 22. Conceptual schematic of ground-source bridge deck deicing (Bowers & Olgun, 2014)	26
Figure 23. (a) A schematic of a possible culvert deicing system based on previous studies on the use of geothermal energy in tunnels and underground structures, (b) Various pipe configuration (c) An energy geotextile installed in an energy tunnel (Loveridge et al., 2020).....	27

Figure 24. (a) Photo of the bridge (b) schematic layout of heating system (Chen et al., 2020)	28
Figure 25. (a) Variation of heat flux, q , with the difference between the inlet fluid and the ambient temperatures, $T_{in}-T_0$, (b) the required inlet fluid temperature and heat flux to keep the deck surface temperature above freezing point (Chen et al., 2020).....	30
Figure 26. (a) Location of the studied section of the bridge (b) photo of bridge deck before pouring concrete (c) layout of bridge deck deicing (Kong et al., 2019).....	31
Figure 27. Surface condition of deck surface at different hours (Kong et al., 2019).....	32
Figure 28. (a) Change in the ambient and bridge deck temperatures, (b) variation of the inlet and outlet circulating fluid temperature and the heating power of the deicing system (Kong et al., 2019)	32
Figure 29. (a) Photo of the bridge (b) schematic of a SERSO system in Switzerland (Eugster, 2007).....	33
Figure 30. Comparison of the measured ambient and surface temperature during operation (Eugster, 2007)	33
Figure 31. (a) Longitudinal closed loop on the bridge deck and (b) approach road loops in Klamath Falls, Oregon (Boyd, 2003)	34
Figure 32. Hydronic heating system using underground water storage on a mountain road in Japan (Yoshitake et al., 2011).....	35
Figure 33. Road surface condition on snowy day (a) snow covered road (b) after 9h operating of the system (Yoshitake et al., 2011).....	35
Figure 34. Temperature histories of the water storage, the bridge deck, and the approach road over one year (Yoshitake et al., 2011).....	35
Figure 35. Outline of “pipe in pile” snow melting system (a) heat storage mode during Summer (b) snow melting mode during winter (Nagai et al., 2009).....	36
Figure 36. Surface condition of heated and unheated segments of the bridge deck in Fukui City, Japan in January, 2008 (Nagai et al., 2009)	36
Figure 37. Plan view of the heated deck on Silver Creek bridge, Oregon (Minsk, 1999).....	37
Figure 38. (a) Heating circuits before pouring concrete (b) close-up of supply and return manifolds (pipes in center) and thermocouple conduits terminating in enclosure at right on a bridge deck in Amarillo, Texas. (Minsk, 1999).....	38
Figure 39. (a) Location and spacing of energy piles and observation wells (b) experimental deck model. Pipes spacing are 20 cm and 30 cm in the left-side and right-side model deck, respectively. (Bowers Jr, 2016)	39
Figure 40. Photo of the deck model surface during the storm. Heat exchanger pipes have spacing of 30 cm and 20 cm in left-side and right-side model deck, respectively (Bowers Jr, 2016).	41
Figure 41. (a) The layout of experimental set-up (b) initial stage of snow melting process (c) after 30 min operation of snow melt system (Balbay & Esen, 2010).....	42
Figure 42. Variation of top surface temperatures of bridge deck and pavement slab, and air temperatures (a) borehole depth 30 m (100 ft) (b) borehole depth 90 m (295 ft)(Balbay & Esen, 2010).....	42
Figure 43. Photo of bridge surface condition during the test (SFAR: Snow Free Area Ratio) (Liu, 2005)43	
Figure 44. Recorded average surface temperature of the bridge (Liu, 2005)	44

Figure 45. (a) The schematic of experimental set-up (b) laboratory setup (Yu et al., 2020).....	44
Figure 46. (a) Experimental set up (b) temperature contours after 0.5 day (Ghasemi-Fare et al., 2015) ...	45
Figure 47. Primary heat transfer mechanisms in a thermo-active foundation with heat exchanger pipe embedded in a concrete pile and surrounded by soil (not to scale) (Atalay, 2019)	46
Figure 48. Heat transfer paths in soil (Alrtimi et al., 2016).....	46
Figure 49. Thermal conductivity and dry density of MICP-treated sand versus MICP treatment cycles (Wang et al, 2019).....	48
Figure 50. Effect of degree of saturation on (a) thermal conductivity of the MICP-treated and untreated sand (b) improvement in thermal conductivity of the MICP-treated soil (Venuleo et al., 2016)	49
Figure 51. (a) The mesh of deck model (b) distribution of temperature within the bridge deck using boreholes depths of 90 m (295 ft) (Balbay & Esen, 2013)	51
Figure 52. Meshed 3D model (Chowdhury, 2019)	51
Figure 53. Weather data and numerical model results in the coldest day of 2016, December 19, 2016, for inlet fluid temperatures of (a) 22°C (b) 38°C (Chowdhury, 2019)	52
Figure 54. Numerical baseline model configuration of the bridge deck (Yu et al., 2017).....	53
Figure 55. Effect of inlet fluid temperature on (a) average deck surface temperature (b) time required to reach above-freezing point (Yu et al., 2017).....	53
Figure 56. Effect of flow rate on (a) average deck surface temperature (b) time required to reach above-freezing point (Yu et al., 2017).....	53
Figure 57. 3D Finite Element model meshing for: (a) whole model, (b) serpentine pipes, and (c) pipes and surrounding concrete (Feng & Yin, 2019).....	54
Figure 58. Surface temperature with variation of inlet flow rate (Feng & Yin, 2019)	54
Figure 59. Contours of (a) surface temperature of heated deck (b) circulating fluid temperature variation, inlet fluid temperature 30°C (86°F), ambient temperature of -25°C (-13°F), and flow rate of 0.21 l/s (0.05 gal/s) (Ho et al., 2019)	55
Figure 60. Temperature of heated pavement versus volumetric flow rate for ambient temperature of (a) -25°C (-13°F) (b) -15°C (5°F)(Ho et al., 2019).....	56
Figure 61. Comparison of surface temperature difference with (a) different pipe embedded depth in terms of pipe spacing of 15 cm (b) different pipe spacing in terms of pipe embedded depth of 15 cm (5.9 inch) (Feng & Yin, 2019).....	56
Figure 62. (a) Numerical baseline model configuration, (b) Numerical modeling mesh (Bowers Jr, 2016)	57
Figure 63. Contours of deck surface temperature for different pipe spacing when the average surface temperature reached above freezing point (Bowers Jr, 2016).....	58
Figure 64. (a) Average deck surface temperature, and (b) time required to reach above-freezing point at top surface of bridge deck (Yu et al., 2017).....	58
Figure 65. (a) Average deck surface temperature and area of deck surface above 0°C (32°F) for different ambient temperatures (b) Distribution of injected energy to the deck and lost energy for different air temperatures (Bowers Jr, 2016)	59

Figure 66. (a) Average deck surface temperature and area of deck surface above 0°C (32°F) for different wind speeds (b) Distribution of injected energy to the deck and lost energy for different wind speeds (Bowers Jr, 2016).....	60
Figure 67. (a) Average deck surface temperature (b) time required to reach above-freezing point at bridge deck surface (Yu et al., 2017)	60
Figure 68. (a) Average deck surface temperature with different snowfall rate (b) deck heating flux per surface area for different snowfall rates (Bowers Jr, 2016).....	61
Figure 69. (a) Mesh of bridge deck model and snow melting system (b) accumulated energy consumption with various snowfall rate (Liu et al., 2019).....	61
Figure 70. Effects of key parameters on the efficiency of a geothermal piles after 12 hrs and 60 days of operation (Ghasemi-Fare & Basu, 2016)	62
Figure 71. (a) Grid arrangement of boreholes (b) the Meshing of the pile and heat exchanger pipes (Bowers Jr & Olgun, 2020).....	63
Figure 72. Different extraction strategies (Bowers Jr & Olgun, 2020).....	64
Figure 73. Comparison of the net energy remaining within the energy pile grids at the end of extraction and end of operational year for three scenarios (Bowers Jr & Olgun, 2020)	64
Figure 74. Temperature distribution and BHE workloads for the optimized case. Each circle represents a BHE with its corresponding load in grayscale. Darker color shades illustrate higher BHE loads. The subsurface temperature distribution at a depth of 50 m (164 ft) is shown by colors, where high absolute temperatures appear in red and lower temperatures in blue (de Paly et al., 2012).	65
Figure 75. The subsurface temperature distribution at depth of 50 m for the optimized case and the equal heat extraction case (Beck et al., 2013)	67

LIST OF TABLES

Table 1. Fundamental strategies of MDT for road maintenance operation in winter	5
Table 2. The lowest practical melting temperature of winter maintenance materials.....	6
Table 3. MDT Winter Maintenance Annual Averages (Goodwin & Pisano, 2003).....	7
Table 4. Montana statewide car crashes due to slippery road surface conditions.....	8
Table 5. Average daily weather data obtained for five major cities in Montana	13
Table 6. Case/Field studies of bridge deck deicing/anti-icing using GSHP systems.....	29
Table 7. Experimental studies of bridge deck deicing – Secondary Unit	40
Table 8. Experimental studies of bridge deck deicing – Primary Unit	40

STANDARD CONVERSION TABLE – ENGLISH TO METRIC				
<u>Symbol</u>	<u>To convert from</u>	<u>Multiply by</u>	<u>To determine</u>	<u>Symbol</u>
<u>LENGTH</u>				
IN	inch	25.4	millimeters	mm
FT	feet	0.3048	meters	m
YD	yards	0.9144	meters	m
MI	miles	1.609344	kilometers	km
<u>AREA</u>				
SI	square inches	645.16	square millimeters	mm ²
SF	square feet	0.09290304	square meters	m ²
SY	square yards	0.83612736	square meters	m ²
A	acres	0.4046856	hectares	ha
MI ²	square miles	2.59	square kilometers	km ²
<u>VOLUME</u>				
CI	cubic inches	16.387064	cubic centimeters	cm ³
CF	cubic feet	0.0283168	cubic meters	m ³
CY	cubic yards	0.764555	cubic meters	m ³
GAL	gallons	3.78541	liters	L
OZ	fluid ounces	0.0295735	liters	L
MBM	thousand feet board	2.35974	cubic meters	m ³
<u>MASS</u>				
LB	pounds	0.4535924	kilograms	kg
TON	short tons (2000 lbs)	0.9071848	metric tons	t
<u>PRESSURE AND STRESS</u>				
PSF	pounds per square foot	47.8803	pascals	Pa
PSI	pounds per square inch	6.89476	kilopascals	kPa
PSI	pounds per square inch	0.00689476	megapascals	Mpa
<u>DISCHARGE</u>				
CFS	cubic feet per second	0.02831	cubic meters per second	m ³ /s
<u>VELOCITY</u>				
FT/SEC	feet per second	0.3048	meters per second	m/s
<u>INTENSITY</u>				
IN/HR	inch per hour	25.4	millimeters per hour	mm/hr
<u>FORCE</u>				
LB	pound (force)	4.448222	newtons	N
<u>POWER</u>				
HP	horsepower	746.0	watts	W
<u>TEMPERATURE</u>				
°F	degrees Fahrenheit	5 X (°F – 32)/9	degrees Celsius	°C
<u>DENSITY</u>				
lb/ft ³	pounds per cubic foot	16.01846	kilograms per cubic meter	kg/m ³
<u>ACCELERATION</u>				
g	freefall, standard	9.807	meters per second squared	m/s ²

TO CONVERT FROM METRIC TO ENGLISH, DIVIDE BY THE ABOVE CONVERSION FACTORS.

CHAPTER 1: INTRODUCTION

This task report contains the results of a comprehensive literature search on the topic of geothermal foundations and its application for deicing and anti-icing road culverts and bridge decks. This literature search is in support of a research project being conducted for the Montana Department of Transportation (MDT) by the Department of Civil Engineering at Montana State University (CE-MSU). The project is designed to examine the feasibility of a ground-coupled system that utilizes heat energy harvested from the earth as an alternative for deicing bridges and culverts. This report documents research performed to establish the state-of-the-practice for this application. Experimental and field data from different projects is reviewed to demonstrate the feasibility and applicability of this innovative technology and to indicate where knowledge gaps exist. Studies involving numerical modeling of shallow geothermal foundation are summarized to evaluate recent advances in Ground Source Heat Pump (GSHP) systems with a focus on Montana climate. The results from a survey designed to examine and document MDT's current bridge deck and culvert deicing and anti-icing practices are discussed. This report concludes by summarizing the body of literature available on this topic and its relationship to the work being conducted in this research project.

Problem Statement

Snow accumulation on roads and bridges reduces their capacity, decreases safety, and increases travel delays. Ice accumulation in culverts causes flooding and associated economic losses when they remain blocked with ice after spring runoff begins. Ice accumulation can also lead to propagation of the freezing front into the frost susceptible subsoil around the culvert and increase the risk of frost heave in road sections adjacent to the culvert. Therefore, deicing bridge decks and culverts is a major maintenance concern in areas with extreme cold weather. Reduction of ice and snow on bridges also leads to safer roadways and enhances winter traffic mobility. The most common deicing solution for bridge decks is the use of salts and other debonding chemicals. However, salt is ineffective for snow melting or deicing for temperatures below -9.4°C (15.1°F). Long-term use of salts and deicing chemicals also increases the maintenance and repair cost for reinforced concrete (RC) bridges. It accelerates the corrosion of the steel used in reinforced concrete, reduces the available reinforcement area over time, and could result in premature bridge and culvert rehabilitation. The removal of problematic culvert ice after it has developed is usually accomplished by the application of heat or other mechanical means. Electric heating cables have been used in Alaska and other locations to thaw holes through ice-filled culverts (Carey, 1984). The cables are usually installed in the fall, removed in the spring, and can be connected to a local power supply or on-site generators. Alternatively, steam deicing (Figure 1) can be used to melt holes through the ice to allow drainage to proceed. These methods are labor intensive, expensive and require frequent monitoring of high-risk culverts.



Figure 1. Culvert deicing using hot, glycol filled hoses is Saskatchewan, (www.canadianundergroundinfrastructure.com)

Recently, new materials and innovative techniques such as hydronic heating systems have been used to remove ice and snow from transportation infrastructure. Several heated pavement systems have been proposed including electrically heated pavements and hydronically heated pavements. Electrically heated pavements can be utilized wherever electricity is available, however, the high voltage required and the high operation cost of using electricity discourage the widespread use of this system (Fliegel et al., 2010). Using a hydronic heating system for removing snow and ice from bridge decks has received more attention in recent years. Heat can be extracted from shallow or deep layers of earth through thermo-active foundations or boreholes based on mechanisms of heat transfer including convection, conduction and radiation (Lund & Boyd, 2016). Seasonal variation of ground temperature is minimal at a depth approximately 6-9 m (20-30 ft) below the ground surface (Kusuda & Achenbach, 1965). Shallow geothermal loops below that depth are, thus, good alternatives to piles and wells for harvesting geothermal energy through heat exchange with the ground.

A conceptual schematic of a ground-source bridge deck deicing system is shown in Figure 2. Heat is transported to and from the ground through heat exchanger pipes by circulating fluid through a closed loop system embedded within the ground. The circulating fluid is then circulated through the pipes embedded under the pavement surface. The efficiency of a hydronically heated system was shown to depend on many factors, including material properties (e.g. soil and concrete conductivity) and design parameters of the system such as inlet fluid temperature, pipe depth, and pipe spacing. The efficiency of the de-ice bridge system increases as fluid temperature and concrete thermal conductivity increase. Greater pipe embedded depth and wider pipe spacing are not desirable for the efficiency of system (Ghasemi-Fare & Basu, 2016). The harvested energy from the ground can be used to de-ice bridge decks and culverts in the winter. Hydronically heated pavement systems can also reduce the temperature fluctuation on the surface of the bridge deck and thermal stresses within the concrete. A reduction in thermal stresses results in prevention of expansion cracks.

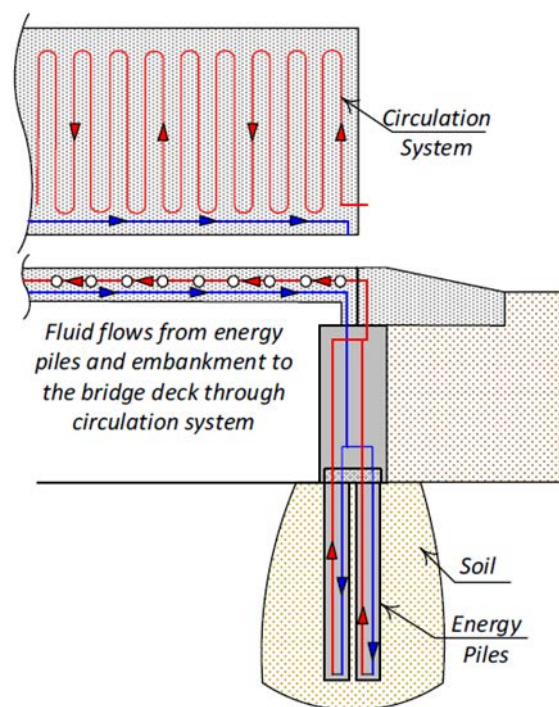


Figure 2. Schematic of Ground Source Heat Pump (GSHP) for bridge deck deicing (redrawn after (Bowers & Olgun, 2014))

Overview and Outline

The proposed research program will investigate the feasibility of the use of a ground-coupled system that utilizes heat energy harvested from the earth as a potential alternative for deicing bridge decks and culverts. The results of this research are expected to provide benefits in safety, operation, and maintenance of transportation infrastructure in the state of Montana.

In this report, the available literature on the use of geothermal energy for bridge decks and pavement deicing applications is compiled. Chapter 2 discusses the results of an initial survey conducted to determine the type and extent of anti-icing and deicing technology currently in use in the state of Montana. The survey also summarizes the weather data from Road Weather Information System (RWIS) from 2015 to 2020. The weather data includes air temperature, snowfall accumulation, snowfall rate, wind speed and direction, pavement surface temperature, and pavement temperature (2 to 10 cm (0.8 to 3.9 inch) below the pavement surface). Chapter 3 provides an overview of closed loop and open loop GSHP systems, addressing the different components, different construction techniques, different circulating fluids, and power sources. Chapter 4 includes successful application case studies on the use of geothermal energy for bridge decks and pavement deicing applications. Chapters 5 and 6 summarize the results from a series of model scale lab experiments and numerical simulations performed to investigate the effects of important parameters on the efficiency of GSHP systems.

CHAPTER 2: SURVEY RESULTS

One of the objectives of this project is to design a larger, and more definitive future study based on a life-cycle cost analysis and an analysis of the energy required to maintain ice-free bridge decks and culverts. The design report will include an economic feasibility study to compare the cost of different snow melting methods including chemical methods (e.g., using salt and other chemical debonding) and GSHP systems using both geothermal energy piles and geothermal energy wells. In order to understand MDT's perceptions and preferences about deicing/anti-icing measures, a survey was designed and distributed to staff at MDT. The survey consisted of three main parts:

- 1) *Survey of Culvert Maintenance Activities within the State of Montana:* The first part was developed to assess current MDT practices to mitigate ice jams in culverts as well as those from the literature. This part included the following questions:
 - What are the fundamental strategies of MDT for culvert maintenance operations in winter?
 - Please provide the average annual cost of each technology used.
 - What are the factors used in decisions about which chemicals to use?
 - What are the factors considered in the maintenance of culverts?
 - Please provide an estimate of the average annual maintenance and repair cost due to corrosion.
- 2) *Survey of Road Maintenance Activities within the State of Montana:* The second part focused on the current MDT deicing/anti-icing measures for bridge decks, as well as those from the literature and included the following questions:
 - What are the fundamental strategies of MDT for bridge maintenance operations in winter?
 - Please provide an estimate of the average annual cost of each product (e.g. sand, chemicals) used.
 - Please provide an estimate of the average annual maintenance and repair cost due to corrosion.
 - What are the factors used in decisions about which chemicals to use?
 - Which abrasive materials are being used by MDT?
 - Does MDT have an abrasive clean-up plan in place?
 - How important is entry of abrasives into waterways as a negative aspect of using abrasives?
- 3) *Request for Weather and Crash Dataset:* In the third part of the survey, the following information was requested from MDT:
 - The time histories of the average snowfall accumulation, average temperature, wind speed, pavement surface temperature over the period of 2015 to 2020 from 73 stations of Road Weather Information System (RWIS).
 - Montana statewide car crashes with snow or ice as a contributing factor.

The collected information will be used to perform an economic feasibility study and compare deicing and anti-icing systems using geothermal energy with the current methods being used by MDT.

Current Practice in Montana

As a first step to compare the costs of different deicing/anti-icing methods, it is important to understand current MDT's deicing/anti-icing practices. The first two parts of the survey questionnaire focused on the current methods of removing ice and snow from transportation infrastructure that are used by MDT.

Road Maintenance

As summarized in Table 1, the survey identified the following three activities as the most used winter maintenance strategies by MDT:

- Anti-icing to prevent snow or ice accumulation on the surface before a winter storm
- Deicing to remove snow and ice during and after a storm
- Mechanical removal

The results of the survey indicated that the factors that aid in the decision about which material to use are cost of material, environmental impacts, ease of application, effectiveness, availability, public feedback, and decreased corrosion.

The effectiveness of each of these solutions depends on pavement temperature, the thickness of snow and ice accumulation, and weather conditions. Before a cold-weather event or in the early stages of a storm, MDT may employ an anti-icing strategy. During a cold weather event, a combination of tactics including snow plowing, sanding, and deicing are typically used to clear roads and enhance traction. When the pavement surface is covered with significant amounts of snow, corresponding to a "Low" pavement condition as shown in Table 1, MDT typically employs a deicing approach. Abrasives are most used during low temperature events.

Table 1. Fundamental strategies of MDT for road maintenance operation in winter

Strategies and Tactics	Pavement Condition**			Pavement Condition**		
	Within-winter weather event			After/end-of-winter weather event		
	Low ¹	Medium ²	High ³	Low ¹	Medium ²	High ³
Anti-icing/Pre-wetting	X	X	X			X
Deicing	X			X		
Mechanical removal alone	X	X	X			
Mechanical removal and abrasive	X	X	X			
Mechanical removal and anti-icing	X	X	X			
Mechanical removal and deicing	X					

** Pavement Condition Categories

Pavement Condition	Pavement Snow and Ice Conditions
¹ Low	Conditions 5 and 6
² Medium	Conditions 3 and 4
³ High	Conditions 1 and 2

Condition 1: Dry/wet pavement conditions.

Condition 2: Snow accumulation occurs occasionally. There are patches of ice or packed snow.

Condition 3: Snow accumulation occurs regularly. Loose snow or slush ranging up to 5 cm (2 inches) are accumulated on the pavement surface.

Condition 4: Snow accumulation occurs regularly. Ice or packed snow with only bare wheel tracks.

Condition 5: Pavement surface is covered with ice and compacted snow.

Condition 6: Pavement surface is covered with significant amounts of snow.

The most common deicing/anti-icing solution for bridge decks in Montana is the use of salts and other debonding chemicals such as Sodium Chloride (NaCl), Magnesium Chloride (MgCl₂), and Potassium Acetate (KAc). Based on MDT's official state website, Sodium Chloride is primarily extracted from the evaporation of seawater, and MgCl₂ is primarily extracted from the Great Salt Lake. Debonding chemicals used are in the form of solids and liquids. Dry solid chemicals are more effective if there is sufficient moisture on the pavement. There are two effective solutions to improve the effectiveness of this treatment method: 1) applying the solid chemicals after adequate precipitation has fallen, and 2) prewetting the materials. A commonly used dry solid material by MDT is sodium chloride (NaCl). Pre-wetting of a solid chemical is usually conducted in a stockpile, spreader, and at the point of discharge. A common liquid chemical for deicing/anti-icing purposes are NaCl, MgCl₂, and KAc. However, the chemical solutions are ineffective for snow melting or deicing for temperatures below -12 degrees Celsius (10 degrees Fahrenheit). The effective working temperatures for magnesium chloride and sodium chloride are -12 degrees Celsius (10 degrees Fahrenheit) and -9.4 degrees Celsius (15 degrees Fahrenheit), respectively. The lowest practical melting temperatures of the winter maintenance materials are summarized in Table 2.

Table 2. The lowest practical melting temperature of winter maintenance materials (Frederickson et al., 2005)

<i>NaCl</i>		<i>MgCl₂</i>	<i>KAc</i>
<i>Solid</i>	<i>Liquid</i>	<i>Liquid</i>	<i>Liquid</i>
-9.4°C (15.1°F)	-9.4°C (15.1°F)	-12°C (10°F)	-9.4°C (15.1°F)

Previous studies have shown that deicing chemicals have negative impacts on the environment (e.g. Kelting & Laxon, 2010; Shi et al., 2018). Long-term use of deicing chemicals also increases the maintenance cost for reinforced concrete (RC) bridges. It accelerates the corrosion of steel reinforcement used in reinforced concrete, reduces the available reinforcement area over time, and may result in the collapse of RC bridge decks (e.g. Baboian, 1992; Granata & Hartt, 2009; Virmani et al., 1983; Virmani et al., 1984; White et al., 2005; Yunovich et al., 2003). Bridge deterioration is one of the major national infrastructure concerns ((AASHTO), 2008). The annual direct cost of corrosion in bridges is in the range of \$6 to \$10 billion (Koch et al., 2002). Including indirect costs, the total cost can be as much as 10 times higher than what was reported by Koch et al. (2002) (Yunovich et al., 2003).

Abrasive materials are used for winter road maintenance in extremely cold winter weather. The use of abrasives (e.g., sand, cinders, ash, tailings, and crushed stone) has been popular for many years due to their low cost. Abrasives are not ice-control chemicals and are used when a rapid increase in surface friction is required. The abrasive material employed by MDT is crushed stone from local gravel sources. Abrasive use can contribute to negative impacts on water quality, air quality, drainage facilities, wildlife habitats, vegetation, and soil quality, and increase maintenance costs (i.e., road and shoulder clean-up after the winter season) (Fischel, 2001).

Cost of Material

Information on costs associated with products used by MDT for winter road maintenance purposes is gathered as follows in terms of average annual costs of products:

- NaCl is \$70/ton
- Salt Brine is \$0.32/gallon

- MgCl₂ is \$150/ton
- KAc is \$4.66/gallon

The results of the survey indicated that over the period of 2015 to 2020, the average annual costs based on total winter material use was 10.7 million dollars. The total cost of labor and equipment for winter road maintenance will be updated in future project reports.

In a case study performed by MDT in 2003, the effectiveness of two different winter maintenance strategies, anti-icing and deicing were investigated (Goodwin & Pisano, 2003). The strategies were investigated during a storm that affected two road sections of State Highway 200, Thompson Falls section and Plains section. On the Plains section, an anti-icing strategy was used while deicing was employed on Thompson Falls section. The anti-icing strategy on the Plains Section included 11355 liters (3000 gallons) of MgCl₂ used during and after the storm. On the Thompson Falls section in addition to 3028 liters (800 gallons) of chemicals used to pre-wet abrasive, another 2839 liters (750 gallons) of MgCl₂ were used for deicing. Figure 3 shows the road surface conditions of the Thompson Falls section and Plains section after applying different treatments. As can be seen, the pavement was bare in the Plains section, while the pavement surface in the Thompson Falls section was covered with ice and compacted snow.



Figure 3. Road surface conditions of (a) Thompson Fall Section (b) Plains Section (Goodwin, 2003)

As summarized in Table 3, the Plains section (anti-icing strategy) required 44% less sand and labor costs were reduced by 52%. Although more chemicals were applied, the overall cost per lane mile of the anti-icing strategy used on the Plains section was 37% less compared to the deicing section used in Thompson Falls (Goodwin & Pisano, 2003). The results highlighted the benefits of preventive versus reactive treatment strategies.

Table 3. MDT Winter Maintenance Annual Averages (Goodwin & Pisano, 2003)

	Thompson Falls Section	Plains Section
Sand Costs per lane mile	\$724	\$407
MgCl ₂ Costs per lane mile	\$136	\$233
Equipment Costs per lane mile	\$327	\$182
Labor Costs per lane mile	\$564	\$273
Total Costs per lane mile	\$1,750	\$1,095

Culvert Maintenance

Culverts allow water to flow under roads and keep water from collecting along roadway embankments. Snow and ice accumulation in culverts, which reduces flow capacity, causes flooding, and associated economic losses when they remain blocked with ice after spring runoff begins. Ice accumulation can also lead to propagation of the freezing front into frost susceptible subsoil around the culvert and increase the risk of frost heave in road sections adjacent to the culvert.

The removal of problematic culvert ice after it has developed is usually accomplished by the application of heat or other mechanical means. The survey identified mechanical removal as MDT's most used winter maintenance strategy. The budget for snow and ice removal of culverts was not available, however the results of the survey indicated that the total cost for cleaning drainage structures was \$301,659 in State Fiscal Year (SFY) 2020.

Request for Weather and Crash Dataset

In this section, a summary of the data collected in the third part of the survey is presented. The data includes: 1) the number of car crashes due to slippery road conditions between 2010-2019, and 2) weather data from 73 RWIS stations over the period of 2015-2020.

Car Crashes in Montana

According to the Federal Highway Administration (FHWA), from 2002 to 2012, approximately 5,878,000 car accidents occurred per year on U.S. roadways, 23% of which were due to weather events (FHWA, 2013). Annually, car accidents on snowy, slushy, or icy pavements resulted in 1300 deaths, over 116,800 injuries, and an estimated economic cost of nearly \$42 billion in the U.S. (Beran & Wilfong, 1998; FHWA, 2013). The number of car crashes in Montana with snow or ice as a contributing factor between 2010-2019 is shown in Table 4. The results indicate that, on average, 5,430 car crashes occurred annually due to slippery road conditions (ice/frost, slush, and snow). The data considers all crashes, however, for a life-cycle cost-benefit analysis of different deicing/anti-icing strategies, the average annual number of crashes on bridges is required.

Table 4. Montana statewide car crashes due to slippery road surface conditions

	<i>Ice/Frost</i>	<i>Slush</i>	<i>Snow</i>	<i>Total</i>
2010	2951	232	2174	5357
2011	2922	251	2081	5254
2012	2060	272	1572	3904
2013	2737	233	1905	4875
2014	3491	296	2725	6512
2015	2466	206	2063	4735
2016	1929	253	1904	4086
2017	3509	360	2967	6836
2018	3668	331	2138	6137
2019	3342	220	3041	6603
Total	29075	2654	22570	54299
Average	2907	265	2257	5430

The accident records for a two-year period from 1972 to 1973 by Agent and Dean (1976) showed that almost 8% of all accidents involved bridges. The study included 350 overpasses and 360

underpasses on the interstate and parkway system with dual bridges counted as one bridge. Based on their records, the severity of bridge-related accidents on primary and secondary highways was almost equal to that of the bridge-related accidents on the interstate and parkway system. Habibzadeh-Bigdarvish et al. (2019) collected data on car crashes across Texas due to slippery road surface conditions. They also reported that a minimum of 8% percent of all crashes occurs on bridges. Therefore, it is estimated that approximately 434 car crashes occur annually on Montana bridges.

Weather in Montana

Many state transportation agencies have adopted the Road Weather Information System (RWIS) to monitor, report, and forecast road related weather conditions. RWIS provides detailed weather information which can be used for winter road and bridge maintenance (Al-Kaisy & Ewan, 2017). There are 73 RWIS stations in the state of Montana. Figure 4 shows the locations of the 73 RWIS sites. Each of these 73 stations includes an air temperature and humidity sensor, wind speed and direction sensor, in-pavement temperature sensor, subsurface temperature sensor, precipitation sensor, and a camera. Six sites (or fewer) also equipped with advanced precipitation sensors, visibility sensors, or infrared illuminators for nighttime camera images (Al-Kaisy & Ewan, 2017).

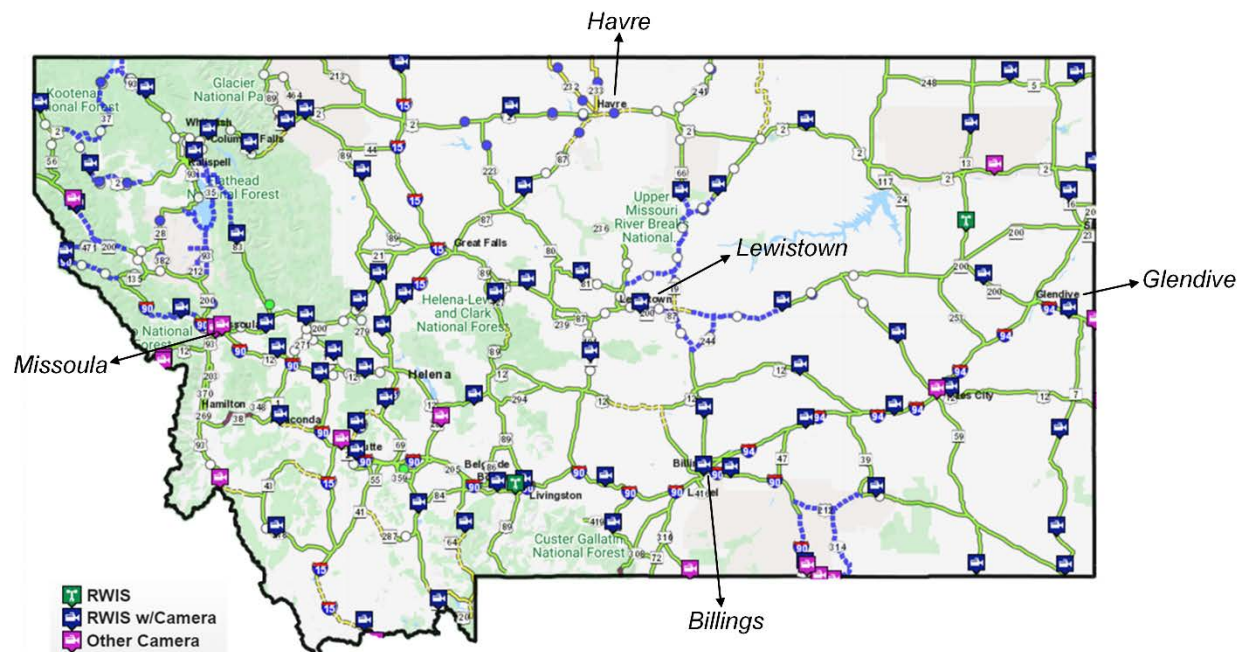


Figure 4. Locations of MDT RWIS Sites (Map Source: <https://roadreport.mdt.mt.gov/>)

As the third part of the survey, the time histories of weather data including ambient temperature, pavement surface temperature, sub-surface temperature, relative humidity, wind speed, and average snowfall accumulation over the period of 2015 to 2020 were collected from 73 RWIS stations and a summary of the results are presented in this section. The data were averaged over each month for the last five years. Representative examples of the weather data recorded at the Lookout Pass station near Missoula from 2015 to 2020 are shown in Figure 5. Figure 5(a) displays the monthly average ambient air temperatures. The black line shows the monthly average (mean) temperature, while the red and blue lines show the maximum and minimum monthly average temperatures, respectively. The observed weather data from RWIS stations in different parts of Montana indicated that the coldest months of the year for 2015 to 2020 were November,

December, January, and February. In western Montana, temperatures were highest in July 2018 and lowest in February 2019. The largest difference between the monthly average maximum and monthly average minimum temperatures was seen in July 2018, with the monthly average temperature ranging between 10.7°C (51.3°F) and 26.7°C (80.1°F).

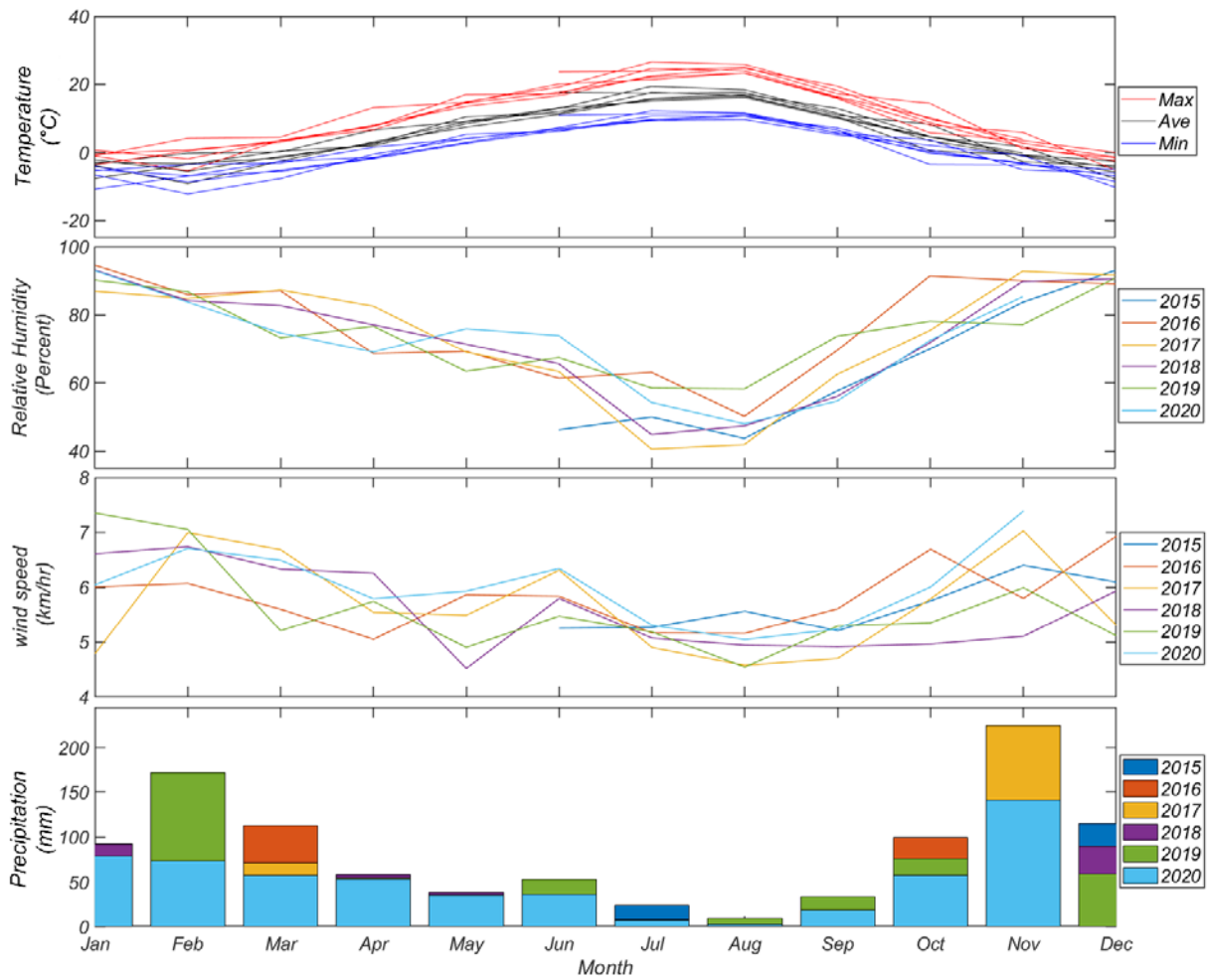


Figure 5. Monthly average weather data for 2015-2020: (a) ambient temperature, (b) relative humidity (c) wind speed, and (d) precipitation

Figure 5(b) shows the monthly average relative humidity of western Montana over the period from 2015 to 2020. In Montana, the winter months have higher relative humidity with a high of 95% in January. Summer months have lower relative humidity with a low of 40% in July. The monthly average wind speed over the last five years is shown in Figure 5(c). The monthly average wind speed varied from 4.0 to 7.4 km/hr (2.5 to 4.3 mph). One of the most important parameters in designing a snow melting system is the snowfall rate. The monthly average precipitation at the Lookout Pass station near Missoula is presented in Figure 5(d) for the period of 2015 to 2020. Snowfall amount is presented as its water equivalent. The observed data indicated that western Montana had higher levels of precipitation in the winter months (November–Feb) with a monthly average of over 112 mm (4.4 inch) in Nov. In the summer months (June–September), the monthly average precipitation rates dropped drastically, to less than 7.2 mm (0.3 inch) per month in July.

Figure 6 presents the average daily temperatures of five major cities in northern (Figure 6(a)), western (Figure 6(b)), southern (Figure 6(c)), eastern (Figure 6(d)), and central (Figure 6(e)) Montana during February 2019. The locations of these five major cities are shown in Figure 4. Spatially, the temperature was relatively consistent across the state, with temperatures slightly lower in the northern region in the city of Havre. As shown in Figure 6(a), the lowest ambient temperature in Northern Montana during February 2019 was -35°C (-31°F). The Sunburst station recorded the lowest temperature among the other stations. The lowest ambient temperatures in western, southern (Figure 6(c)), eastern (Figure 6(d)), and central (Figure 6(e)) Montana were -22.5°C (-8.5°F), -26°C (-15°F), -31.5°C (-24.7°F), and -30.2°C (-22.4°F), respectively.

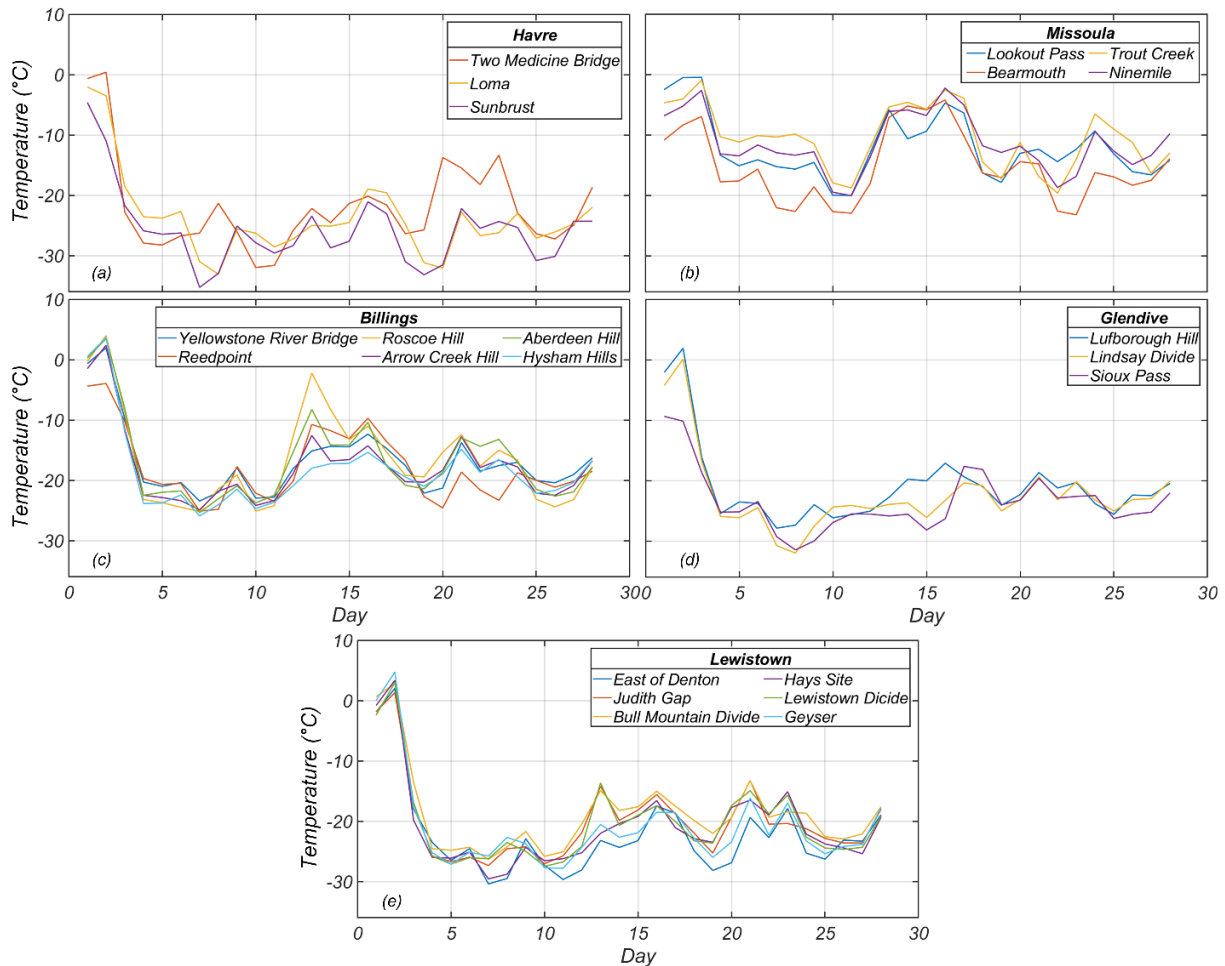


Figure 6. Average daily temperature during coldest month, February 2019, in (a) Northern (b) Western (c) Southern (d) Eastern, and (e) Central Montana

Monthly average ambient air temperatures indicated that July 2018 was the warmest month over the period of 2015 to 2020. Figure 7 shows the average daily temperature of five major cities in northern (Figure 7(a)), western (Figure 7(b)), southern (Figure 7(c)), eastern (Figure 7(d)), and central (Figure 7(e)) Montana during July 2018. Spatially, the temperature was relatively consistent across the state, with temperatures slightly higher in the northern region (Havre). As shown in Figure 7(a), the highest average daily temperature in Northern Montana was 37°C (99°F). The Sunburst Inverness station recorded the highest temperature among the other stations from the

selected cities. The highest ambient temperatures recorded in western, southern, eastern, and central Montana was 37°C (99°F), 38°C (100°F), 35.5°C (95.9°F), and 35°C (95°F), respectively.

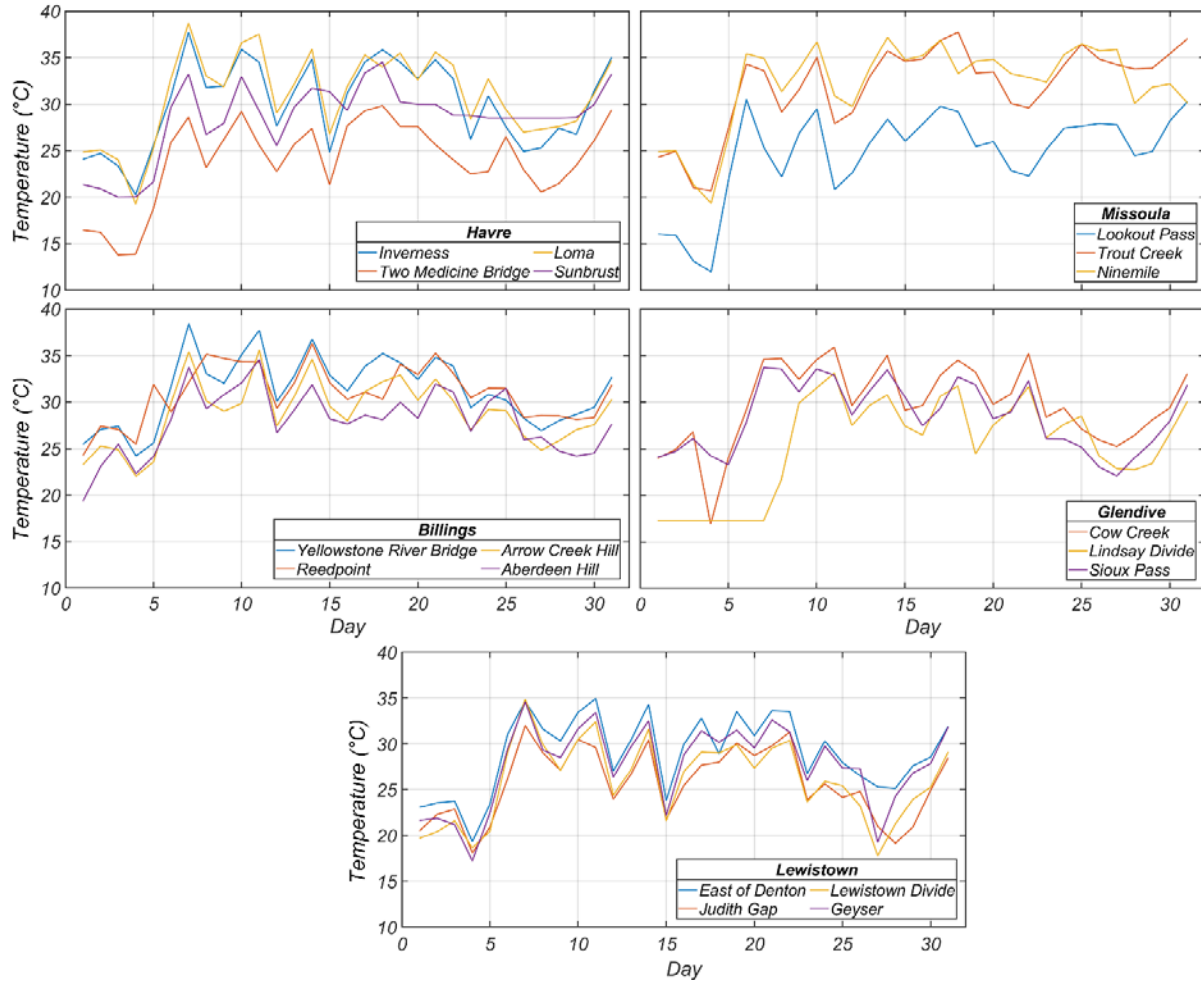


Figure 7. Average daily temperature during warmest month, July 2018, in (a) North (b) West (c) South (d) East (e) Center of Montana

Table 5 presents the maximum and minimum average daily ambient air temperature, surface temperature, subsurface temperature, and relative humidity for selected cities in Montana (Missoula, Billings, Lewistown, Havre, and Glendive) over the period of 2015 to 2020. The maximum snowfall rate, snowfall accumulation, and wind speeds are also presented in this table. Surface temperature is the temperature of the pavement surface, and subsurface temperature indicates the temperature approximately 43 cm (17 inches) below the top of the pavement. The observed data indicate that the temperature was relatively consistent spatially across the state, with ambient air, surface, and subsurface temperatures slightly higher in Western Montana, near Missoula. The lowest ambient air, surface, and subsurface temperatures were observed east of Denton near Havre (Northern Montana) and in Cow Creek near Glendive (Eastern Montana). The maximum wind speed recorded was 54.3 km/hr (33.7 mph) at Geyser station near Havre (Northern Montana).

Table 5. Average daily weather data obtained for five major cities in Montana

Area	Description	Site ID	Ambient Temperature (° C)		Surface Temperature (° C)		Sub-Temperature (° C)		Relative Humidity (%)		Wind Speed (km/hr)
			Max	Min	Max	Min	Max	Min	Max	Min	Max
Missoula	Lookout Pass	A150000	36.57	-23.57	33.65	-16.93	31.05	-7.96	100	22.00	20.75
	Bearmouth	A150002	41.64	-31.89	37.28	-20.98	32.65	-11.26	94.96	9.00	15.17
	Trout Creek	A150003	42.78	-28.27	39.04	-17.39	34.48	-8.58	93.00	24.34	9.77
	Ninemile	A150005	42.19	-27.52	38.64	-20.66	34.08	-8.86	95.00	27.76	9.3
Billings	Yellowstone River Bridge	A263000	40.96	-27.74	38.45	-19.00	31.86	-8.02	90.95	15.94	31.87
	Reedpoint	A263001	38.14	-34.11	36.00	-20.69	N/A	N/A	98.42	17.07	40.93
	Roscoe Hill	A263002	37.22	-26.35	35.35	-18.61	29.76	-9.90	87.70	9.93	33.99
	Arrow Creek Hill	A263003	38.82	-26.49	37.41	-16.58	32.92	-6.72	89.00	15.07	34.05
	Aberdeen Hill	A263004	38.06	-26.16	36.49	-17.25	30.87	-8.43	100	15.02	42.05
	Hysham Hills	A263005	39.724	-29.41	37.97	-17.92	32.26	-6.43	93.69	16.68	28.16
Lewistown	East of Denton	A268000	40.64	-34.55	38.02	-20.24	31.79	-8.88	95.00	17.00	35.23
	Judith Gap	A268001	36.19	-30.12	34.65	-19.09	30.76	-12.75	99.03	17.29	44.05
	Bull Mountain Divide	A268003	37.69	-28.01	36.13	-15.74	33.09	-8.79	100	12.39	44.2
	Hays Site	A268004	39.09	-29.56	N/A	N/A	28.78	-8.12	92.00	15.85	48.92
	Lewistown Divide	A268005	37.05	-31.45	N/A	N/A	29.97	-12.89	99.00	4.18	25.59
	Geyser	A268006	39.09	-30.42	N/A	N/A	30.01	-10.87	97.59	15.42	46.86

Table 5. Average daily weather data obtained for five major cities in Montana (Continued)

Area	Description	Site ID	Ambient Temperature (° C)		Surface Temperature (° C)		Sub-Temperature (° C)		Relative Humidity (%)		Wind Speed (km/hr)
			Max	Min	Max	Min	Max	Min	Max	Min	Max
Havre	East of Denton	A629000	41.11	-38.44	38.34	-23.39	N/A	N/A	92.00	14.42	48.10
	Judith Gap	A629001	N/A	N/A	39.49	-22.51	31.58	-13.09	N/A	N/A	-
	Bull Mountain Divide	A629002	35.74	-33.71	34.05	-26.00	28.75	-13.35	100	19.92	51.99
	Hays Site	A629003	39.78	-33.67	38.19	-21.06	N/A	N/A	100	17.36	41.84
	Lewistown Divide	A629004	39.15	-35.27	N/A	N/A	N/A	N/A	100	17.96	47.95
	Geyser	A629005	38.53	-30.71	35.71	-22.28	29.47	-11.11	100	16.55	54.32
Glendive	Lufborough Hill	A302000	39.48	-31.20	39.02	-20.29	31.55	-8.77	100	11.71	36.45
	Cow Creek	A302001	40.31	-41.60	38.72	-25.19	32.48	-12.49	100	26.69	38.71
	Lindsay Divide	A302002	38.45	-33.44	37.77	-22.02	31.16	-10.37	100	18.40	42.21
	Sioux Pass	A302004	39.68	-32.68	39.36	-24.12	31.63	-11.74	100	23.44	40.50

CHAPTER 3: SHALLOW GEOTHERMAL ENERGY: OVERVIEW

The application of Geothermal Energy as a renewable heat source is well developed around the world due to its environmental advantages and long-term economic benefit (Sinyak, 1994). Geothermal heat can be extracted from shallow or deep layers of earth through thermo-active foundations or boreholes based on mechanisms of heat transfer, including convection, conduction, and radiation. Typical underground locations in which thermal energy is stored are: 1) aquifers, which are mostly considered for open-loop systems, 2) boreholes, and 3) rock caverns or pits (McCartney et al., 2016). Geothermal energy has been used for a wide variety of applications, from power generation to snow melting for bridges and sidewalks. Geothermal energy can be categorized as low-temperature, medium-temperature, and high-temperature (Abbasy, 2009). Low temperature and medium temperature sources can be served for snow melting purposes or residential and industrial heating and cooling by employing a geothermal cycle. High temperature sources are used primarily for power generation. Lund and Boyd (2016) reviewed the application of geothermal energy in 82 countries and summarized various categories of direct-use of global geothermal capacity. As shown in Figure 8, the highest percentage of global capacity (70.9%) is associated with geothermal heat pumps (GHP) or ground source heat pumps (GSHP). GHP systems are among the best energy-saving technologies in heating systems and are among the most rapidly growing renewable energy applications (Lund & Toth, 2020).

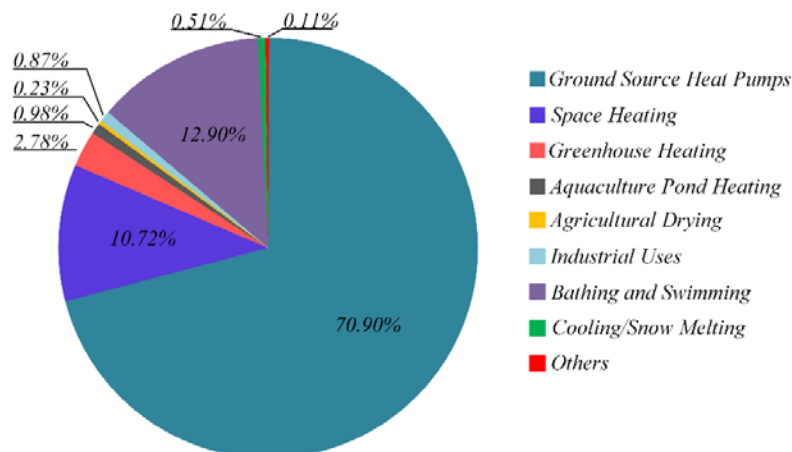


Figure 8. Percentage of global capacity used by various forms of direct geothermal energy in 2015 (Lund & Boyd, 2016)

This study focuses on the application of GSHP systems for snow and ice melting on bridge decks and ice melting inside culverts. GSHP relies on relatively constant ground temperatures below a certain depth. Seasonal variation of ground temperature is minimal at a depth of approximately 6-9 m (20-30 ft) below the ground surface. Heat exchangers can be employed within a thermo-active system to use the constant ground temperature as a thermal source to heat or cool above-ground structures (Brandl, 2006; Faizal et al., 2016; Kusuda & Achenbach, 1965).

A GSHP system consists of three main units, as shown in Figure 9, namely (Brandl, 2006):

- Primary unit (ground heat exchanger)
- Heat pump system, and
- Secondary unit (pipe network that delivers the heat energy to the receiving infrastructure).

The primary unit consists of a ground heat exchanger in a system of pipes called a loop, used to exchange heat with the surrounding ground. The secondary unit interacts with an above-ground structure to be heated or cooled (including building, bridge deck, or pavement). The primary unit and secondary unit are connected by either a circulating pump or heat pump. A heat pump is used to increase the temperature of the heat extracted from the ground.

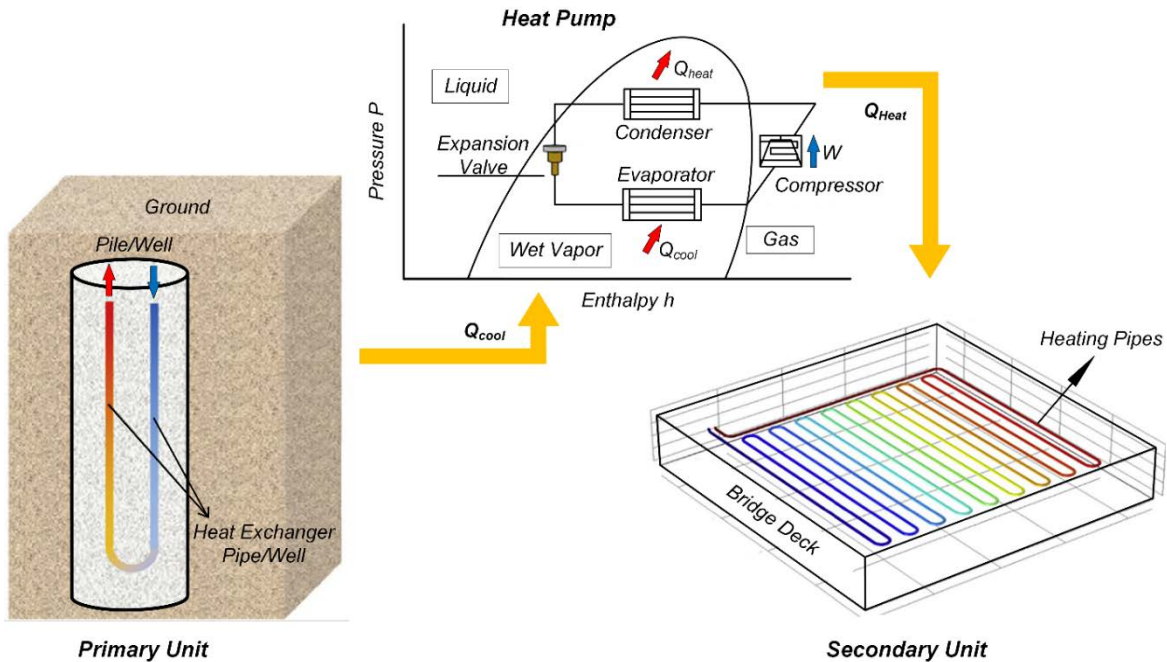


Figure 9. GSHP system (Han & Yu, 2017)

A GSHP system can be operated in either heating or cooling mode. Figure 10 depicts a closed-loop GSHP system for heating and cooling of a secondary unit. The ground serves as a heat sink during warmer times of the year as its temperature is less than the ambient temperature. During colder times of the year, the ground heat exchanger extracts the thermal heat energy through the temperature gradient that exists between the circulating fluid and the ambient ground. The amount of heat needed to be exchanged from or to the earth depends on the heating or cooling energy consumption of the super-structure (Faizal et al., 2019).

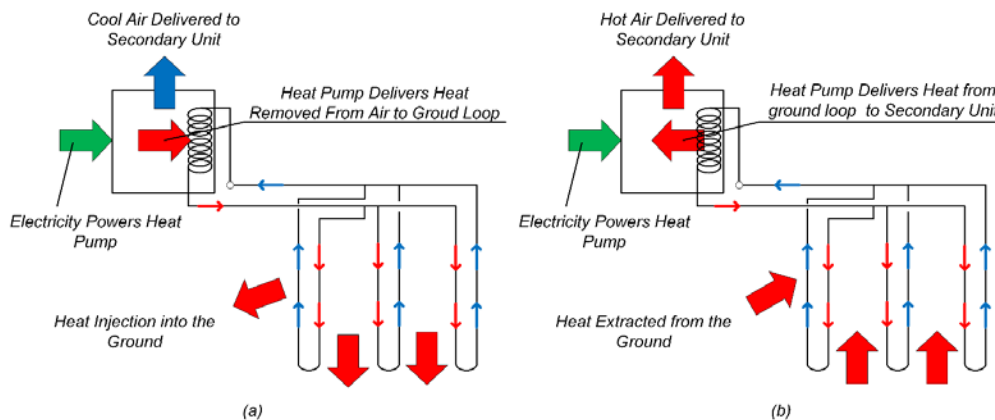


Figure 10. Closed loop GSHP using for (a) cooling (b) heating of secondary unit (Kavanaugh, 2006)

Primary Unit

There are two common primary unit system types: borehole heat exchangers (BHE) or geothermal wells, and geothermal energy pile foundations (GEP). BHE systems have been utilized for energy extraction and storage purposes over the last several decades (Brandl, 2006) and are categorized as either open-loop or closed-loop systems (Preene & Powrie, 2009). An open-loop system, which is also known as a groundwater system, uses an underground aquifer as a heat source during colder times of the year and a heat sink during warmer times of the year. As shown in Figure 11(a), an open-loop system includes extraction and rejection wells. The groundwater is extracted from the extraction well and circulated through the heat pump. Depending on whether heating or cooling is required, heat is extracted or rejected by the system. The water is then returned through the discharge well to the ground. Since the open-loop system cycles natural groundwater, the chemical composition of the water that passes through the heat pump and heat exchanger must not be altered prior to its return to the groundwater. Moreover, the aquifer must be shallow and permeable enough to allow water to move through it at a rapid rate. The aquifers should contain a low concentration of undesirable chemicals (e.g., chlorinated solvents) which could result in erosion of the pump components. The PH of the water in an open-loop system must be low enough to minimize corrosion and fouling of coils and control valves. Moreover, the cost of well maintenance can be prohibitively high (Rafferty, 2009).

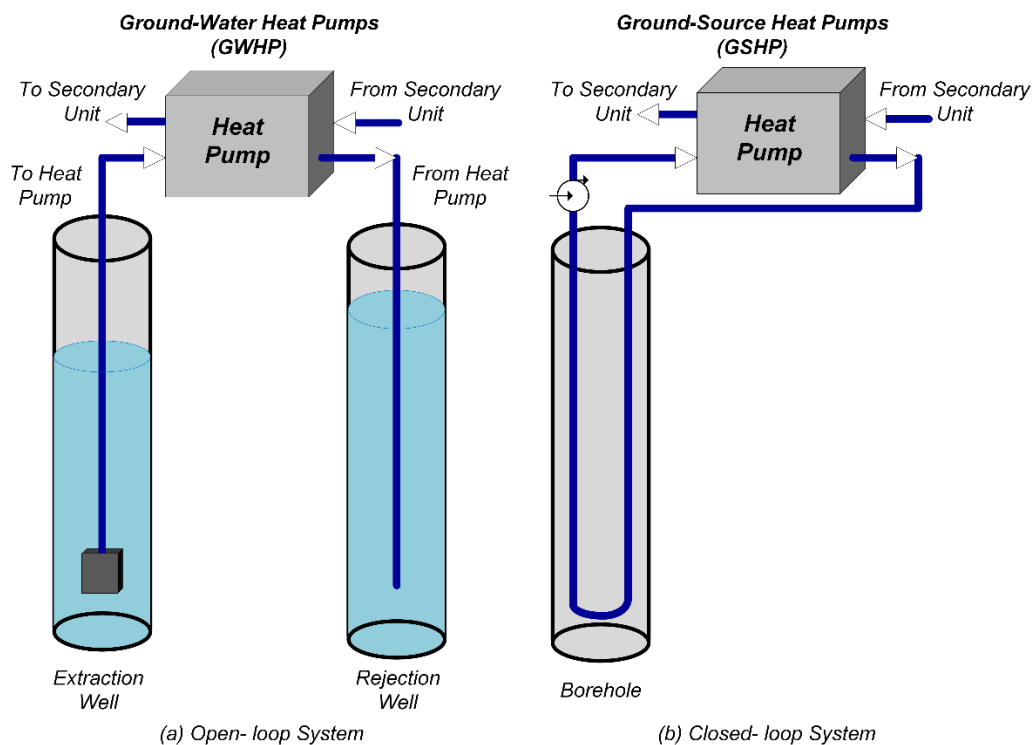


Figure 11. (a) Open-loop system (b) closed-loop system

Closed-loop (or ground-coupled) systems use an embedded heat exchanger to extract heat energy from the ground. Closed-loop systems can be installed either vertically or horizontally (Bloomquist, 2000). A simplified schematic of a vertical, closed-loop system is shown in Figure 11(b). In a closed-loop system, the circulating fluid circulates through the heat exchanger pipes and transfers heat from the ground to the heat pump. The pipes in a horizontal closed-loop system are placed in an excavated trench, below the frost line, or even embedded in the bridge's backfill

abutment. In vertical closed-loop systems, the heat exchanger pipes, usually in U-shape configurations, are installed in vertical boreholes or subsurface structural elements (e.g. piles). Boreholes are usually filled with thermally enhanced grout to improve the heat flow from the surrounding soil to the heat exchanger pipes. Grout material is used to fill the space between the borehole wall and heat exchanger pipes. The choice of grout depends on factors such as thermal conductivity, hydraulic conductivity, bonding quality, and workability (Hiller, 2000). Hydraulic conductivity is an important factor as it inhibits leakage through defective joints in the primary loops (Allan & Philippacopoulos, 1999). To enhance the heat transfer capabilities of grout materials, additives have been found to be a preferable solution from an economical and practical standpoint. Lee et al. (2010) compared silica sand and graphite as additives to bentonite-based grouting materials. They concluded that graphite improved the thermal properties of grout more than the silica sand. It has been shown that increasing quartz content will enhance the thermal properties of grouting materials (Kim et al., 2015).

The other common primary unit type, Geothermal Energy Pile (GEP) foundations are dual-purpose structural elements - transferring the structural loads to the ground and acting as a ground heat exchanger. Because of their multiple functions, GEPs can be highly cost-effective. GEPs are primarily comprised of reinforced concrete, due to its high thermal conducting properties and high thermal storage capacity, and U-shaped pipes. The pipes are typically made from high-density Poly-Ethylene/Poly-Propylene, Polyvinyl-chloride, or Polybutylene (Adam & Markiewicz, 2009; Akrouch et al., 2014; Gao et al., 2008; Hamada et al., 2007; Loveridge, 2012; Park et al., 2012). Pile foundations can exploit geothermal energy via circulating heat-absorbing fluids in a system of looped pipes embedded within the piles. The heat is extracted or injected through conduction or convection heat transfer mechanisms resulting from the thermal gradient in the soil mass. Piles can be either cast-in-place or precast piles (driven piles). A cast-in-place pile is preferred as a ground heat exchanger since it causes less damage to the heat exchanger system attached to the reinforcing cage (Mimouni, 2014). Enhancing the thermal conductivity of standard concrete has been the subject of recent studies for improving the geothermal efficiency of GEPs. A concrete mix with higher aggregate content and lower cement ratio results in more efficient heat transfer within the energy piles due to the lower heat conductivity of cement compared to aggregates (Loveridge, 2012).

Construction Technique

Direct pressing, ramming, and drilling are three common construction techniques for a geothermal borehole. Direct pressing and ramming are the most common techniques in soft soils. They provide better borehole stability and more efficient thermal contact with the surrounding soil. However, these techniques are only applicable for depths up to 10 m (32 ft) (Sanner & Knoblich, 1991). Drilling techniques include using a hollow stem auger, solid stem auger, sonic methods, or rotatory methods. Each of these techniques has its advantages and disadvantages in terms of depth, cost, and penetration rates. The selection of the drilling technique depends on the site condition and project criteria. The drilled hole can be supported by casing or grouting. Based on the International Ground Source Heat Pump Association (IGSHPA, www.igshpa.okstate.edu), in their 2010 Design and Installation standards, the bore annulus needs to be uniformly grouted from the bottom to the top via tremie pipe. The heat exchanger pipes are then inserted into the fresh grout mortar in the last step of the construction process.

GEPs are installed using either soil displacement techniques or soil excavation systems. Various techniques including bored piles, spun piles, or continuous flight auger piles can be employed to construct GEPs. In bored hole piles, a temporary casing is first driven into the ground. The soil inside is then excavated using an auger, a reinforcing cage with the attached heat exchanger is placed, concrete is poured, and finally, the casing is removed (Mimouni, 2014; Pahud, 2013). This technique is usually employed for constructing large diameter piles, in which several U loops will be embedded in the GEP. As an example, five U-shape pipes were embedded in GEPs with a depth of 26.8 m (88 ft) at the Dock Midfield, one of the terminals in Zürich airport (Mimouni, 2014). When constructing spun piles, precast concrete with a central hole is installed into the ground, followed by the heat transfer pipes, and finally filling the hole with wet sand, fine gravel (Mimouni, 2014), or cement (Park et al., 2013). In continuous flight auger pile construction, a hollow auger is first driven into the ground and then concrete is poured through the hollow bore. The auger is then pulled out, and the reinforcing cage and heat exchanger pipes are installed into the fresh concrete (Mimouni, 2014)

Heat exchanger pipes

Figure 12 illustrates different attachment arrangements of the heat exchanger pipes on the reinforcing cage. The heat exchanger pipes can be attached to the inside (Figure 12(a)) or outside (Figure 12(b)) of the reinforcing cage prior to installing the cage (Sani et al., 2019). The loops can also be installed beyond the rebar cage by clipping the loop to high-strength steel rebar and plunged into the center of the wet pile concrete to utilize the high thermal conductivity and thermal storage of the concrete compared to the soil (Figure 12(c)). In precast concrete piles, a coring technique can be utilized to place pipes into the hardened concrete. This technique is not a cost-effective method due to high installation cost (Sani et al., 2019). Figure 13(a) and (b) illustrate two examples of cast-in-place bored GEPs with U-shaped configuration for a residential building located at Monash University (Melbourne, Australia).

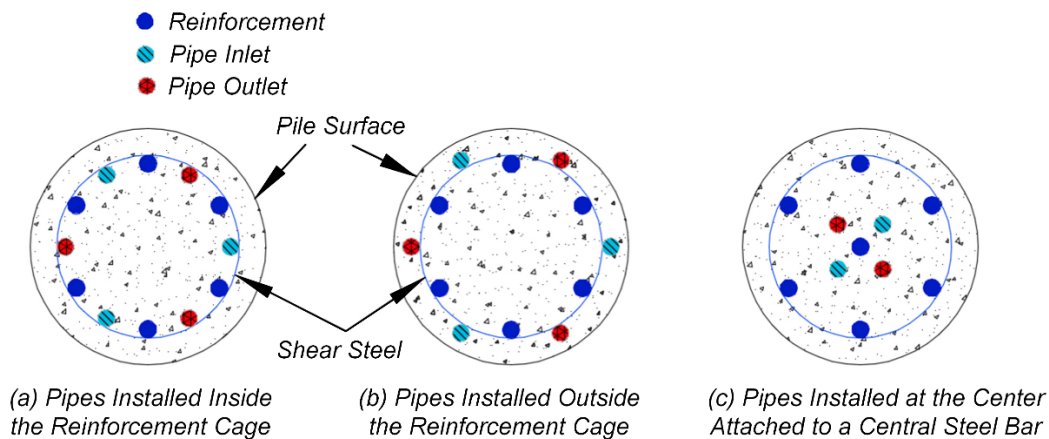


Figure 12. Various attachment arrangements of heat exchanger pipes on the reinforcement cage (Sani et al., 2019)



Figure 13. (a) U-shaped pipes inside an energy pile reinforcing cage (b) instrumented energy pile (Faizal et al., 2019)

Vertical loop pipes can be installed in various configurations within the pile heat exchangers. Figure 14 shows four typical heat exchanger pipe arrangements including U-shaped, double U-shaped, W-shaped, and spiral shaped configurations (Gao et al., 2008; Hamada et al., 2007; Park et al., 2012; You et al., 2016). Figure 13(a) shows an example of a U-shaped pipe configuration utilized inside an energy pile reinforcing cage that supplies heat to a six-story student dormitory building at Monash University, Melbourne, Australia (Faizal et al., 2019). Figure 15(a) and (b) show energy piles with double U-shaped and spiral shaped pipe configurations tested at a project located at the high-speed railway station in the city of Xinyang in Henan Province, China.

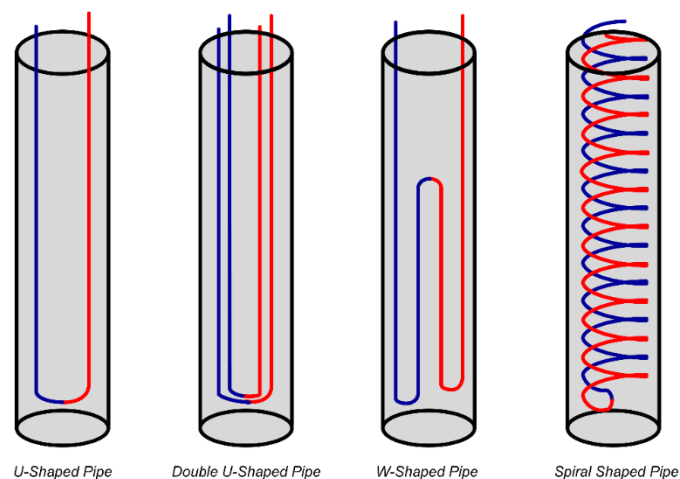


Figure 14. Different configurations of energy loops within a GEP (Sani et al., 2019)

Previous studies have demonstrated the influence of heat pipe configuration on the efficiency of GSHP systems (i.e. Bozis et al., 2011; Lee & Lam, 2013; Park et al., 2013; Wood et al., 2012). Gao et al. (2008) conducted field experiments of heat transfer efficiency with four different loop configurations: U-shaped type, single U-shaped, double U-shaped and triple U-shaped, and W-shaped type. A GEP heat exchanger with a W-shaped type was found to be the most efficient based on its thermal performance. Zarrella et al. (2013) evaluated, via field experiments, the performance

of three different pipe configurations: helical (spiral shaped), double U-shaped, and triple U-shaped. The results showed that the pile with helical pipe configuration produced 23% and 40% higher thermal performance than those with triple U-shaped and double U-shaped configurations, respectively. Based on a recent study by Kuishan et al. (2007), a parallel triple U-shaped had a higher heat transfer performance and efficiency compared to single U-shaped, double U-shaped, W-shaped, and spiral type. The heat release per meter of the heat exchanger pipes with a parallel triple U-shaped configuration was approximately 87% higher than a single U-shaped type under a similar initial condition.

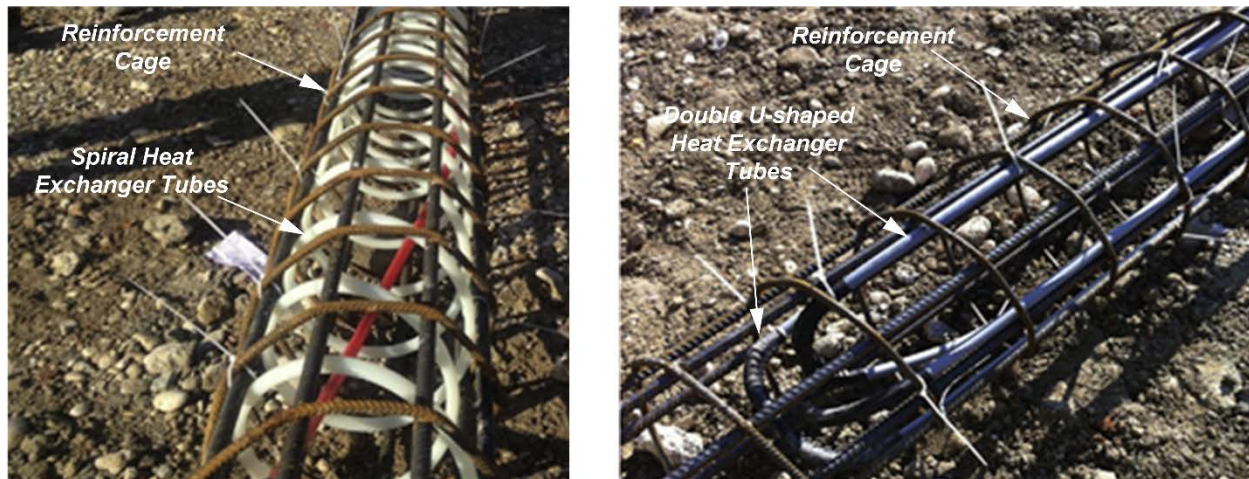


Figure 15. The reinforcement cage of tested energy piles (a) spiral shaped (b) double U-shaped (Zarrella et al., 2013)

Thompson III (2013) compared the effect of the number of loops on GSHP system performance. In this study, 120 cm (3.9 ft) diameter piles with three different loop configurations were compared. Four, five, and six loop systems were investigated and all other parameters were unchanged. Comparing the outlet fluid temperature of the three different loop configurations indicated that the fluid temperature reduced as the number of loops increased. It was concluded that the heat transfer area is higher when the number of loops increases. The additional heat transfer area allowed heat to be dissipated within the pile and led to a lower fluid temperature. It was also noted that increased pumping power is required as the number of loops increases.

Circulating Fluid

Circulating fluid is the liquid that flows in the heat exchanger pipes and, in its heating mode, exchanges heat between the ground and heat pump. In GSHPs, several circulating fluid options are available for the primary unit. An ideal circulating fluid has low viscosity, is environmentally friendly, and is cost-effective (Rawlings & Sykulski, 1999). The circulating fluid can be water, a mixture of water and antifreeze, or a saline solution. Water-antifreeze solution is widely used as a circulating fluid to prevent freezing. Commonly used antifreezes are ethylene glycol or propylene glycol (Brandl, 2006). The drawback to adding antifreeze is that the viscosity of the antifreeze increases at low temperatures, thereby increasing the overall electricity consumption of the heat pump system (Loveridge et al., 2020; Rawlings & Sykulski, 1999). If the antifreeze solution includes corrosion inhibitors it can become toxic and extra care should be taken to prevent leaks in the system. The Agency for Toxic Substances and Disease Registry (ATSDR, 1997), US Department of Health and Human Services, considers propylene glycol a safer chemical than

ethylene glycol, which is a toxic chemical. Additionally, if leakage occurs, quick degradation of the propylene glycol is expected. Propylene glycol is completely soluble in water. Based on ATSDR (1997), the half-life of propylene glycol in water is between 1 to 4 days under aerobic conditions and between 3 to 5 days under anaerobic conditions. The half-life of propylene glycol in the soil is expected to be equal to or slightly less than that in water (ATSDR, 1997).

Heat Pump System

A heat pump system serves as the energy carrier that transfers harvested geothermal energy to the secondary unit. Geothermal heat pump systems are classified into two categories based on their heat source (ASHRAE & Design, 2011). If the Geothermal Heat Pump (GHP) uses groundwater as a heat source or sink, it is called a Ground Water Heat Pump (GWHP). Otherwise, if the pump uses the ground as a heat source or sink, it is called a Ground Source Heat Pump (GSHP). The advantages of GWHP systems are a low initial cost and small area requirements (American Society of Heating & Engineers, 2003). The restrictions associated with a GWHP system are limited availability of groundwater and high maintenance costs. GSHP systems, which are also called a closed-loop heat pumps, are more environmentally friendly. Another advantage of the GSHP is that the collector loops are in contact with soil rather than water, which has a smaller temperature variation (Sarbu & Sebarchievici, 2014). In contrast to GWHP systems, the initial cost is higher due to utilizing expensive equipment.

A heat pump system is comprised of four main components: the evaporator, condenser, compressor, and expansion valve, as shown in Figure 16 (Bach et al., 2016). In heating mode, the circulating fluid is first pumped through the pipes embedded in geothermal piles. The circulating fluid absorbs thermal energy from the ground through conduction and convection. Then the absorbed heat is transferred directly to the evaporator. The evaporator contains refrigerant, which is colder than the circulating fluid. The refrigerant absorbs heat from the circulating fluid and evaporates. The evaporated refrigerant then enters the compressor, which raises the pressure and temperature of the gas. The heat pump joins with the secondary unit where the high-temperature refrigerant transmits its heat to the secondary unit where condensation occurs. The refrigerant then passes through an expansion valve where the pressure and temperature of the refrigerant is returned to its original condition and then flows into the evaporator where the cycle repeats (Brandl, 2006; De Moel et al., 2010; Johnston et al., 2011).

The terms coefficient of performance (COP) and energy efficiency ratio (EER) describe the heating and cooling efficiency of a geothermal system that includes a heat pump. COP is defined as the ratio between produced energy and absorbed power; the higher the number, the more efficient the system is. COP of a heat pump is related to EER by Equation 1 (Sarbu & Sebarchievici, 2014):

$$\text{COP} = \text{ERR} / 3.413 \quad (1)$$

The COP of a GSHP system, designed for a closed-loop heating system, ranges between 2.5 to 4.0, while the ERR for a closed-loop cooling system varies from 10.5 to 20.0 (Heinonen et al., 1996).

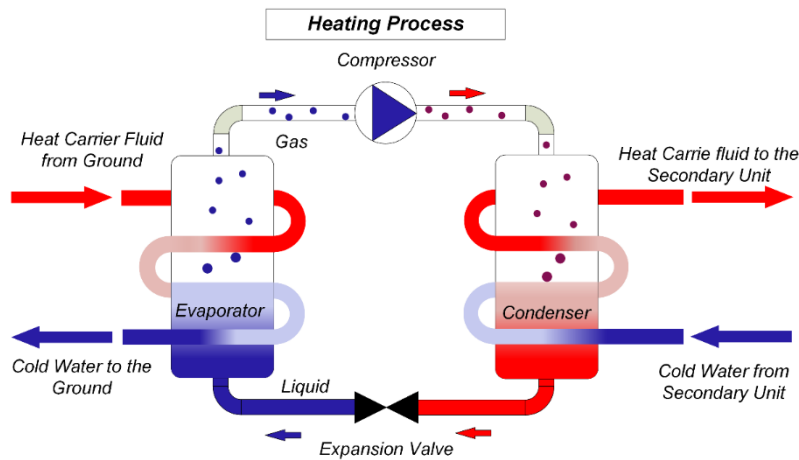


Figure 16. Process of the overall heating only in heat pump system

Power Source

As a promising approach for energy savings, heat pumps can be coupled with other renewable energy sources to provide higher efficiency. Solar energy has been found to be the most adaptable source for hybridization with a GSHP system (Leenders et al., 2000; Tagliabue et al., 2012). Solar energy hybridized with a geothermal energy system can be exploited to reduce the thermal load of boreholes or to generate solar power (Bakker et al., 2005; Shahed & Harrison, 2009).

Solar thermal collectors and GSHPs can be connected in parallel configuration or in series. In a parallel arrangement, solar energy and a GSHP system can directly provide the demanded heat. In this case, each system can operate separately and act as a primary energy source for the structure. A control system can be used to select the most efficient thermal source during the operation of the deicing system (Duffie et al., 2020). Figure 17(a) shows a schematic view of a parallel configuration. In the series configuration, which is also known as a solar augmented heat pump system (Figure 17(b)), the heat pump evaporator is supplied with energy from the solar thermal collectors through a heat exchanger loop. Such systems can potentially be used for seasonal thermal energy storage (Shahed & Harrison, 2009).

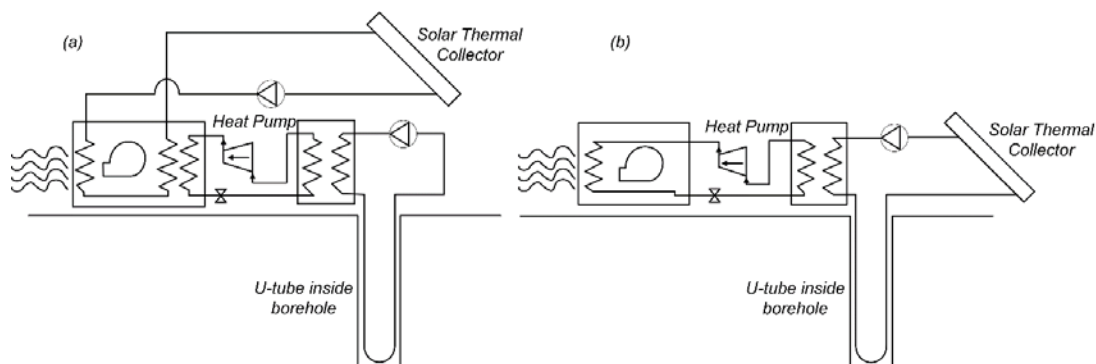


Figure 17. Simplified schematic of a solar assisted ground-source heat pump system (a. parallel, b. series) (Shahed & Harrison, 2009)

Trillat-Berdal et al. (2006) investigated the performance of a GSHP used in a 180 m² private residence and hybridized with thermal solar collectors. The system configuration was in series and employed two 90 m (295 ft) boreholes as the ground loop. Solar energy was utilized as a primary

source for heating the water tank to a specific temperature. Then the excess solar energy is injected into the ground through embedded heat exchanger loops. The schematic view of the system is shown in Figure 18. The circulating fluid was a 35 percent propylene glycol water solution. By studying the system's behavior and energy balances it was concluded that continuous operation of the heat pump did not result in optimum performance. An average COP value of 3.75 in heating mode was achieved. The extracted thermal energy from the ground was 6253 kWh, and the injected solar heat to the ground was 2121 kWh. Finally, it was concluded that solar thermal collectors may decrease the number of boreholes and their corresponding installation costs.

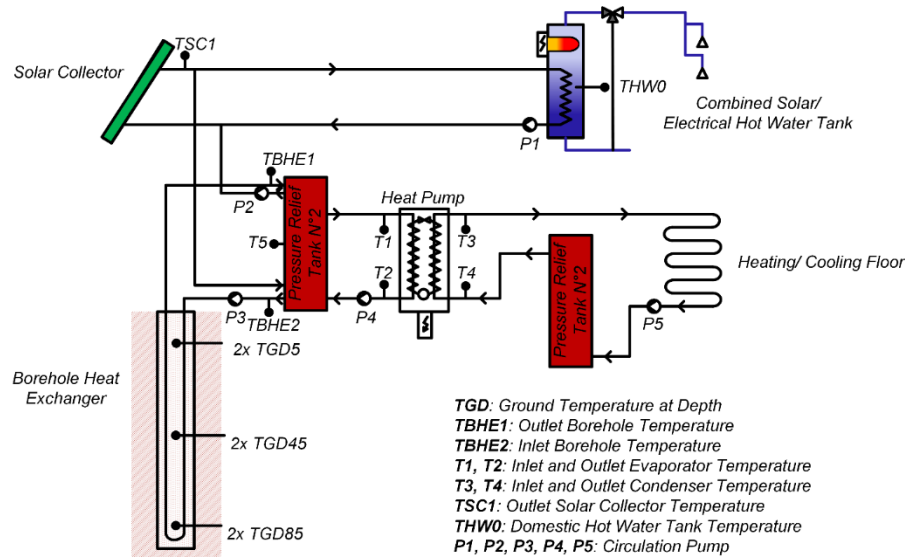


Figure 18. Schematic view of ground-coupled heat pump combined with thermal solar collectors (Trillat-Berdal et al., 2006)

Bakker et al. (2005) studied the performance of a solar-assisted GSHP system at the Energy Research Centre of the Netherlands. They employed a photovoltaic/thermal (PVT) panel, which combined photovoltaic cells with a solar thermal collector to generate solar electricity and solar heat concurrently. Figure 19 shows the front and back of a PVT panel tested in the study. Using an array of PVT panels, the heat is generated and stored in a storage vessel using a heat exchanger. During the summer, the excess generated heat from the PVT panels is injected and stored into the ground via embedded loops. During winter, the stored heat is extracted from the ground via a heat pump and the same embedded loop system. A schematic view of the system is shown in Figure 20. The results of the ten-year average energy balance of this system showed that the PVT system was able to provide approximately 96 % of the electricity used by the system, including pumps, electrical heater, and heat pump. Additionally,



Figure 19. Front and back of a PVT panel (Bakker et al., 2005)

A schematic view of the system is shown in Figure 20. The results of the ten-year average energy balance of this system showed that the PVT system was able to provide approximately 96 % of the electricity used by the system, including pumps, electrical heater, and heat pump. Additionally,

the ground injected heat from the PTV system was effective in maintaining a constant ground temperature during long-term use of the system, which results in an increase in the COP of the heat pump from 2.6 to 2.66.

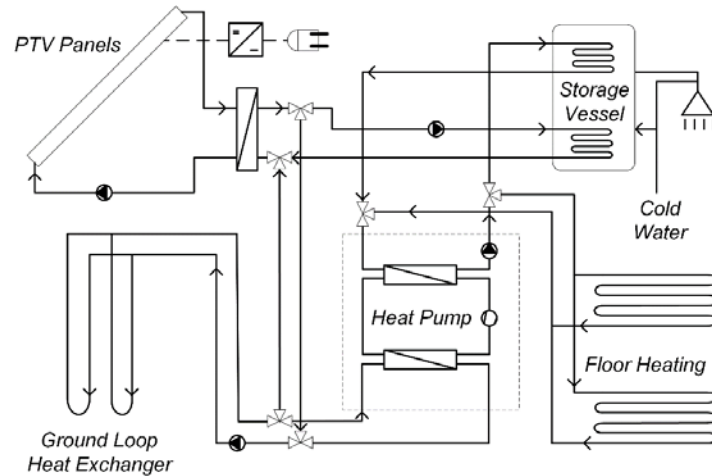


Figure 20. Schematic view of tested hybrid system (Bakker et al., 2005)

Bernier and Shirazi (2007) investigated the performance of a modified solar assisted heat pump system. In the proposed system, two independent U-pipe loops were embedded in the borehole, as shown in Figure 21. One of the U-loops was connected to the heat pump, and the other was connected to the thermal solar collectors. During the summer, solar energy was used for heating the water tank, and the excess solar heat was injected into the ground. During winter, the solar energy was either transferred directly to the other U-loop if the heat pump was in operation or to the ground when the pump was not working. They concluded that this arrangement resulted in increased ground temperature, leading to a reduction of the borehole depth and increased heat pump performance.

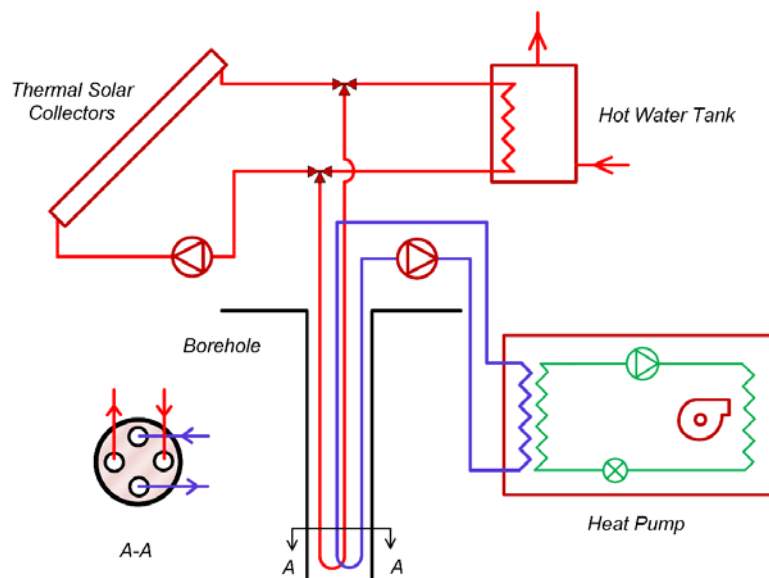


Figure 21. Schematic of the modified system proposed by Bernier and Shirazi (2007)

Secondary Unit

The secondary unit comprises the pipes embedded in bridge decks, pavements, and other infrastructure. It utilizes the extracted thermal energy during colder times of the year to heat the surface and receives unwanted heat from its surroundings during warmer times of the year to transfer into the ground. Using a hydronic heating system for snow melting and deicing on bridge decks has received more attention in recent years. The harvested energy from the ground may also be used for deicing culverts. However, the feasibility of the use of GSHP system for deicing culverts has not been studied.

A schematic of a GSHP system for heating bridge decks is illustrated in Figure 22. By installing circulation pipes in the sub-structural elements of a bridge, foundation elements are converted to energy foundations. For additional heat exchange with the ground and increased efficiency of the system, the heat exchanger loops can also be embedded in the embankment of the bridge. The circulating fluid is warmed as it circulates through the energy piles, approaches the embankment and is then circulated in the deck, heating the deck.

The fluid can be pumped directly from the foundation to the bridge deck (passive system) or can be distributed through a heat pump (active system). In an active system, the heat pump uses the heat energy from the fluid for efficient heating of the circulation fluid for bridge deck deicing (Liu et al., 2007). Due to the absence of a heat pump in the passive system, the temperature of the circulating fluid is primarily controlled by the ground temperature. The main advantage of a passive system is that the only energy required to operate the system is the energy required for operation of the circulation pumps. An active system requires an external power source for the operation of the heat pump.

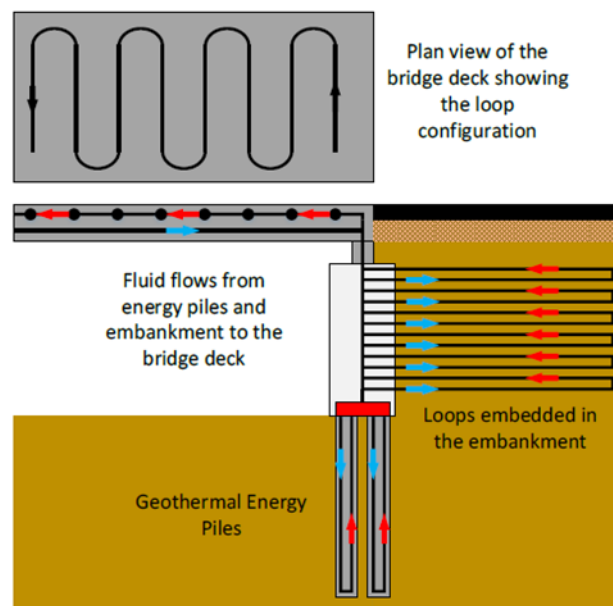


Figure 22. Conceptual schematic of ground-source bridge deck deicing (Bowers & Olgun, 2014)

A GSHP system may also be used for ice jam mitigation and prevention in culverts. The possible application of geothermal energy for culvert deicing and anti-icing has not been published to date. Therefore, there is not a typical design for a culvert system or clear guidelines and best practices supported by practical experiences. A schematic of a possible culvert deicing system is shown in Figure 23(a). The schematic is based on previous studies on the use of geothermal energy in tunnels and underground structures. As shown in Figure 23(a), the lining and deck of the culverts can be equipped with heat exchanger pipes. As discussed in the primary unit section, pipe configuration plays a significant role in system efficiency. Three common pipe configurations that can be used in culvert systems are: 1) longitudinal along the culvert axis, 2) transverse, and 3) slinky (Figure 23(b)). The heat exchanger pipes can be either embedded at the bottom of the culvert or inside the primary lining (e.g., concrete) or installed between the primary

lining and an external lining with high thermal conductivity (e.g., an energy geotextile (Figure 23(c)) (Loveridge et al., 2020).

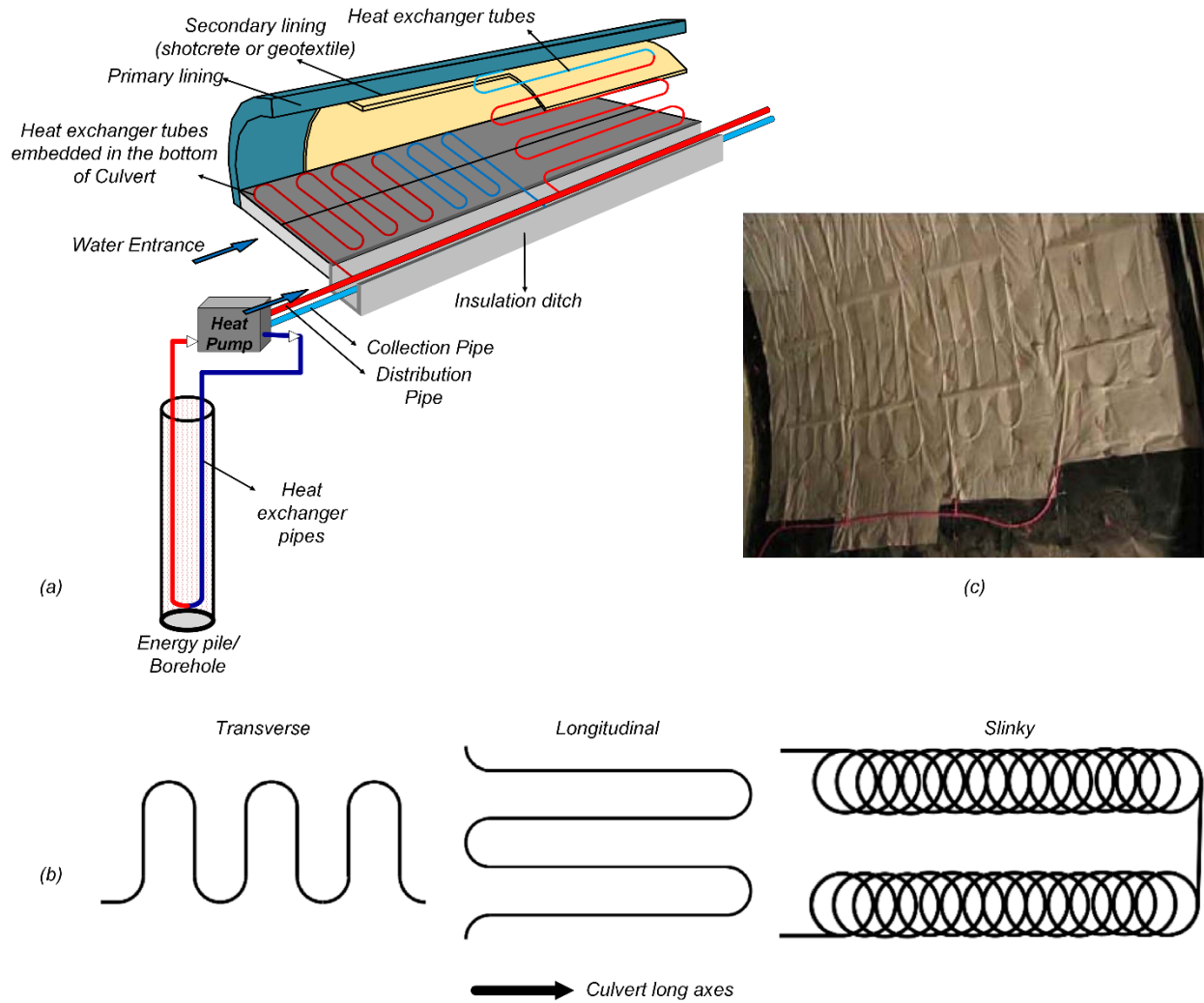


Figure 23. (a) A schematic of a possible culvert deicing system based on previous studies on the use of geothermal energy in tunnels and underground structures, (b) Various pipe configuration (c) An energy geotextile installed in an energy tunnel (Loveridge et al., 2020)

CHAPTER 4: USE OF GEOTHERMAL ENERGY FOR ROAD CULVERT/BRIDGE DECK DEICING: CASE/FIELD STUDIES

This chapter will briefly introduce several case studies where geothermal energy was used for deicing or snow melting of bridge decks. The list of case studies investigated in the current report is shown in Table 6.

Case Study 1: Jiangyin, China

Chen et al. (2020) presented the results of field tests of a bridge deck located in China. The heated deck was 30 m (98.4 ft) long, 26 m (85.3 ft) wide, and 80 cm (2.6 ft) thick. Figure 24 shows a photo of the bridge deck after construction, the schematic layout of the heating system, and the locations of the sensors. The annual average and minimum ambient temperatures of the city were 17°C (63°F) and -5°C (23°F), respectively. The minimum ambient temperature during the night was 10-20°C (50-68°F), and the maximum ambient temperature during the day was 20-30°C (68-86°F) during the test period. The secondary system used Polyethylene Raised Temperature pipes (PERTs) with an inner diameter of 16 mm (0.6 inch), a thickness of 2 mm (0.08 inch), and a spacing of 25 cm (10 inch). A water tank was utilized as the heat source for bridge deck deicing. Three inlet fluid temperatures of 30.5°C (86.9°F), 35.5°C (95.9°F), and 41°C (106°F) were considered to study the effect of inlet fluid temperature on the performance of the system. The volumetric flow rate of the heat carrier fluid was maintained at 0.79 m³/h (27.9 ft³/h) during the tests. Two thermostats and a flowmeter were used to monitor the inlet and outlet fluid temperatures and the volumetric flow rate.

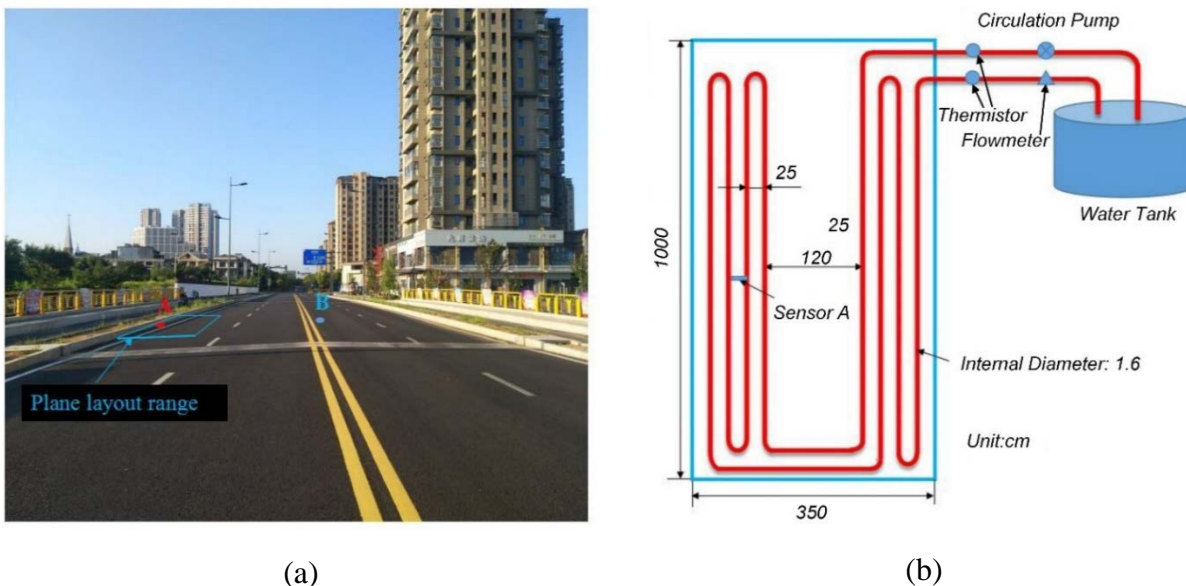


Figure 24. (a) Photo of the bridge (b) schematic layout of heating system (Chen et al., 2020)

Table 6. Case/Field studies of bridge deck deicing/anti-icing using GSHP systems

Source	Location	Snow Melting system	Heat Extraction System	Temperature Range
Xin Chen et al. (2020)	Jiangyin, China Bridge length: 30 m Bridge Width: 26 m Deck Thickness: 80 cm	Heated area: 20 m ² Fluid: Water Pipe material: Polyethylene raised temperature pipes (PERTs) Pipe diameter: 20 mm Horizontal spacing of the pipes: 25 mm	Water Tank Temperature Control Temperature: 30.5°, 35.5°, 41°	Average = 17°C Minimum = -5°C
Kong et al. (2019)	Jiangyin, China Bridge length: 36 m Bridge Width: 26 m Deck Thickness: 80 cm	Heated area: 20 m ² Fluid: Water Pipe material: Polyethylene raised temperature pipes (PERTs) Pipe diameter: 20 mm Horizontal spacing of the pipes: 25mm	Energy Pile Heat Exchange rate: 1200 W Pile length: 20 m Pile diameter: 1 m Pipe Arrangement: U shape	Ambient T = -1.5°C
Eugster (2007)	Central Switzerland	Heated area: 1300 m ² Heat Output: 100 W/m ²	Number of boreholes: 91 Depth of boreholes: 65 m	Outflow T = 10°C
Boyd (2003)	Klamath Falls, Oregon, Bridge length: 48 m Bridge width: 12.8 m	Heated area: 345.6 m ² Heat Output: 189 W/m ² Fluid: Propylene glycol solution Pipe material: Polyethylene Pipe diameter: 16 mm	Geothermal heat exchanger Well water flowing: 2.5 L/s	Inlet Fluid T to deck = 66°C Output Fluid T to deck = 43°C
Minsk (1999)	Silver Creek, in the Cascade Mountain, Oregon Bridge length: 32 m Bridge Width: 12.2 m	Heated area: 576 m ² Heat Output: 394 W/m ² Fluid: Propylene glycol solution Pipe material: Cross-linked polyethylene (PEX) Pipe diameter: 12.7 mm Horizontal spacing of the pipes: 114 mm	Ground surface heat pump Heat input: 37 W/ft ² Well water flowing: 568 L/min	Ambient T = -23°C Inlet Fluid T to deck = 49°C Output Fluid T to deck = 32°C
Minsk (1999)	Two-lane bridges on US 287 in Amarillo, Texas, Deck Length: 44.5 m Deck Width: 17.7 m	Heated area: 799 m ² Fluid: Propylene glycol-deionized water Pipe diameter: 19 mm Horizontal spacing of the pipes: 152 mm	Well Depth: 53.6 m Well Diameter: 102 mm Pipe Arrangement: Two pipe loops Filling Material: Non-shrinking bentonite	Ambient T = 1.7°C
Yoshitake et al. (2011)	Mountain road in western Japan, Bridge deck area: 430 m ² , Road area: 265 m ²	Deck Material: Concrete mixture with Polypropylene Fiber, Pipe material: Steel Pipe Horizontal spacing of the pipes: 150 mm	Underground water tank Diameter*Height: 5.5 m * 9.5 m	Ambient T = 2°C Ground temperature at a depth of 15 m = 12°C

The results of this study showed that the transient heat flux of the system varied linearly with the difference between the inlet fluid temperature and the air temperature. As shown in Figure 25(a), for a constant fluid inlet temperature, the transient heat flux increased as the ambient temperature decreased. The thermal efficiency of the deicing system was found to be affected by: 1) concrete thickness above the heating pipes, 2) the thermal conductivity of the concrete, and 3) the heat transfer coefficient from the heated layer to the ambient air. Thermal efficiency is defined as the portion of the heat transferred to the top surface of the deck from the heated layer. The average rate of heat transfer to the deck surface reported in this study was 0.52. Considering the heat efficiency of the deck, an equation for estimating the deck surface temperature (T'_s) was developed as Equation 2:

$$T'_s = 0.3T_{in} + 0.7T_0 \quad (2)$$

where T_{in} is the inlet fluid temperature ($^{\circ}\text{C}$) and T_0 is the air temperature ($^{\circ}\text{C}$). Figure 25(b) shows the inlet fluid temperature and heat flux required to keep the deck surface temperature above 0°C (32°F) under different ambient temperatures. Based on the results, at an air temperature below 0°C (32°F), the minimum inlet fluid temperature required to maintain the deck surface temperature above 0°C (32°F) should be 2.3 times the ambient temperature. In winter, the minimum ambient temperature in the project site was -5°C (23°F), therefore, the inlet temperature of the fluid should be greater than 11.5°C (52.7°F).

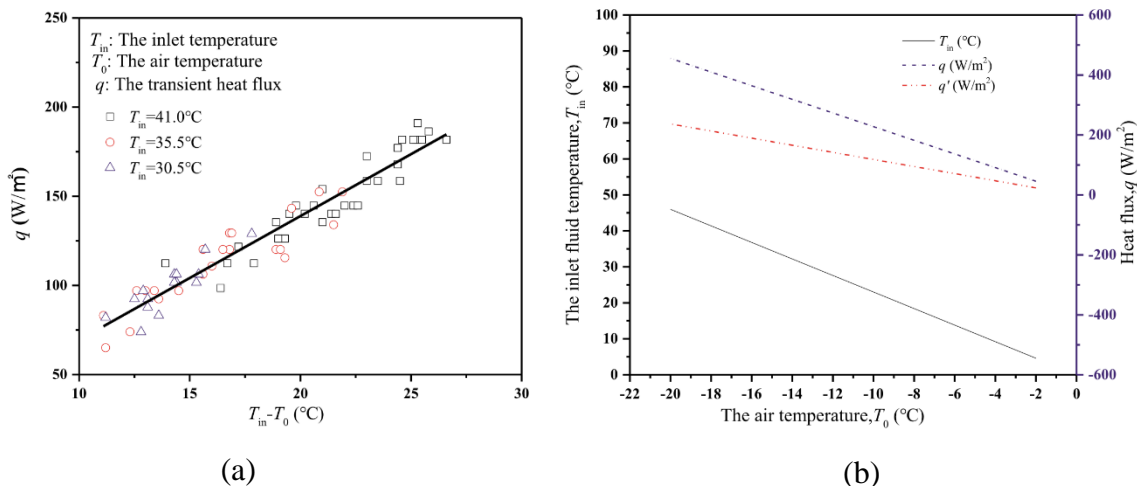


Figure 25. (a) Variation of heat flux, q , with the difference between the inlet fluid and the ambient temperatures, $T_{in}-T_0$, (b) the required inlet fluid temperature and heat flux to keep the deck surface temperature above freezing point (Chen et al., 2020)

Case Study 2: Jiangyin, China

Kong et al. (2019) investigated the performance of a geothermal energy deicing system for bridge decks using a pile heat exchanger during snowfall conditions. The project was located in Jiangyin, China. The design objective of the bridge deck deicing system was to accelerate the snow-melting process. In this project, a 10 m (32.8 ft) long, 3.5 m (11.5 ft) wide, and 0.8 m (2.6 ft) thick section of the bridge deck was studied. Figure 26 shows the section of the bridge deck with heat pipes (Figure 26(a)), a photo of the study section before pouring concrete (Figure 26(b)), and a schematic of the bridge deck deicing system (Figure 26(c)). PERT pipes with an inner diameter of 16 mm (0.6 inch) and a thickness of 2 mm (0.08 inch) were placed in the upper 10-cm (3.9-inch) of the reinforced concrete deck. The pipe spacing was 25 cm. The primary system consisted of 1-m

diameter energy piles with a depth of 20 m (65.6 ft) and a total heat exchange rate of 1200 W per pile. U-shaped polyethylene pipes with an outer diameter of 25 mm (1 inch) were installed inside the pile. A water tank was utilized to store the circulating fluid. The initial fluid temperature in the water tank was about 2°C (35.6°F) when the ambient temperature was -1.5°C (29.3°F). The inlet flow rate of the circulating fluid was 1.27 m/s (3.3 f/s). The deck temperature was measured during the test using sensors placed in the bridge deck.

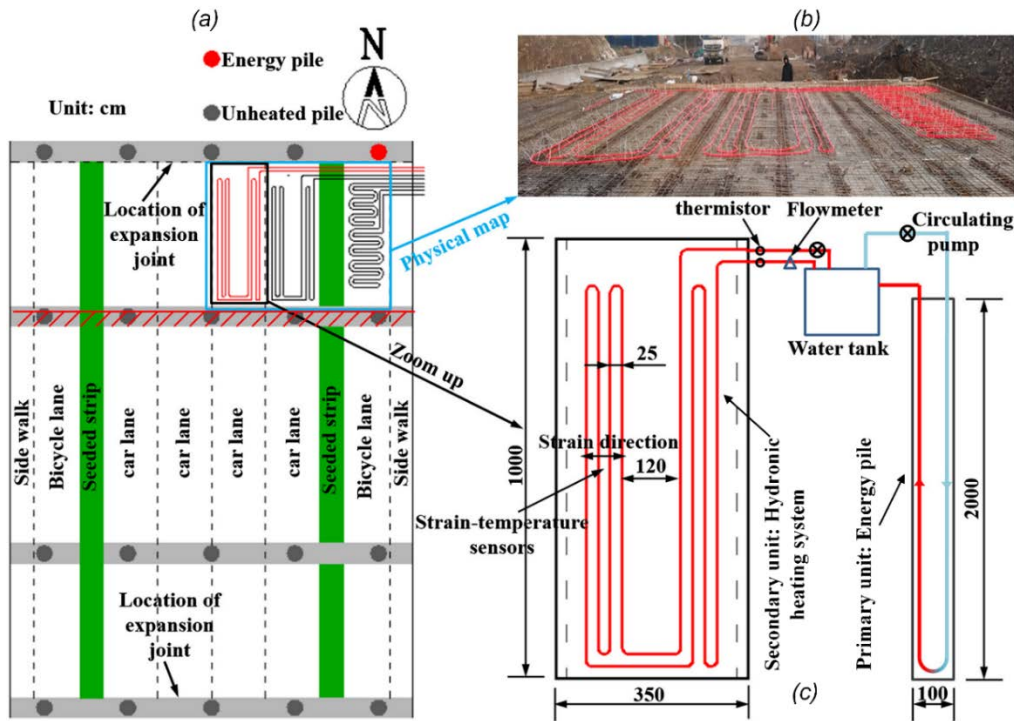


Figure 26. (a) Location of the studied section of the bridge (b) photo of bridge deck before pouring concrete (c) layout of bridge deck deicing (Kong et al., 2019)

Figure 27 illustrates the surface condition of the bridge deck during the operation of the deicing system (after 0, 3, 7, 17, 25, and 27 hours). As shown in Figure 27, the snow melting system was not very effective for melting snow during snowfall (the first 7 hours of the experiment). However, as shown in Figure 28(a), continuous operation of the snow melting system maintained the bridge deck temperature at a constant value of 1°C (34°F). The ambient temperature did not affect the temperature of the bridge deck or the circulating fluid when the bridge deck was covered with a layer of snow due to snow's natural insulation characteristics. Bridge deck snow melting started once the snowfall stopped (from 16 to 25 hours during the test). Figure 28(a) shows that the deck temperature increased by 2.8°C (37.0°F) a few hours after snowfall reaching a temperature of 3.8°C (38.9°F) (point F on Figure 21) and stayed above 0°C (32°F) when the ambient temperature dropped below the freezing point. The results of the study suggested that the snow melting process can be accelerated using a geothermal energy system after the snowfall.

The variation of inlet and outlet circulating fluid temperature is presented in Figure 28(b). The results showed that the variation of inlet and outlet circulating fluid temperatures was similar to the change in bridge deck temperature. However, the temperature of the outlet fluid was about 3°C (37°F) higher than the deck, which could be attributed to the high flow velocity of the inlet fluid

(1.27 m/s (4.2 f/s)). The heating power of the system was computed as 55 to 70 W/m², which was lower than the upper limit of the heat flux, 80 W/m². The upper limit was determined according to a maximum value of the heat exchange rate of 60 W/m for an energy pile with a diameter larger than 0.6 m (23.6 in). The discrepancy between the obtained heating power of the system and the upper limit of the heat flux was attributed to heat loss between the hydronic heating system and the energy pile.

Han and Yu (2017) computed snow melting heat flux demand for bridge decks with 10 different design conditions. The results indicated that the heat fluxes that achieve 95 % reliability of snow-free areas vary between 280 to 792 W/m². The heat flux provided by a deicing system was found to be lower than the level of heat flux required to keep the deck free from snow during snowfall (Kong et al., 2019). Therefore, it was concluded that a shallow geothermal bridge deck deicing system without a heat pump might not keep the deck surface free from snow during snowfall; however, the system could accelerate the snow melting process, as shown in Figure 27.

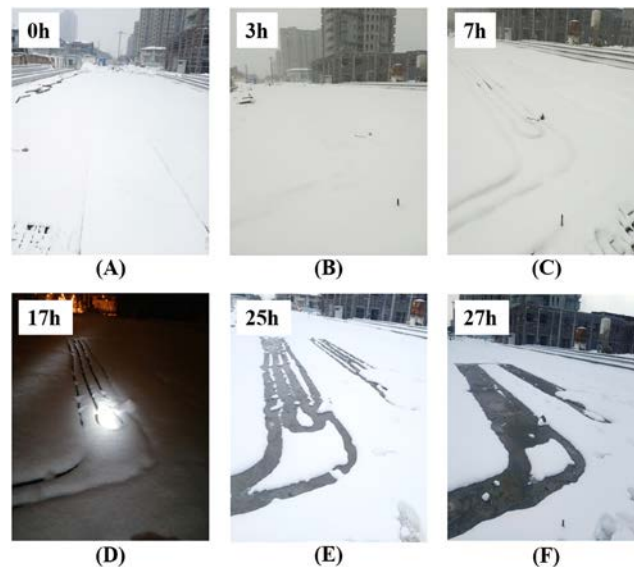


Figure 27. Surface condition of deck surface at different hours (Kong et al., 2019)

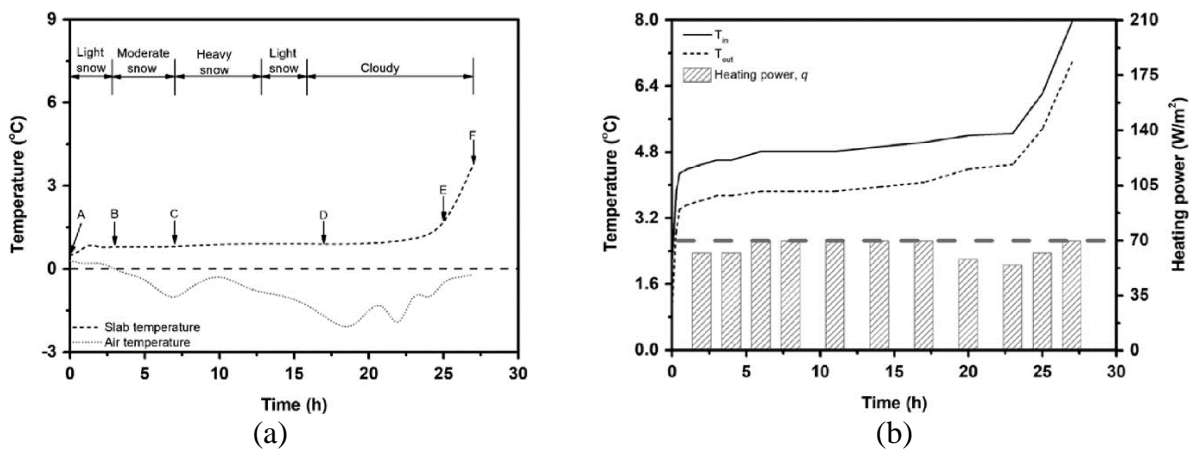


Figure 28. (a) Change in the ambient and bridge deck temperatures, (b) variation of the inlet and outlet circulating fluid temperature and the heating power of the deicing system (Kong et al., 2019)

Case Study 3: Central Switzerland

The SERSO system in Switzerland, with a total heated area of 1300 m² (13993 ft²), is one of the longest running hydronic geothermal bridge deck deicing projects in the world. The system has been continuously operating since 1994 (Eugster, 2007). Figure 29(a) and (b) show a photo of the SERSO system in operation and a schematic of the SERSO deicing system, respectively. The design objective of the system was to prevent accumulation and freezing of snow and other precipitation on the deck surface. The system utilizes 91 borehole heat exchangers with a depth of 65 m (213 ft) and operates by storing thermal energy during the summer in 55,000 m³ (1942306 ft³) of rock. In the winter, the thermal energy stored in the rock was used preemptively to prevent snow accumulation on the bridge deck. Figure 30 shows typical ambient and surface temperatures measured during operation in the winter. The results of this study suggested that continuous operation of the heating system reduces the heat demand during the winter and allows the system to operate without a GSHP. The heat collected in the summer is usually more than what is required to prevent snow accumulation on the surface. The extra heat collection serves to stabilize the road surface temperatures during the year, which could increase the lifetime of the bituminous surface.



Figure 29. (a) Photo of the bridge (b) schematic of a SERSO system in Switzerland (Eugster, 2007)

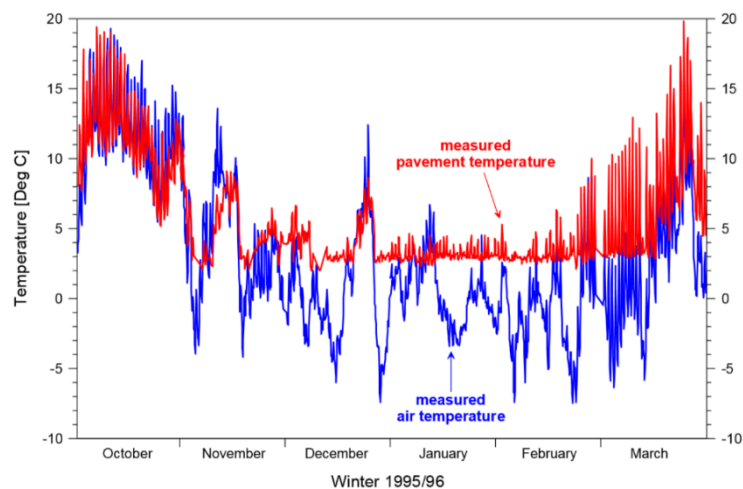


Figure 30. Comparison of the measured ambient and surface temperature during operation (Eugster, 2007)

Case Study 4: City of Klamath Falls, Oregon

A snow melting project using geothermal energy was defined in a joint effort by the Oregon Department of Transportation and city of Klamath Falls. (Boyd, 2003). The Wall Street bridge and approach road employed a snow melting system using geothermal energy. Geothermal heat was provided by the city of Klamath Falls's District Heating System. The heated area of the bridge deck and sidewalks was 345.6 m^2 (27 m by 12.8 m) and the approach road and sidewalk snow melt area was 614.4 m^2 (3720 ft^2) (48 m (157 ft) by 12.8 m (42 ft)). The district heating system included two production wells, a geothermal water transmission pipeline, a heat exchanger and pumping facility, and a closed-loop heating water delivery system. The circulating fluid in the bridge and approach road loop was a 35% propylene glycol mixture. The heat exchanger pipes were made of cross-linked polyethylene with an inner diameter of 16 mm (0.6 inch). The closed-loop system of pipes was placed longitudinally and transversally on the bridge deck and approach road, respectively. The heat exchanger pipes were placed longitudinally on the bridge and the approach road sidewalks. Figure 31(a) and (b) show the bridge deck and approach road loops, respectively. The temperature of inlet and outlet fluid, circulated into the bridge and approach road, was 66°C (151°F) and 43°C (109°F), respectively. The system was designed to clear surfaces of snow and ice during heavy snowfall and a temperature down to -24°C (-11.2°F).



Figure 31. (a) Longitudinal closed loop on the bridge deck and (b) approach road loops in Klamath Falls, Oregon (Boyd, 2003)

Case Study 5: Mountain Road in Japan

An underground water storage tank (9.5 m (31.1 ft) height and 5.5 m (18 ft) diameter) has been used to provide geothermal energy for a bridge system on a mountain road in Japan (Yoshitake et al., 2011). The schematic of the bridge with the hydronic heating system is illustrated in Figure 32. This system does not include a heat pump and the water in the tank was heated by the ground to roughly ambient ground temperature. The annual average ambient air temperature at the site project was 12°C (54°F), but the temperature during winter nights and early morning drops below 0°C (32°F). The system was automatically controlled and operates whenever the temperature in the bridge deck was less than 0.5°C (33°F). The total area of the bridge deck and the road are 430 m^2 (4628 ft^2) and 265 m^2 (2852 ft^2), respectively. The water was circulated through embedded steel pipes with an inner diameter of 15 mm (0.6 inch), a thickness of 3.5 mm (0.14 inch), and a thermal conductivity of 43 W/m.k. The horizontal spacing of the pipes was 150 mm (5.9 inch). The bridge

deck was constructed with a mix of concrete and polypropylene fiber to reduce cracking potential of the concrete during the cooling and heating cycles. The pipes were embedded 50 mm (2 inch) below the road surface.

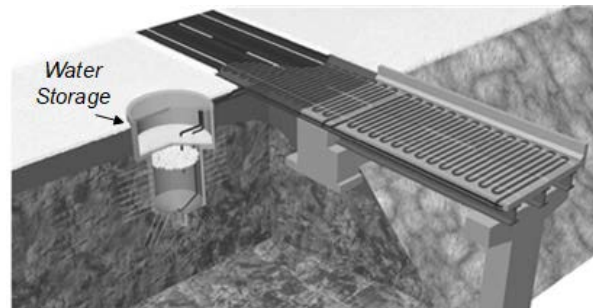


Figure 32. Hydronic heating system using underground water storage on a mountain road in Japan (Yoshitake et al., 2011)

Figure 33 illustrates the condition of the road before and after a 9 hour long operation of the deicing system. As shown in the figure, the system was effective at melting the accumulated snow. The temperature of the water storage, bridge deck, and approach road operation of the deicing system from April 2007 to March 2008 is shown in Figure 34. The results indicated that the continuous operation of the heating system could maintain the temperature of the bridge deck and road surface above 0.5°C (33°F) and prevent snow accumulation on the ground during the winter. Operation of the system during the summer increased the temperature of the water in the tank.

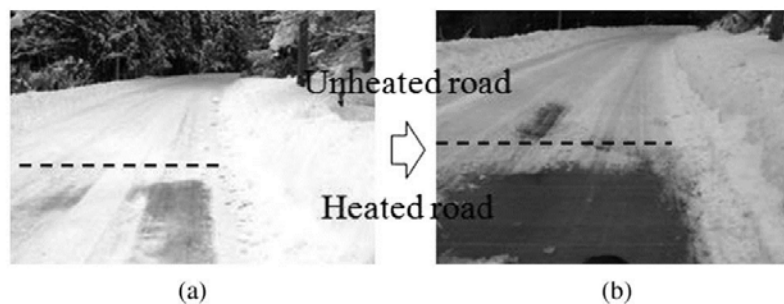


Figure 33. Road surface condition on snowy day (a) snow covered road (b) after 9h operating of the system (Yoshitake et al., 2011)

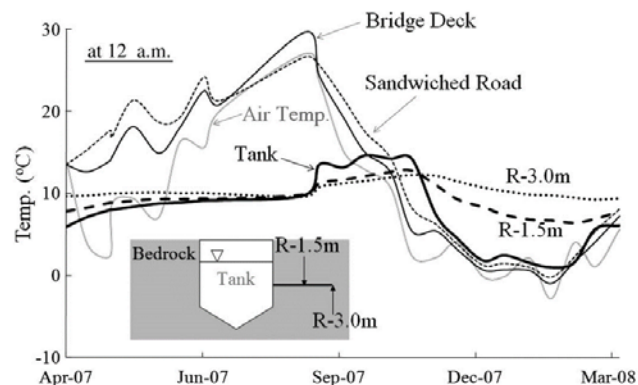


Figure 34. Temperature histories of the water storage, the bridge deck, and the approach road over one year (Yoshitake et al., 2011)

Case Study 6: Fukui City, Japan

A snow melting system named “pipe in pile snow melting system” was utilized for bridge deck deicing in Fukui city in Japan (Nagai et al., 2009). In this system, concrete piles functioned as a heat exchanger between the ground and the circulating fluid (Figure 35). The surface area of the bridge was 1300 m² (13993 ft²), and 378 piles with 128 mm (5 inch) diameter and 23 m (75.4 ft) length were installed under the abutments of the bridge. During the summer, the system absorbs solar radiation at the pavement surface and stores the heat into the ground. During the winter, the heat collected during the summer was extracted from the ground through water flow in pipes. Figure 36 shows the condition of the heated and unheated segments of the bridge deck surface in January 2008. It can be seen that in the segments where heat dissipation pipes were placed, there was no snow on the deck surface. In contrast, the road segments without heat dissipation pipes were covered with snow.

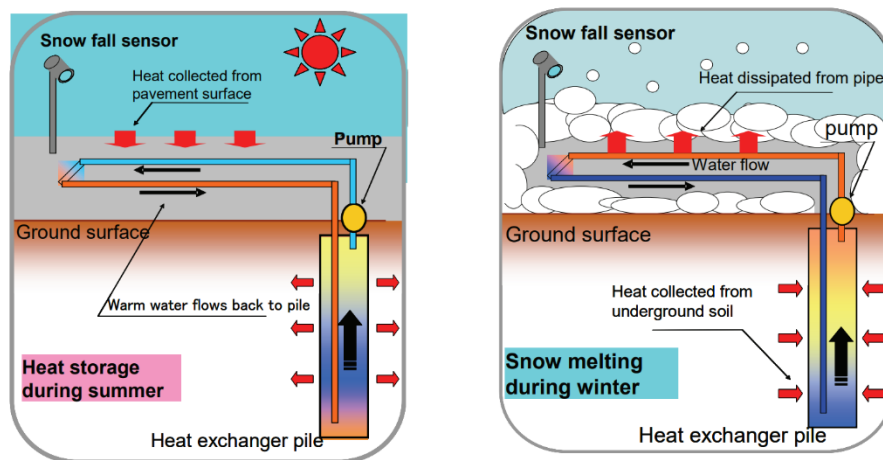


Figure 35. Outline of “pipe in pile” snow melting system (a) heat storage mode during Summer (b) snow melting mode during winter (Nagai et al., 2009)

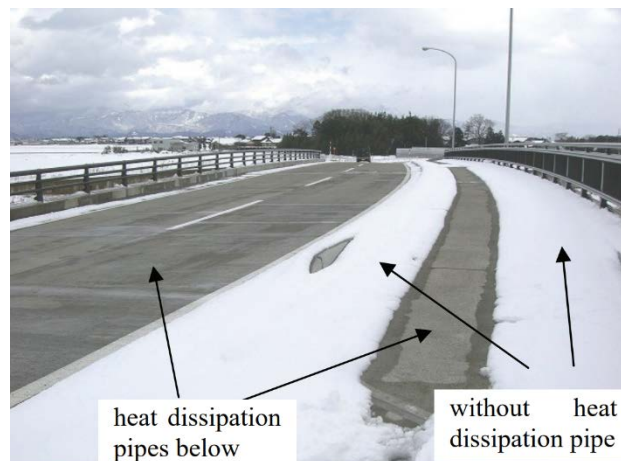


Figure 36. Surface condition of heated and unheated segments of the bridge deck in Fukui City, Japan in January, 2008 (Nagai et al., 2009)

Case Study 7: North Fork of Silver Creek, Oregon

A 32.0 m (105 ft) × 12.2 m (40 ft) two-lane bridge deck was built over the North Fork of Silver Creek, in the Cascade Mountains, with an embedded hydronic heating system. The heated area was 576 m² (6200 ft²). Figure 37 shows the plan view of the heated deck on Silver Creek bridge. Design air temperature was 23°C (73.4°F), and the average wind speed was 1.9 m/s (4.25 mph). The circulating fluid was a 35 percent propylene glycol-water solution. The hydronic system consisted of a closed-loop system with longitudinally placed pipes. The pipes were made of cross-linked polyethylene with an inner diameter of 12.7 mm (0.5 inch) and a wall thickness of 1.6 mm (0.06 inch). The pipe spacing was 114 mm. The heat extraction system consisted of well water flowing at a temperature of 11°C (52°F). A Trane liquid scroll chiller with a capacity of 50 tons was in a building near the bridge. A deck temperature sensor, ambient temperature probe, and an electronic controller were installed in the bridge deck to control the operating system. The controller system ensured that the well pump motor and heat pump ran at an appropriate time by monitoring heating system variables, inlet and outlet fluid temperatures and pressures in the hydronic system, inlet and outlet well water temperature and pressure, deck surface and air temperature, and flow rate. The controller system also prevents slush formation in the circulating fluid which increases the viscosity of the fluid and overloads the pump capacity. The average inlet and outlet fluid temperatures were recorded as 49°C (120°F) and 32°C (90°F), respectively. The results confirmed that the bridge deck deicing system had operated successfully since January of 1995 and could clear the deck surface of snow and ice during cold weather conditions (Minsk, 1999).

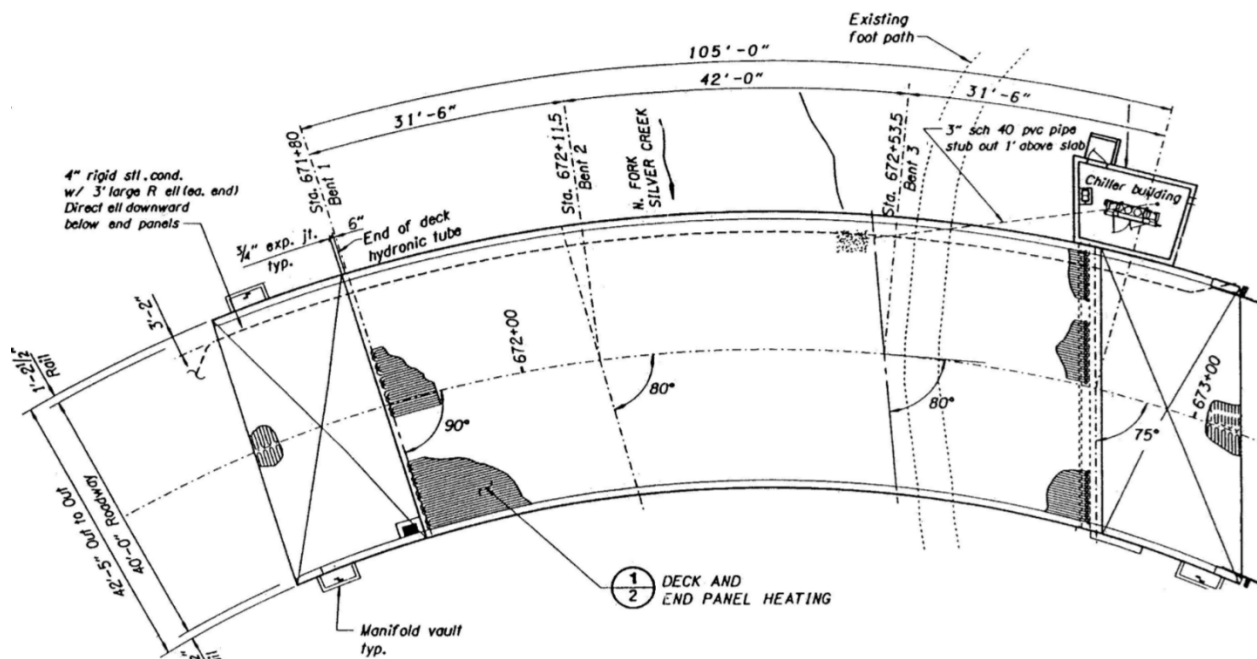


Figure 37. Plan view of the heated deck on Silver Creek bridge, Oregon (Minsk, 1999)

Case Study 8: Amarillo, Texas

Two-lane bridge decks, located in Amarillo, Texas, were heated using a hydronic system using geothermal wells (Minsk, 1999). The design objective of the deicing system was to prevent ice

bonding, not snow melting. The project site experiences many freeze-thaw cycles in the winter, and the ground surface usually freezes at night. Each bridge was in 44.5 m (146) length and 17.7 m (58 ft) in width. The total heated area and the designed heat flux of each bridge were 799 m² and 129 W/m², respectively. Fifty wells in star patterns were used for extracting energy. The diameter and depth of the energy wells were 102 mm (4 inch) and 53.6 m (176 ft), respectively. The depth of the geothermal wells did not reach the groundwater level. Geothermal heat was extracted through two closed-loop pipes inside the well. To ensure good thermal contact with the ground, non-shrinking bentonite was used as a grouting material. The circulating fluid was 50 percent propylene glycol-deionized water circulated through pipes with an internal diameter of 19 mm (0.75 inch). Figure 38(a) shows deck heating circuits before pouring concrete. A Vaisala road weather information system was utilized to monitor the bridge and road condition and control the hydronic heating system. Type K thermocouples were installed near the deck surface and in each deck at the outside shoulder and the right travel lane line. The manifolds and thermocouple conduits are shown in Figure 38(b). Heating was automatically started when the bridge deck temperature reached 1.7°C (35.1°F), and weather reports forecast precipitation. The operating heating system experience showed that to achieve a maximum operating temperature, a three-hour time period is required to extract enough heat for the heating system (Minsk, 1999). The results showed that the operation of the heating system had no problems. The operation of the designed system over two winters could confirm the effectiveness of the applied system.



(a)



(b)

Figure 38. (a) Heating circuits before pouring concrete (b) close-up of supply and return manifolds (pipes in center) and thermocouple conduits terminating in enclosure at right on a bridge deck in Amarillo, Texas. (Minsk, 1999)

CHAPTER 5: LABORATORY STUDIES OF BRIDGE DECK DEICING SYSTEMS

This chapter briefly discusses several laboratory studies of GSHP bridge deck deicing systems and their performance. The effects of pipe spacing in the secondary unit, borehole depth in the primary unit, preheating and snowfall rate, external heating systems, inlet flow rate, and temperature will be discussed. Table 7 and 8 present the features of the GSHP bridge deck deicing systems investigated in these laboratory studies.

Pipe Spacing in the Secondary Unit

The thermal performance of a small-scale bridge deck deicing system was investigated by Bowers Jr (2016) at the Virginia Tech Geotechnical Research Facility. A total of five energy piles (micropiles) were constructed as a heat extraction system. The diameter and depth of the energy piles were 30.5 m (100 ft) and 25.4 cm (10 inch), respectively. In order to measure the ground temperature during the test, four observation boreholes were installed. The location and spacing of the energy piles and observation wells are illustrated in Figure 39(a). HDPE pipes with a diameter of 19 mm (0.75 inch) in a single closed-loop and PEX pipes with a diameter of 25.4 mm (1 inch) in both single and double closed-loop systems were installed in the energy piles. Two bridge deck models were constructed (1.3 m (4.3 ft) wide, 3.05 m (10 ft) long, and 0.254 m (10.4 inch) deep). The experimental deck models are shown in Figure 39(b). The heat exchanger pipes had a spacing of 30 cm (12 inch) and 20 cm (8 inch) in the left-side and right-side model deck, respectively. The inner and outer diameter of the pipes was 16 mm (0.62 inch) and 22 mm (0.87 inch), respectively. The circulating fluid was a 20% glycol solution with a flow rate of 15.1 L/m (1.2 gal/ft). In order to measure deck temperatures, 36 thermistors were placed inside the deck.

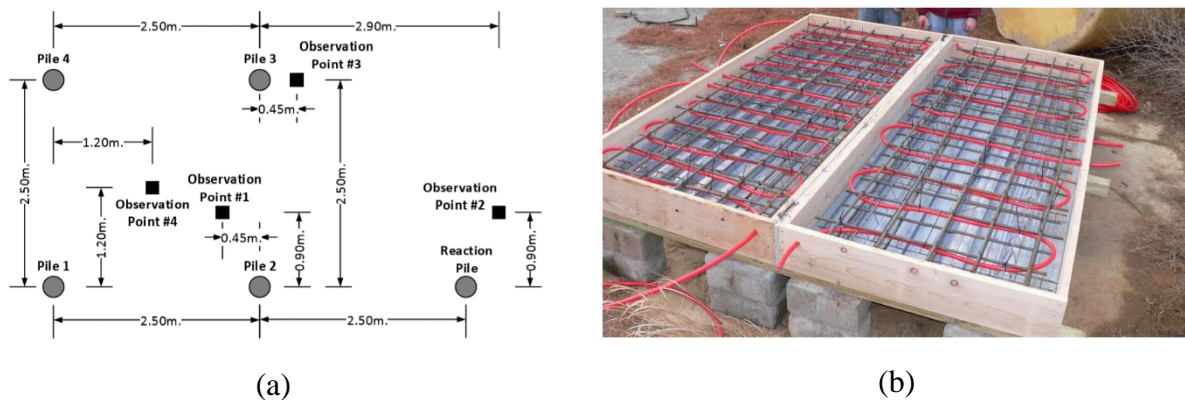


Figure 39. (a) Location and spacing of energy piles and observation wells (b) experimental deck model. Pipes spacing are 20 cm and 30 cm in the left-side and right-side model deck, respectively. (Bowers Jr, 2016)

Table 7. Experimental studies of bridge deck deicing – Secondary Unit

Authors	Snow Melting System							Circulating Fluid
	Deck			Pipe				
	Area (m ²)	Thickness (cm)	Thermal Conductivity W/m/k	Inner Diameter (mm)	Thickness (mm)	Spacing (cm)	Material	
Bowers Jr (2016)	7.2	25.4	3.0	16.0	3.0	20.3 and 30.5	PEX	40% glycol by volume, and water
Balbay and Esen (2010)	2.1	20.0		16.0	2.4	20.0	Polyethylene PX-b	25% glycol by volume, and water
Liu (2005)	112.0	20.3	1.4	25.0	2.0	15.2	High-Density Polyethylene	42% glycol by volume, and water
Yu et al. (2020)	2.2	10.2	1.9	13.0	3.0	15.2	Cross-linked polyethylene (PEX)	water and antifreeze mixture
Ghasemi-Fare et al. (2015)								Water

Table 8. Experimental studies of bridge deck deicing – Primary Unit

Authors	Heat Source				Ambient Temperature
	Ground Source (Energy pile or wells)			Water Tank	
	Depth (m)	Diameter (cm)	Filling Material		
Bowers Jr (2016)	30.5	25.4	Grout		0° C
Balbay and Esen (2010)	30, 60, 90	15.0	Bentonite		7.3° C
Liu (2005)	66.1	13.0	Grout		17.2° C
Yu et al. (2020)				21° C to 40° C	4.3° C to 17.1° C
Ghasemi-Fare et al. (2015)	1.4	10.0	Concrete		19° C

This study demonstrated the effect of pipe spacing on the efficiency of a bridge deck deicing system during a snowstorm. Figure 40 shows the model deck surface during a winter storm for pipe spacing of 30 cm (12 in) (left-side model deck) and 20 cm (8 inch) (right-side model deck). The results showed that there was no snow on the model deck with the pipe spacing of 20 cm (8 inch) (right-side of the model deck), while on the deck with pipe spacing of 30 cm (12 inch) the GSHP system was not able to keep the deck free from snow. In this case, an additional snow removal technique may be needed to keep the bridge deck free from snow and ice. In both cases, the GSHP system maintained the deck temperature above 0°C (32°F).



Figure 40. Photo of the deck model surface during the storm. Heat exchanger pipes have spacing of 30 cm and 20 cm in left-side and right-side model deck, respectively (Bowers Jr, 2016).

Borehole Depth in Primary Unit

Balbay and Esen (2010) evaluated the performance of a GSHP system for snow melting of a pavement slab (PS) and bridge slab (BS) as shown in Figure 41. The experimental system consisted of vertical boreholes with three different depths, two slabs, two circulation pumps, and a heat pump. The ambient air temperature during the test was between -8°C (18°F) and -6°C (21°F). High-density polyethylene pipe with a nominal diameter of 40 mm (1.6 inch) was placed in the boreholes which had a diameter of 150 mm (5.9 inch). The U-loop configuration was utilized for the heat extraction system. The boreholes were filled with bentonite as a grout material. The circulating fluid was 25% water-antifreeze solution, and the designed flow rates were 0.43 L/s (0.11 gal/s), 0.40 L/s (0.1 gal/s), and 0.36 L/s (0.09 gal/s) for borehole depths of 30 m (100 ft), 60 m (197 ft), and 90 m (295 ft), respectively. Figure 41(a) shows a schematic view of the experimental test. The prototype-scale slabs were 1.7 m (5.6 ft) long, 1.2 m (3.9 ft) wide, and 20 cm (7.9 inch) deep. The hydronic system was designed with eight parallel lines of pipes at a spacing of 20 cm (7.9 inch). The slab pipe material was polyethylene with an inner diameter of 16 mm (0.6 inch) and a wall thickness of 2.4 mm (0.09 inch). The flow rate of circulating fluid in the hydronic system was set to 0.056 L/s (0.0148 gal/s). The operation of the system was monitored with several temperature sensors installed in the slabs. The maximum and minimum extracted heat from the ground by the GSHP system were 10.5 kW and 7.91 kW, respectively.

Figure 41 shows the pavement and bridge slabs before (Figure 41(b)) and after 30 minutes (Figure 41(c)) running the GSHP system. The measured air and surface temperatures of the bridge deck and pavement slab for borehole depths of 30 m (100 ft) and 90 m (295 ft) are shown in Figure 42(a) and (b), respectively. Generally, the surface temperatures of the bridge deck and pavement slab increased with borehole depth. During an average ambient air temperature of 7°C (45°F), the average surface temperatures of the bridge deck and pavement slab heated by a 30 m (98.4 ft) deep borehole reached 2°C (35.6°F) and 0.2°C (32.4°F), respectively. For a 90 m (295 ft) deep borehole, the average surface temperatures of the bridge slab and pavement slab reached 3°C (37.4°F) and

0.5°C (32.9°C), respectively. The system maintained slab surface temperatures above 0°C (32 °F) in the winter season in Elazig, Turkey.

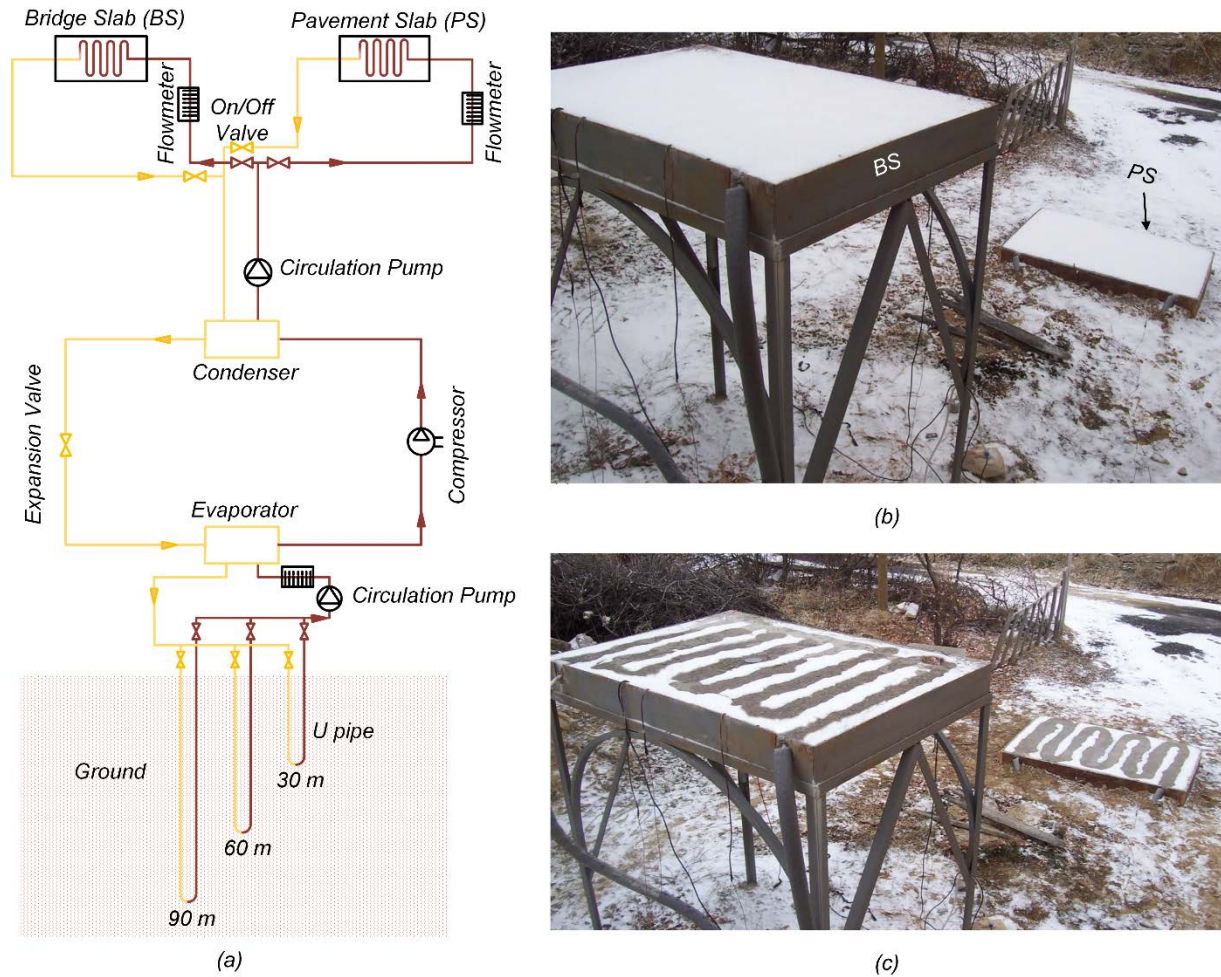


Figure 41. (a) The layout of experimental set-up (b) initial stage of snow melting process (c) after 30 min operation of snow melt system (Balbay & Esen, 2010)

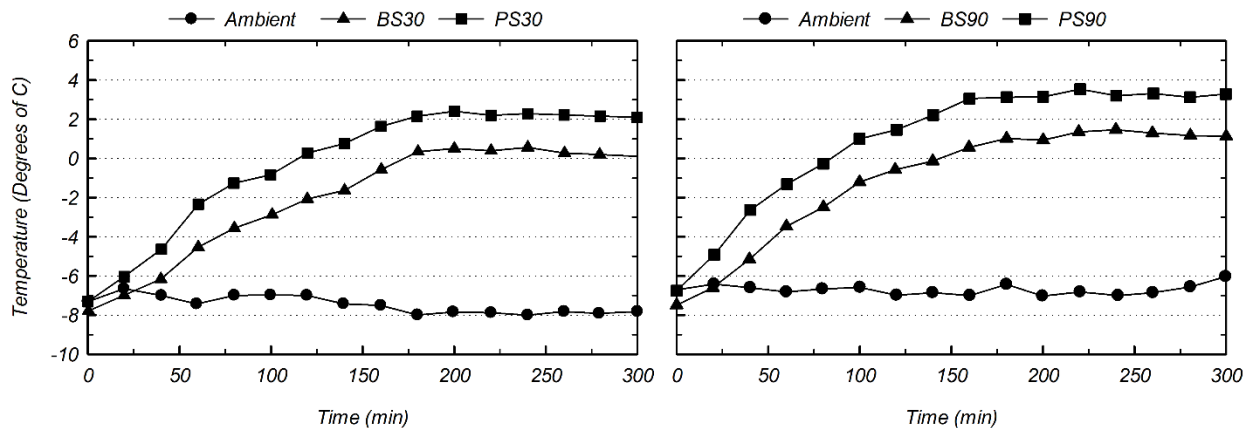


Figure 42. Variation of top surface temperatures of bridge deck and pavement slab, and air temperatures (a) borehole depth 30 m (100 ft) (b) borehole depth 90 m (295 ft)(Balbay & Esen, 2010)

Preheating the deck

A hydronic bridge deicing system was studied experimentally by Liu (2005). The experiment was conducted at Oklahoma State University. The model deck was 18.3 m (60 ft) long and 6.1 m (20 ft) wide. The pipes in the heat distribution system were made of cross-linked polyethylene with an inner diameter of 19 mm (0.75 ft). The circulating fluid was a 39 percent solution of propylene glycol and water. A ground heat pump system was employed to increase the temperature of the circulating fluid. The maximum inlet circulating fluid temperature was 54°C (129°F) during the test. The designed objective of the test was to keep the average deck surface temperature at 4.4°C (39.9°F) when there was a risk of snowfall or ice bonding. Thermistor probes and a flow meter were utilized to monitor the inlet fluid temperature and volume flow rate, respectively. Additionally, the snow-free area ratio has been assessed using images of the bridge surface taken during the test by a digital video system.

Figure 43 shows the bridge surface conditions during the experiment. The recorded average surface temperature during the test is shown in Figure 44. The results of the recorded surface temperature indicated that the deck surface temperature dropped quickly, approximately to 2°C (35.6°F), once snowfall started. Snow accumulated on the bridge deck as snowfall continued. After 3 hours and 38 minutes of heating system operation, the average surface temperature of the bridge deck increased and snow melting began (Figure 43(a)). Thereafter, as shown in Figure 44, the average surface temperature started to increase as the bridge deck surface became free of snow. Then, as deicing continued (Figure 43(b) and (c)), the rate of temperature increase accelerated. The bridge deck surface was free of snow after 8 hours of heating system operation (Figure 43(d)). Thereafter, a model of the transient snow melting process on a heated deck surface was developed and calibrated based on the experimental results. As shown in Figure 44, there was good agreement between the predicted and experimental results. The results of the numerical simulation indicated that preheating the deck 3-5 hours before snowfall with the full heating capacity before snow event can considerably improve the efficiency of the snow melting process. The full heating capacity was obtained based on the surface heat flux requirement as described in the ASHRAE Handbook-HVAC Applications Volume (American Society of Heating & Engineers, 2003).

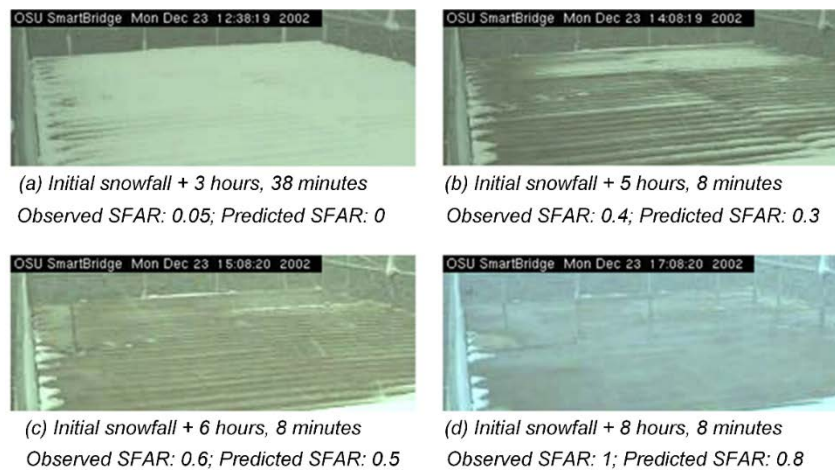


Figure 43. Photo of bridge surface condition during the test (SFAR: Snow Free Area Ratio) (Liu, 2005)

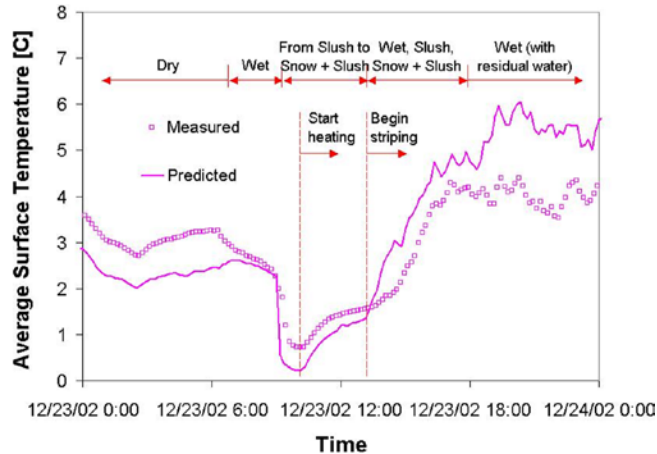


Figure 44. Recorded average surface temperature of the bridge (Liu, 2005)

External Heating Systems

Yu et al. (2020) experimentally investigated the feasibility of an attached, external hydronic heating system for bridge deck deicing. The model bridge deck was 1.83 m (6 ft) long, 1.22 m (4 ft) wide, and 10.16 cm (4 inch) thick. The attached hydronic heating system consisted of 10 parallel lines of cross-linked polyethylene pipes with an inner diameter of 13 mm (0.5 inch), a thickness of 3 mm (0.12 inch), and a spacing of 150 mm (5.9 inch). Geofoam and polyurethane foam were employed for thermal insulation purposes. A water tank with a volume of 95 L (25 gal) connected to a hydraulic pump was utilized to simulate warm fluids provided from a GSHP system. The temperature of the water tank was controlled through heating coils, and the designed temperature range was 21°C (69.8°F) to 40°C (104°F). Figure 45(a) and (b) show the schematic layout of the experimental test and a photo of the laboratory setup, respectively. The ambient air temperature range during the test was 4.3°C (39.7°F) to 17.1°C (62.8°F). In order to monitor the deck temperature, 12 Type-T thermocouples were embedded in the concrete deck. Thermocouples were also installed inside the insulation foam and in inlet and outlet pipes. The inlet fluid flow was measured by a high-pressure flowmeter. The test results showed that the measured temperature of the bridge deck increased gradually with the circulation of warm water. Also, temperature measurement near the outer layer of the geofoam

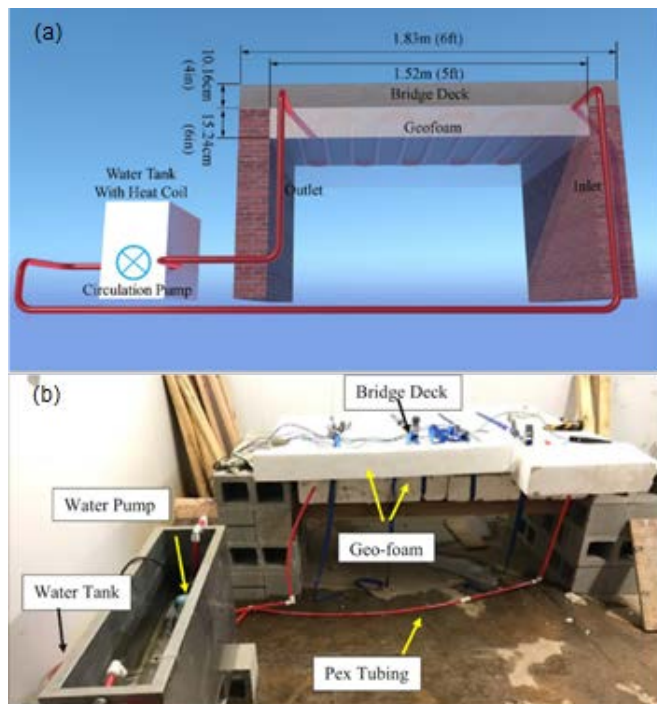


Figure 45. (a) The schematic of experimental set-up (b) laboratory setup (Yu et al., 2020)

showed a value close to the ambient air temperature, indicating the effectiveness of the thermal insulation in reducing heat loss in the system. The measured temperature inside the geofoam dropped quickly as either the heat supply time interval for the system or distance from the heat source increased.

The heat flux analyses showed that the heat flux inside the deck was directly proportional to the difference between the inlet fluid temperature and air temperature. Heat transfer efficiency was shown to depend on thermal conductivity of concrete, thermal insulation and boundary conditions, pipe spacing, void space of geofoam, contact area between pipes and geofoam, and pipe diameter. All test results indicated that approximately 60% of the provided heat was transferred to the bridge deck surface, and the temperature distribution was uniform on the deck surface. The results of this study suggested that an attached hydronic heating system was effective in deicing a bridge deck surface at the range of temperatures studied.

Inlet Flow Rate and Temperature

Ghasemi-Fare et al. (2015) investigated the feasibility of a bridge deck snow melting system using geothermal energy at the Civil Infrastructure Testing and Evaluation Laboratory (CITEL) facility at Pennsylvania State University (PSU). A model-scale energy pile was set up to study the effect of various design parameters, including the inlet flow rate and temperature, on the amount of heat energy extracted from and transferred to the ground (Figure 46). The model concrete pile (diameter 100 mm (4 inch) and length 1.38 m (4.5 ft)) was installed inside a 1.83 m (6 ft) \times 1.83 m (6 ft) \times 2.13 m (7 ft) deep soil bed. A U-loop heat exchanger pipe made of poly-vinyl chloride with an inner diameter of 9.5 mm (0.4 inch) and a wall thickness of 3 mm (0.12 inch) was placed within the pile. A water-reducing concrete admixture at a ratio of 722 ml/m³ was employed to improve the workability of the concrete material of the pile. The slump of the fresh concrete mix was 140 mm (5.5 inch), and the compressive strength of the concrete with the embedded U-shaped pipe was 40.94 MPa (20305 psi). Ninety-four Type-T thermocouples were placed in various locations to monitor the temperature within the soil bed. Figure 46(a) shows the experimental setup and thermocouple data acquisition system. The ambient temperature was kept 19°C during the tests, and the inlet fluid temperatures were 39°C (102°F) and 34°C (93°F) in heating cases and -9°C (16°F) in cooling cases. The linear average flow velocity was varied from 0.11 m/s (0.36 ft/s) to 0.66 m/s (2.16 ft/s).

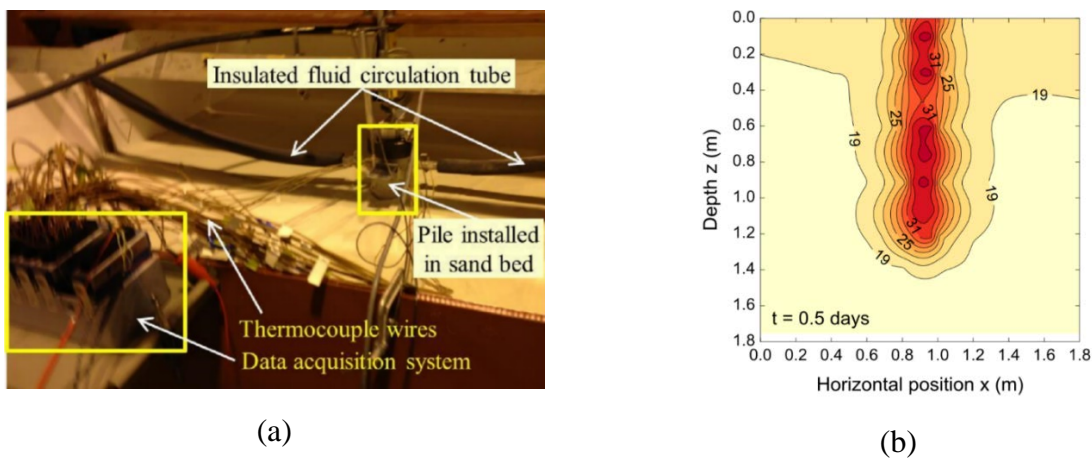


Figure 46. (a) Experimental set up (b) temperature contours after 0.5 day (Ghasemi-Fare et al., 2015)

The temperature contour results showed that the majority of the heat is transferred in the radial direction. Figure 46(b) shows the temperature contours after 12 hours. The thermal influence zone was defined as an important factor in designing the pile group since the thermal efficiency of piles decreases as the thermal influence zones overlap with one another. Additionally, the results indicated that the energy transfer rate increased with increasing the flow rate of the circulating fluid.

Soil Thermal Properties

In a shallow geothermal foundation, heat exchange occurs due to the temperature difference between the pipe network embedded in piles and the surrounding soil. Heat transfer in thermo-active foundations and boreholes occurs primarily by the following heat transfer mechanisms: convective heat transfer due to circulating fluid in the pipes (due to pumping of heat carrier fluid, this mechanism referred to as forced convection), conductive heat transfer across the circulating pipe walls, conductive heat transfer through the pile material (i.e., concrete), and a combination of conductive and convective heat transfer in the soil surrounding the pile/borehole element. Figure 47 shows the primary heat transfer modes between circulating fluid, concrete, and surrounded soil.

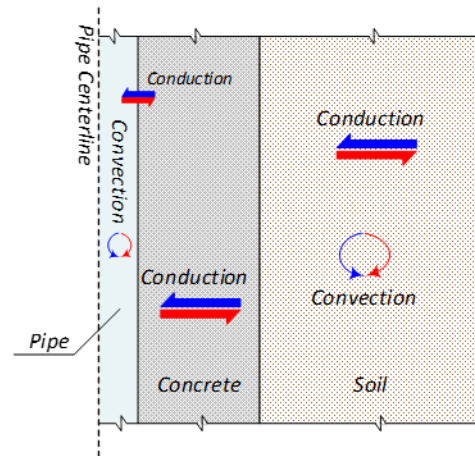


Figure 47. Primary heat transfer mechanisms in a thermo-active foundation with heat exchanger pipe embedded in a concrete pile and surrounded by soil (not to scale) (Atalay, 2019)

Ghasemi-Fare and Basu (2016) used laboratory experiments and finite difference analysis to investigate the performance of geothermal piles with a single U-shaped circulation pipe. Based on their results, the thermal efficiency of a heat exchanger pile (in both long-term and short-term operations) is sensitive to the thermal properties of the surrounding soil. Heat transfer mechanisms in soil are very complicated. Heat transfer in soil consists primarily of three mechanisms: 1) conduction, 2) convection, and 3) radiation. Other mechanisms that are of high importance to heat transfer in soil include: 4) vaporization and condensation, 5) freezing and thawing, and 6) ion exchange (Brandl, 2006). Figure 48 shows the main mechanisms of heat transfer through the soil. The preferred path for heat to transfer through soils is essentially in the solid particles.

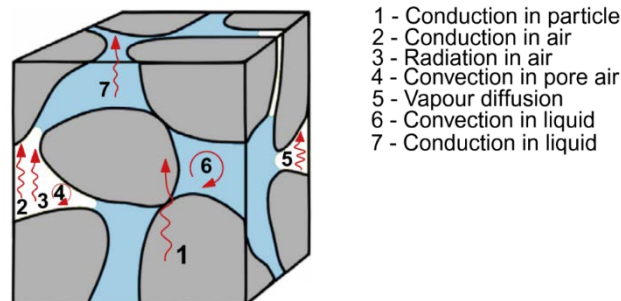


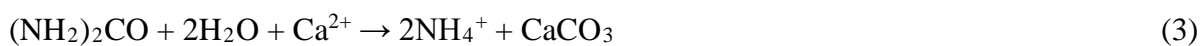
Figure 48. Heat transfer paths in soil (Alrtimi et al., 2016)

Heat transfer by conduction, which is the predominant heat flow mechanism in soil, refers to the flow of heat within solids and fluids (Dawoud et al., 2007). In the convection mechanism, heat transfer occurs through the convection of a fluid and the fluid's bulk motion (Brandl, 2006). Heat transfer by convection can occur by either a natural or forced nature of the flow. In natural convection, the heat largely transfers due to the migration of air and/or water molecules in the soil, which occurs by a difference in density due to temperature change. Forced convection occurs by any external means (i.e., Groundwater flow). Heat transfer by convection is usually negligible in soils with grain sizes smaller than sand (Farouki, 1981). Heat propagation through radiation occurs in pore spaces due to the motion of electromagnetic waves or alternatively by photons. Heat transfer in the soil by radiation is usually negligible, with less than 2% in natural soil (Rees et al., 2000) and up to 10% of total heat transfer in coarse aggregates of 20 mm size (Farouki, 1981). Heat transport by radiation is important only for dry coarse gravel.

One of the objectives of this research is to comprehensively study the effects of bio-cementation on the thermal properties of soil (e.g., thermal conductivity and heat capacity). Heat transfer in the soil varies with grain size, composition, density, and water content of the soil layer. Grain size influences other parameters such as porosity, permeability, fabric, and specific surface area, which also influence the soil's thermal conductivity. Therefore, it is a secondary parameter that should be considered when evaluating the primary parameters (Midttomme & Roaldset, 1998). Other important structural factors influencing the thermal properties of soil are the number and nature of the contacts between the soil particles. Previous studies have indicated that if the soil particles are connected together by bio-cementation, the thermal contact is significantly improved due to precipitation of calcite crystals in the contact areas between the soil particles, and formation of 'thermal bridges' (Venuleo et al., 2016). MICP treatment of sand could lead to a significant increase in soil thermal conductivity by up to 250% (Venuleo et al., 2016).

Effect of Bio-Cementation on Thermal Properties of Soil

Microbes can alter the surrounding chemical environment to induce the precipitation of calcium carbonate, a form of bio-cement (DeJong et al., 2010; Phillips et al., 2013; van Paassen et al., 2010). One mechanism that has been researched extensively is the microbially or plant produced enzyme urease, which promotes the hydrolysis of urea to change saturation conditions, which in the presence of calcium results in the precipitation of calcium carbonate (Cuthbert et al., 2013; Ebigbo et al., 2012; Hommel et al., 2015; Mitchell et al., 2013; Phillips et al., 2016; Phillips et al., 2013). In the presence of urea, the urease enzyme catalyzes the hydrolysis of urea, altering the chemical environment towards favorable saturation conditions for the precipitation of CaCO_3 in the presence of calcium (Equation 3).



In this process, the precipitation of CaCO_3 , often in the stable mineral form of calcite, can serve to bind together porous media including soil particles. Bio-cemented sand treated by MICP has been shown to be effective in reducing soil settlement (DeJong et al., 2006; van Paassen et al., 2010), increasing soil shear strength (Chou et al., 2011; DeJong et al., 2006; Ismail et al., 2002), and improving soil stiffness (Feng & Montoya, 2015; Lin et al., 2016; Montoya & DeJong, 2015).

The MICP treatment primarily affects the average dry density. Precipitation of calcite results in an increase in the solids content and therefore, the average dry density of the soil through the process

of binding particles together at their contacts by calcite bridges (Whiffin et al., 2007). Calcite crystals formed around soil particles also results in a reduction in porosity. As the soil porosity decreases, the number of particle contacts increases. Therefore, the heat path through solid particles with higher thermal conductivity will be enhanced which results in a higher thermal conductivity of the treated soil. As shown in Figure 49, as the number of MICP treatment cycles increases, the amount of calcite formation increases, resulting in a significant enhancement in the thermal conductivity of the soil (up to 120% after four cycles of treatment cycles compared to the untreated sand).

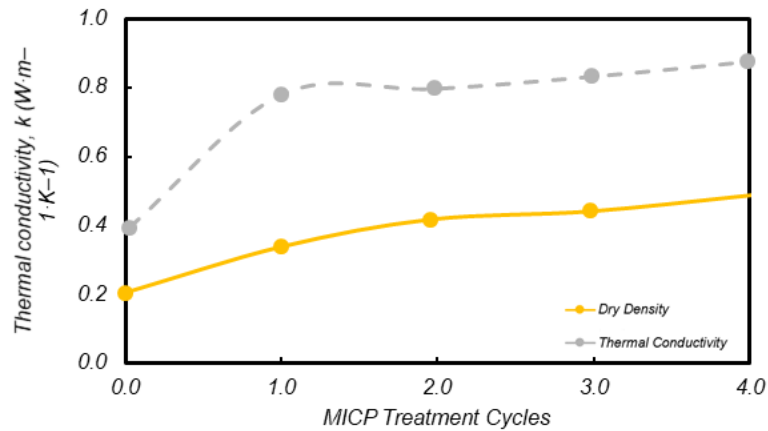


Figure 49. Thermal conductivity and dry density of MICP-treated sand versus MICP treatment cycles (Wang et al, 2019)

Figure 50(a) and (b) presents the variation of thermal conductivity at different degrees of saturation (S), from 0% to 100%, for untreated and bio-treated soil specimens. Thermal conductivity of the water is much higher than air, therefore, as the water content increases, the heat flow in the soil can be enhanced and the soil thermal conductivity increases. Martinez et al. (2019) showed that the thermal conductivity of a dry soil specimen with $S=0$ increased by 860% when the specimen became fully saturated. As shown in Figure 50(a), the effect of water content on the thermal conductivity is most significant at lower degrees of saturation. The increase in thermal conductivity decelerates with an increase in the degree of saturation for both treated and untreated soils. At higher levels of saturation (i.e., capillary and funicular regimes), the particle contacts and presence of water are the governing factors for the increased heat transfer, and small volumes of air have a comparatively insignificant effect on the thermal conductivity of the soil (Likos, 2015).

Figure 50(b) displays the change in the thermal conductivity due to MICP treatment with the degree of saturation (Venuleo et al., 2016). As shown in this figure, the effect of bio-cementation is more pronounced at lower degrees of saturation. It can be seen in Figure 50(b) that improvement in thermal conductivity due to bio-cementation drastically decreases with an increase in degree of saturation. The effect of bio-cementation on the thermal properties of dry soil are more prominent since the thermal conductivity of calcite is much higher than air (around $0.026 \text{ W}\cdot\text{m}^{-1}\cdot\text{K}^{-1}$). In dry sand, the calcite crystals replace the air. Cementation located between the grain particles acted as a highly conductive heat transfer path by increasing the contact area among sand particles. Under dry conditions, bio-cementation could increase the thermal conductivity of the soil by 330%, while the same amount of increase in calcium carbonate led to a 15% increase in thermal conductivity under fully saturated conditions.

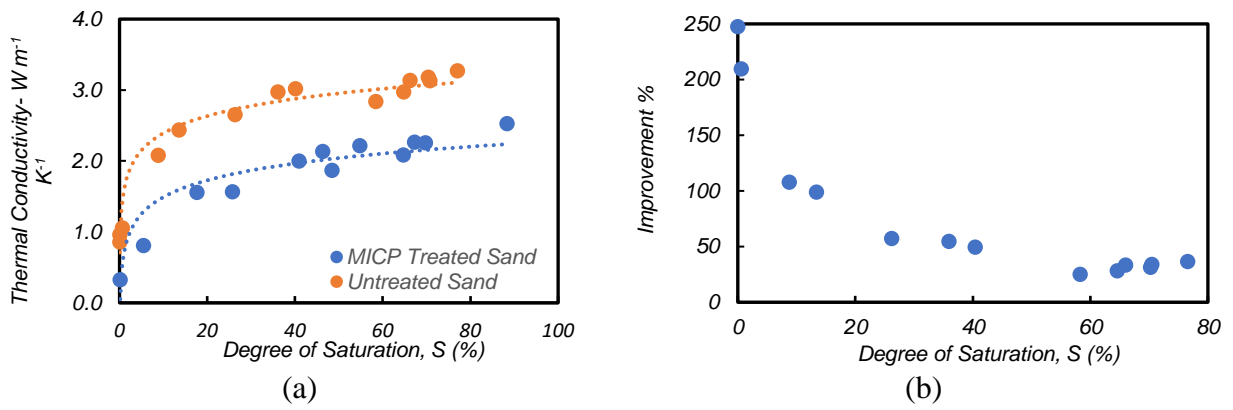


Figure 50. Effect of degree of saturation on (a) thermal conductivity of the MICP-treated and untreated sand (b) improvement in thermal conductivity of the MICP-treated soil (Venuleo et al., 2016)

CHAPTER 6: NUMERICAL MODELING STUDIES ON THE EFFICIENCY OF SHALLOW GEOTHERMAL ENERGY SYSTEMS

Bridge Deck Deicing System

Several numerical modeling studies have been conducted to investigate the energy performance of bridge deck deicing systems. In this section, the key factors that, directly and indirectly, influence the efficiency and performance of the system are highlighted.

Inlet Fluid Temperature and Flow Rate

In this section, the results of previous studies on the effects of inlet fluid temperature and flow rate on the performance of the bridge deck hydronic heating system are discussed. The results include: 1) the average bridge deck surface temperature, 2) the difference between the inlet and outlet fluid temperatures, 3) the time required to heat the deck to above the freezing point of water, and 4) energy consumption. The results indicated that a higher inlet fluid temperature resulted in a higher surface temperature, a higher difference between the inlet and outlet temperatures, and a reduction in the time required to heat the deck to reach 0°C (32°F). A high inlet flow rate has a negligible effect on the performance of a hydronic heating system. However, a low volumetric flow rate could lead to a larger temperature drop and a higher temperature difference on the bridge deck surface, which could cause cracking of the surface. A hydronic heating system with an unnecessarily high inlet fluid temperature and flow rate leads to a higher operating cost. Therefore, the relationship between the inlet fluid temperature and the volumetric flow rate must be defined to achieve a minimum energy consumption.

Balbay and Esen (2013) conducted three-dimensional (3D) finite element modeling using FLUENT computational fluid dynamics (CFD) package program and studied the effect of fluid inlet temperature on the performance of the GSHP system. The effect of inlet fluid temperature on surface temperature distribution was studied numerically by varying the borehole depths. The bridge deck model geometry was the same as the experimental model studied by Balbay and Esen (2010). Figure 51(a) shows the meshed model. The inlet fluid velocity was set at 0.07 m/s, and the outlet pressure was defined as atmospheric pressure. In the modeling procedure, it was assumed that the top boundary was open to ambient air, and the side boundaries were insulated. Additionally, it was assumed that a 1-cm (0.4-inch) thick layer of snow and/or ice was formed on the top surface. The bottom surface and top surface temperatures were set at -7°C (19.4°F) in the initial stage of modeling. The average value of the fluid inlet temperature was 36°C (96.8°C). A sample output from the numerical modeling which illustrates the temperature distribution within the bridge deck model for a borehole depth of 90 m (295 ft) is shown in Figure 51(b). The results of this study showed that: 1) the inlet fluid temperature increases with the depth of the geothermal borehole, and 2) a higher inlet fluid temperature results in an increase in both the average surface temperature and the average temperature difference between the inlet and outlet circulating fluid.

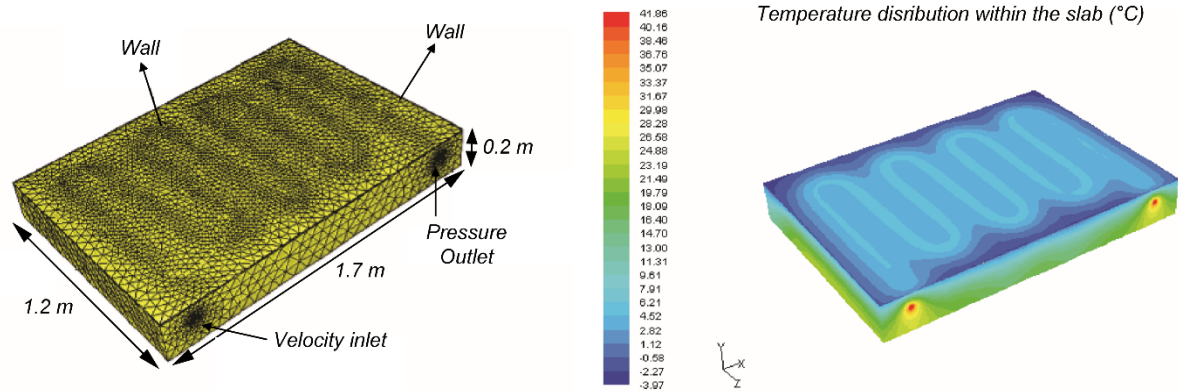


Figure 51. (a) The mesh of deck model (b) distribution of temperature within the bridge deck using boreholes depths of 90 m (295 ft) (Balbay & Esen, 2013)

Chowdhury (2019) developed a 3D numerical simulation using the finite element software COMSOL Multiphysics and studied the influence of inlet fluid temperature on the performance of an externally heated geothermal bridge deck at different weather conditions in the Dallas-Fort Worth area. The geometry of the bridge deck model imitates the experiments conducted by Yu et al. (2020), as presented in the

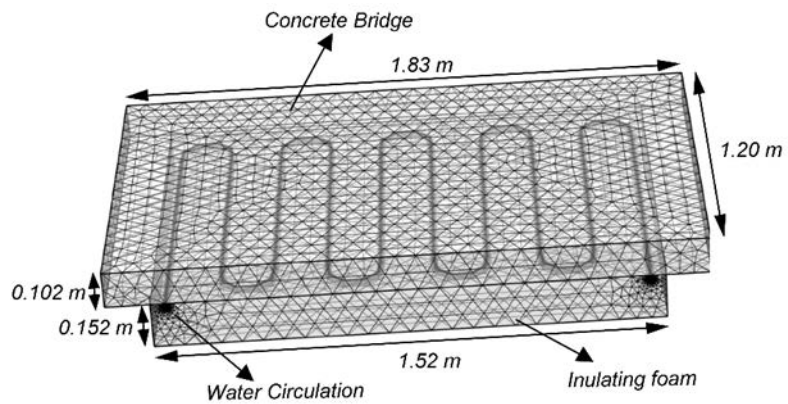


Figure 52. Meshed 3D model (Chowdhury, 2019)

Figure 45 (previous section). Figure 52 shows the meshed model of the bridge deck. The critical model assumption was that the bridge deck was pre-heated during the snowfall, and that no snow had accumulated on the surface. The circulating fluid was water with a flow rate of 7.5 L/min (2 gal/min). The average inlet fluid temperature was maintained around 22°C (71.6°F) during the entire modeling ‘event’. The weather data and wind speed for the extreme weather events from 2014 to 2018 were gathered from National Oceanic and Atmospheric Administrations (NOAA). The model simulation results for the inlet fluid temperatures of 22°C (71.6°F) and 38°C (100.4°F) on the coldest days in 2016, between December 17th and December 20th, are shown in Figure 53 (a) and (b), respectively. The T1 location, shown in the Figure 53, is 1.27 cm (0.5 inch) down from the surface of the deck. The results showed that in an externally heated geothermal deicing system, an inlet fluid temperature higher than 22°C (71.6°F) is required to maintain the deck temperature above freezing (Figure 53(a)). Based on numerical simulation results, an inlet fluid temperature of about 38°C (100.4°F) is needed to keep the surface temperature above freezing in these conditions.

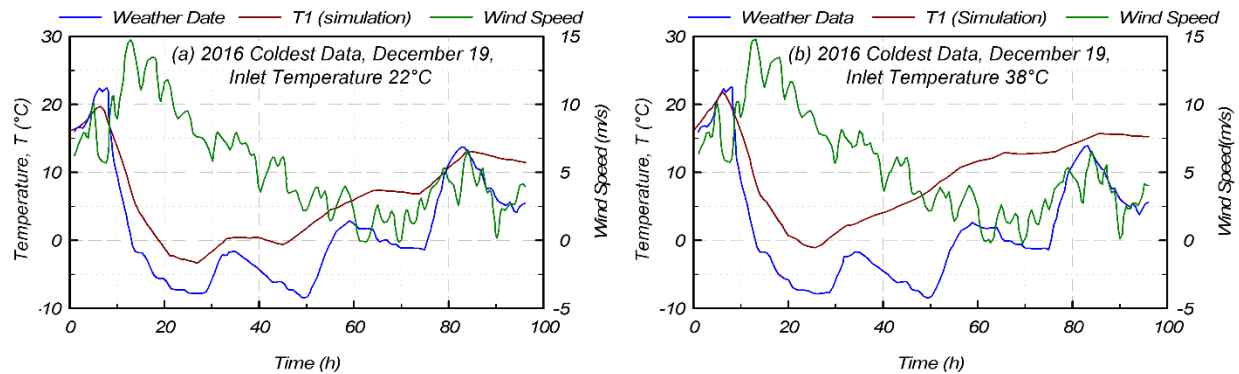


Figure 53. Weather data and numerical model results in the coldest day of 2016, December 19, 2016, for inlet fluid temperatures of (a) 22°C (b) 38°C (Chowdhury, 2019)

Yu et al. (2017) performed a series of 3D numerical simulations using the finite element software COMSOL Multiphysics to investigate the effects of flow rate and inlet fluid temperature on the deicing performance of a bridge deck deicing system. The configuration of the baseline model is shown in Figure 54. The baseline model had dimensions of 3.5 m (11.5 ft) \times (2 times pipe spacing in m) \times 0.25 m (10 inch). The center to center spacing and embedded depth of the pipes in the baseline model were both 20 cm. The circulating fluid, water with 25 % propylene, was circulated in pipes with an inner diameter of 14 mm (0.55 inch) and a wall thickness of 3 mm (0.12 mm). The snow melting process was not considered in this study. It was assumed that the bridge deck was preheated before snowfall and snow accumulation did not occur. The initial temperature of the bridge deck was set at -2°C (28.4°F). The inlet temperature and flow rate of the circulating fluid in the baseline model were 12°C (53.6°F) and 0.6 m/s, respectively. The inlet fluid temperature ranged between 6°C (42.8°F) and 20°C (68°F) and the flow rate varied between 0.3 (1 ft/s) and 1.5 m/s (4.9 ft/s). Figure 55 and Figure 56 show the effects of inlet fluid temperature (Figure 55) and flow rate (Figure 56) on the average deck surface temperature and the required time for the deck surface to reach a temperature above freezing point. The results indicated that the surface temperature increased with the inlet fluid temperature, while the time required for the deck surface to reach a temperature above the freezing point decreased with the inlet fluid temperature. The effect of flow rate on the average deck surface temperature was found to be negligible compared to the effect of inlet temperature, but the required time for the deck surface to reach a temperature above freezing point did decrease with the flow rate.

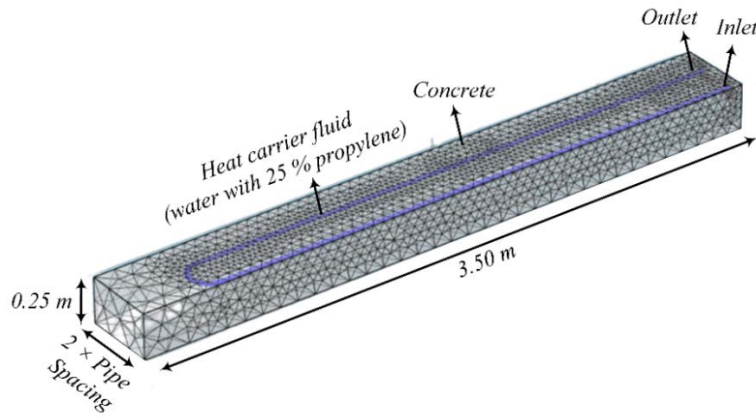


Figure 54. Numerical baseline model configuration of the bridge deck (Yu et al., 2017)

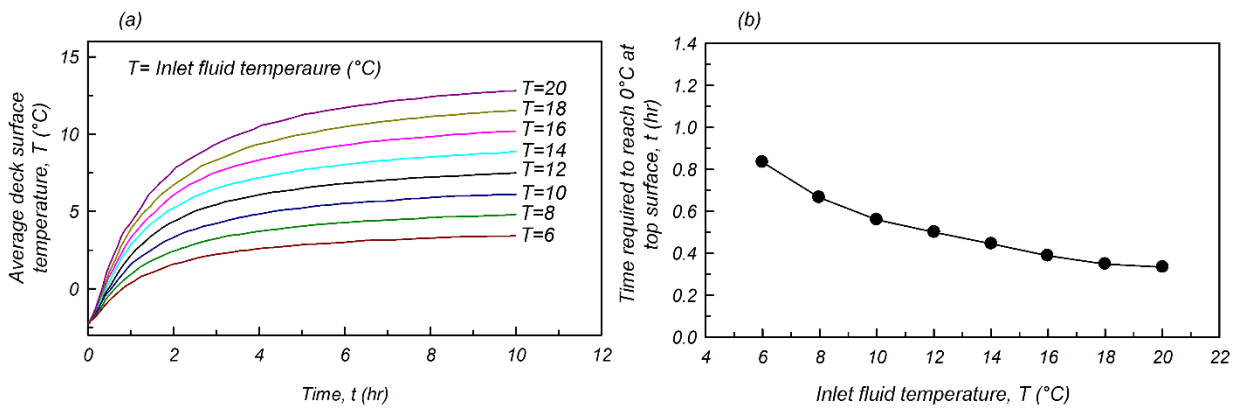


Figure 55. Effect of inlet fluid temperature on (a) average deck surface temperature (b) time required to reach above-freezing point (Yu et al., 2017)

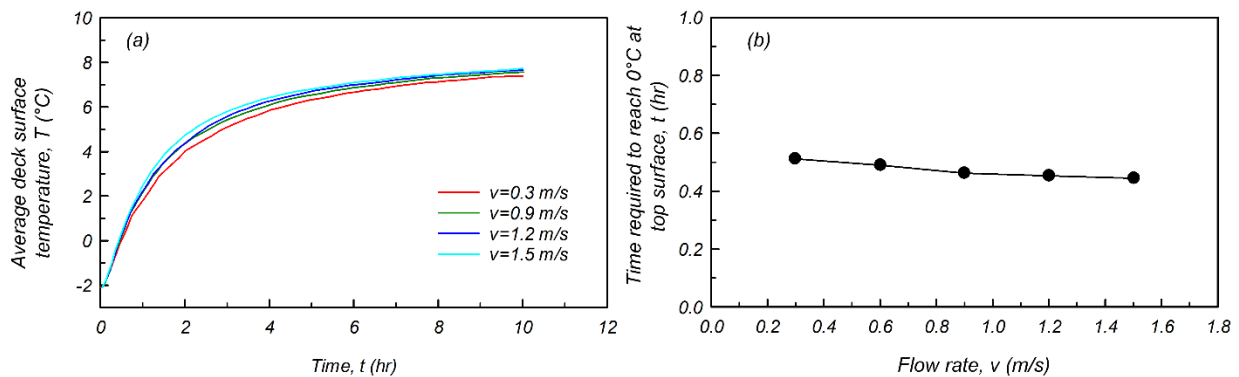


Figure 56. Effect of flow rate on (a) average deck surface temperature (b) time required to reach above-freezing point (Yu et al., 2017)

Feng and Yin (2019) performed 3D numerical simulation of fluid flow and heat transfer in a bridge deck using ANSYS with thermal-fluid hydraulic coupling method to investigate the performance of a bridge deck deicing system. The thermal-fluid coupling method allows for fluid temperature variation along the pipes. Figure 57 shows the numerical model configuration. The side boundaries

of the bridge deck model were adiabatic boundaries. The adiabatic conditions refer to conditions in which no heat flow is allowed across the boundaries. The inlet fluid temperature was 15°C (59°F), and the flow velocity changed from 0.6 m/s (2 ft/s) to 2 m/s (6.6 ft/s).

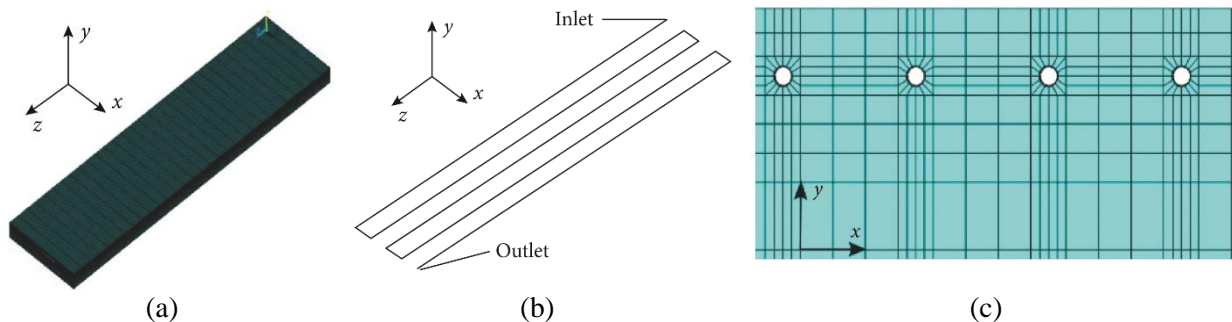


Figure 57. 3D Finite Element model meshing for: (a) whole model, (b) serpentine pipes, and (c) pipes and surrounding concrete (Feng & Yin, 2019)

The time histories of the deck surface temperature for varying inlet fluid temperature are shown in Figure 58. The results indicated that the surface temperature slightly changed with flow rate, suggesting that the effect of flow rate on the surface temperature is negligible. An increase in the flow rate of the circulating fluid, therefore, does not have a significant effect on the heat transfer efficiency of the system.

Ho et al. (2019) investigated the effect of inlet fluid temperature and flow rate on the performance of a hydronic heating system in the extreme continental climate of western and central North Dakota. COMSOL Multiphysics software was used in this study. The average ambient temperature in the winter was -12.4°C (9.7°F). Therefore, North Dakota has higher heat demand in winter compared to the other areas in the United States (Ho & Dickson, 2017). The concrete panel model dimension is 7.31 m (24 ft) × 7.16 m (23.5 ft) × 0.61 m (2 ft). The horizontal spacing and embedded depth of the pipes are 15.2 cm (6 in) and 7.6 cm (3 in), respectively. The side wall boundary conditions of the model were insulated, while heat flow was allowed from the top and bottom boundaries. Heat transfer between the circulating fluid and pipe wall and heat exchange between the pipe wall and concrete were coupled. Additionally, the snow melting process was considered in the model. The inlet fluid temperature ranged from -30°C (86°F) to 60°C (140°F). The ambient temperature range was between -25°C (-13°F) to -5°C (23°F), and the flow rates of fluid varied between 0.0002 m³/s (0.007 ft³/s) to 0.001 m³/s (0.035 ft³/s).

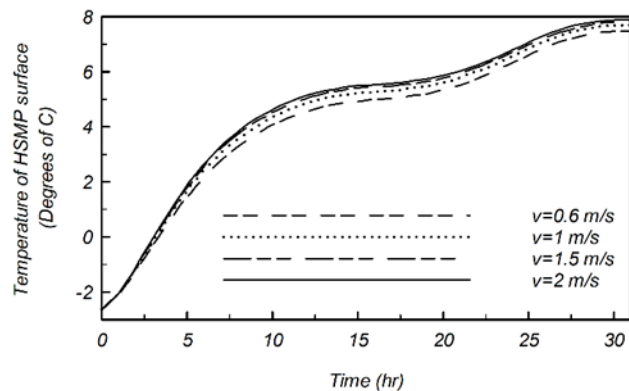


Figure 58. Surface temperature with variation of inlet flow rate (Feng & Yin, 2019)

Figure 59 shows the surface temperature distribution and circulating fluid temperature variation for a fluid inlet temperature of 30°C (86°F), an ambient temperature of -25°C (-13°F), and a flow rate of 0.21 l/s (0.05 gal/s). As shown in Figure 59(a), the pavement surface temperature rarely

went above the freezing point, and the results in Figure 59(b) indicated that there was a considerable temperature difference between the inlet and outlet fluid temperatures. Figure 60(a) shows the effect of inlet fluid temperature on the pavement surface temperature at an ambient air temperature of -25°C (-13°F). Based on the results, an inlet fluid temperature of 60°C (140°F) kept the surface temperature above zero regardless of the volumetric flow rate. For an inlet fluid temperature of 30°C (86°F), the maximum temperatures of the heated pavement were between 3.2°C (38°F) and -1.4°C (29.5°F), depending on the fluid flow rate. The results indicated that both inlet fluid temperature and flow rate were highly dependent on the ambient temperature. For an ambient temperature of -25°C (-13°F), the pavement surface temperature rarely went above 0°C (32°F) for an inlet flow rate higher than $0.0005\text{ m}^3/\text{s}$. Figure 60(b) illustrates that a higher flow rate resulted in a higher surface temperature, while a low volumetric flow rate led to a larger temperature difference on the pavement surface. Non-uniform temperature distribution on the surface could induce an uneven stress distribution along the surface and result in cracking of the surface.

Pipe Spacing and Embedded Depth

The pipe embedded depth is the distance from the pipes to the deck surface, and the pipe spacing is the horizontal distance between two adjacent pipes. These two design parameters can significantly influence the heat transfer through the bridge deck, and thus the performance of the hydronic heating/cooling system. The results of previous studies showed that a wider pipe spacing and a greater pipe embedded depth led to a lower average surface temperature and a longer time required to heat the top of a bridge deck surface to above freezing.

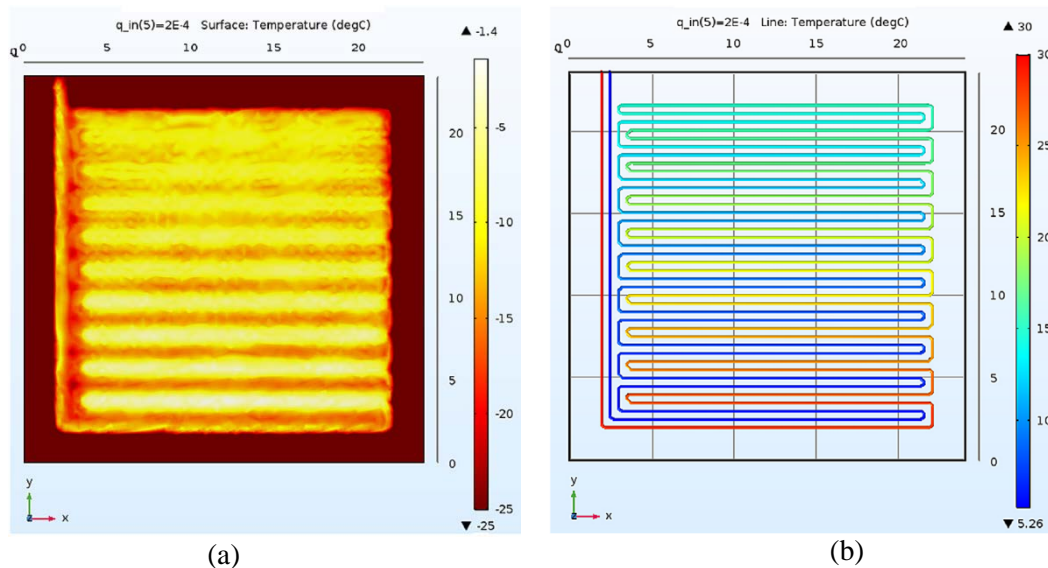


Figure 59. Contours of (a) surface temperature of heated deck (b) circulating fluid temperature variation, inlet fluid temperature 30°C (86°F), ambient temperature of -25°C (-13°F), and flow rate of 0.21 l/s (0.05 gal/s) (Ho et al., 2019)

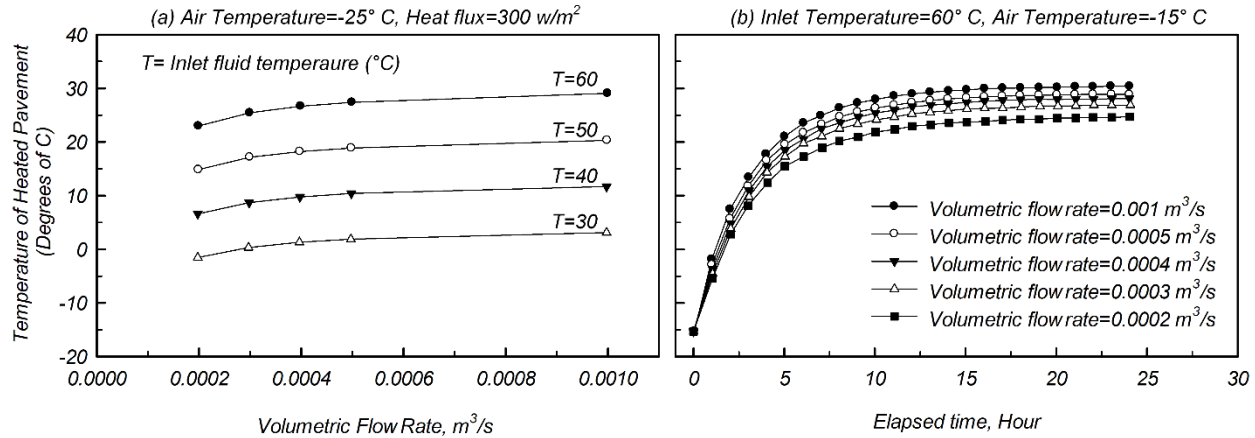


Figure 60. Temperature of heated pavement versus volumetric flow rate for ambient temperature of (a) -25°C (-13°F) (b) -15°C (5°F)(Ho et al., 2019)

Feng and Yin (2019) investigated numerically the effect of pipe embedded depth and pipe spacing on the performance of a bridge deck snow melting system. Figure 61(a) shows the surface temperature distribution after 4.25 hours of heating for a pipe spacing of 15 cm (5.9 inch) and three different embedded depths of 9 (3.5 inch), 10 (3.9 inch), and 11 cm (4.3 inch). As shown in this figure, as the pipe embedded depth increased, more time was required for energy to transfer to the surface and heat it up. Figure 61(b) shows the temperature distribution along the surface of the bridge deck with a pipe embedded depth of 11 cm (4.3 inch) and pipe spacing of 10 cm (3.9 inch), 15 cm (5.9 inch), and 20 cm (7.9 inch). The surface temperature decreased as the pipe spacing increased. An increase in pipe spacing from 10 cm (3.9 inch) to 20 cm (7.9 inch) resulted in a 1.4°C (34.5°F) to 1.7°C (35°F) reduction in the maximum surface temperature. As shown in Figure 50, the wider the pipe spacing, the steeper the temperature curve.

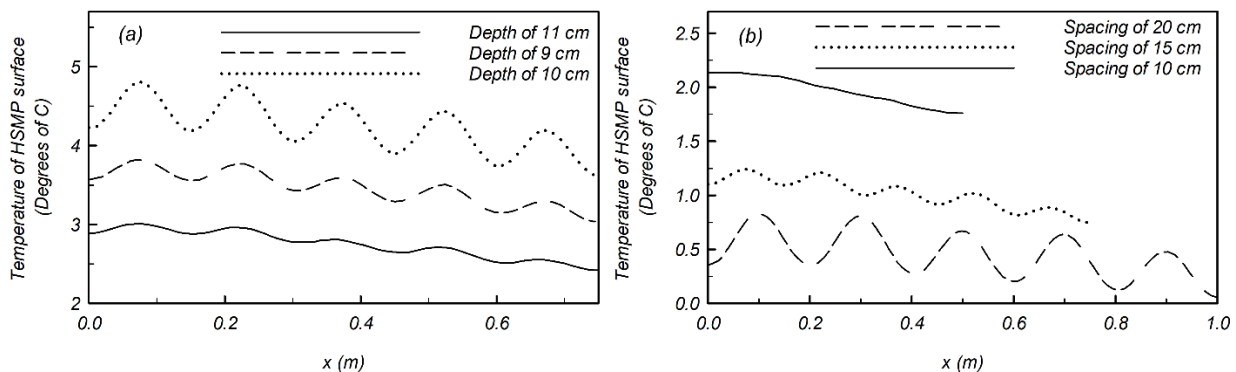


Figure 61. Comparison of surface temperature difference with (a) different pipe embedded depth in terms of pipe spacing of 15 cm (b) different pipe spacing in terms of pipe embedded depth of 15 cm (5.9 inch) (Feng & Yin, 2019)

Bowers Jr (2016) used 3D finite element modeling of a shallow geothermal energy bridge deck deicing system and investigated the performance for different geometric configurations. COMSOL Multiphysics software was used in this study. The bridge deck dimension was 3.7 m (12.1 ft) × (4 times pipe spacing in m) × 25.4 cm (10 inch). The embedded depth of heat exchanger pipes and pipe spacing in the baseline numerical model was 7.45 cm (2.9 inch) and 20 cm (7.9 inch), respectively. Figure 62 shows the model geometry as well as the meshed model. The inlet fluid

temperature in the baseline model was 12°C (53.6°F). The analyses were repeated for four pipe spacing cases of 15 cm (5.9 inch), 20 cm (7.9 inch), 25 cm (10 inch), and 30 cm (12 inch). The side wall boundary conditions of the bridge deck model were insulated, and heat flow was allowed from the top and bottom sides. The contours of average surface temperature for various pipe spacing cases is shown in Figure 63. The average surface temperature, and the required time for attaining surface temperature above the freezing point increased as the pipe spacing and thus the heated surface area around the pipes decreased. The released energy per unit pipe length in a model with 15 cm (5.9 inch) pipe spacing was more than those in models with 25 cm (10 inch) and 30 cm (12 inch) pipe spacing. When the pipe spacing was wider, more time was required for the heat energy to transfer to the midpoint of two pipes. The results of the numerical simulations showed that the surface area above the pipes gets heated up faster than the surface area between the pipes. The model with a wider pipe spacing has a more deck volume to heat per length of the pipe than those with a closer pipe spacing. The energy loss in a model with a wider pipe spacing, however, is less than those with a narrower one. Based on the results of this study, a GSHP system with wider pipe spacing is slightly more efficient.

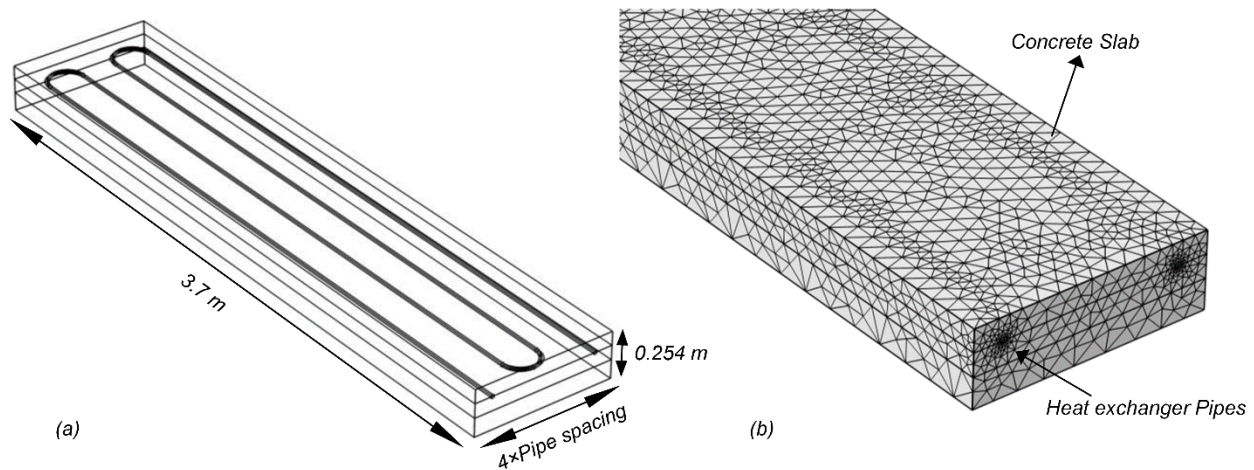


Figure 62. (a) Numerical baseline model configuration, (b) Numerical modeling mesh (Bowers Jr, 2016)

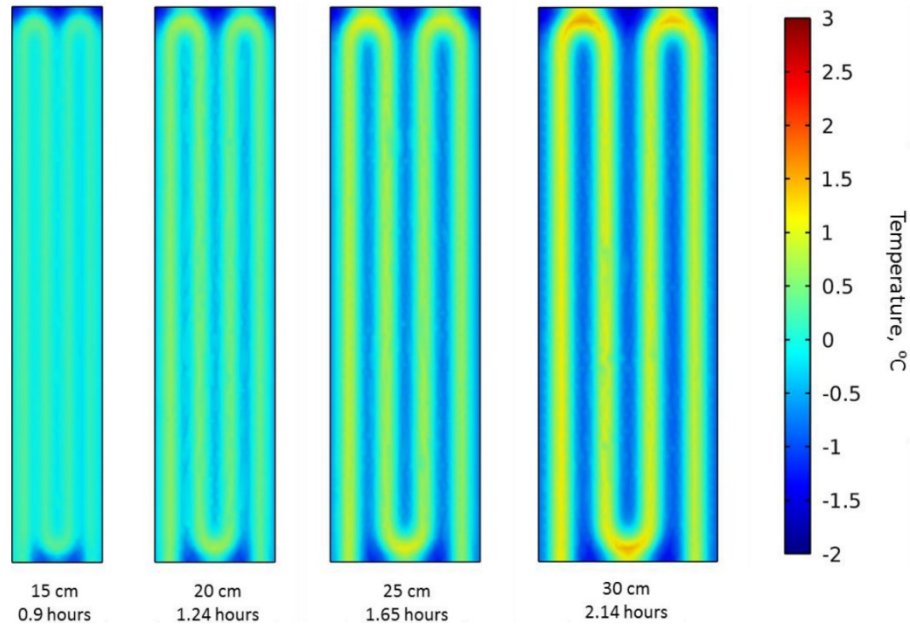


Figure 63. Contours of deck surface temperature for different pipe spacing when the average surface temperature reached above freezing point (Bowers Jr, 2016)

A parametric study by Yu et al. (2017) investigated the effect of pipe embedded depth on the behavior of the bridge deck deicing system and found the pipe embedded depth a critical factor in the design of a geothermal heated bridge deck system. As previously shown in Figure 54, the pipe spacing was 20 cm (7.9 inch) in the baseline model, and the pipe embedded depth ranged between 4 cm (1.6 inch) to 12 cm (4.7 inch). The circulating fluid with a 12°C (53.6°F) inlet temperature was circulated at the flow rate of 0.6 m/s. The ambient temperature was -2°C (28.4°F), and wind was not considered for this investigation. Figure 64(a) shows the average deck surface temperature versus time for varying pipe embedded depths. The average surface temperature decreased as the pipe embedded depth, and thus the distance between the heat source and the bridge deck surface, increased. In contrast, as shown in Figure 64(b), the time required to reach above the freezing point at the top of the bridge deck surface increased significantly with the pipe embedded depth.

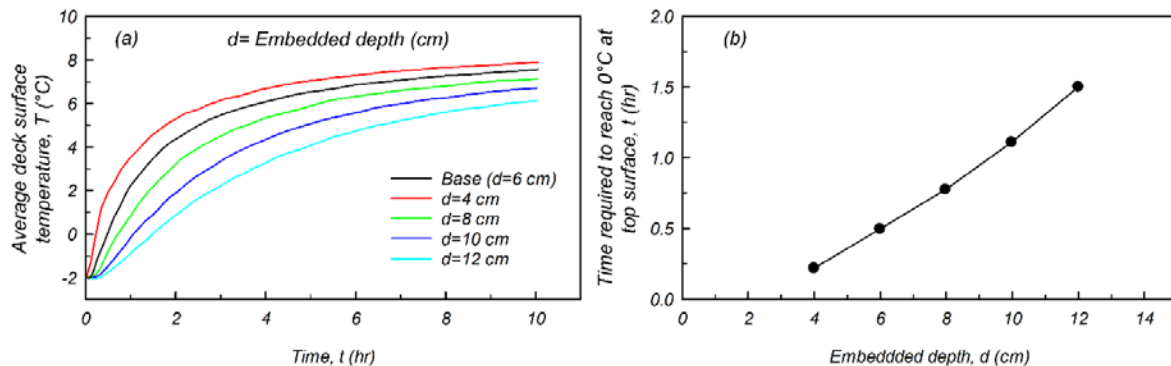


Figure 64. (a) Average deck surface temperature, and (b) time required to reach above-freezing point at top surface of bridge deck (Yu et al., 2017)

Weather Condition (Snowfall Rate, Wind Speed, and Ambient Temperature)

Bowers Jr (2016) compared the performance of a baseline shallow geothermal energy bridge deck deicing system at different air temperatures ranging from -10°C (14°F) to -0.5°C (31°F). Figure 65(a) displays results for variations of the average surface temperature and area of deck surface above 0°C (32°F) over time with ambient air temperature. Based on the results, lower ambient temperatures required a longer time to heat the deck surface above 0°C (32°F). At ambient air temperatures as low as 10°C (50°F), the deck attained a surface temperature above 0°C (32°F) after 4 hours, whereas very little time was required to heat the deck at higher ambient temperatures. The cumulative amount of energy added to the deck in relation to the baseline model is shown in Figure 65(b) for different ambient temperatures. The results also indicated that a reduction in the ambient temperature resulted in an increase in the amount of energy injected to the deck surface. Based on the results, the lower the ambient temperature, the higher is the amount of energy devoted to deck heating and lost to the environment.

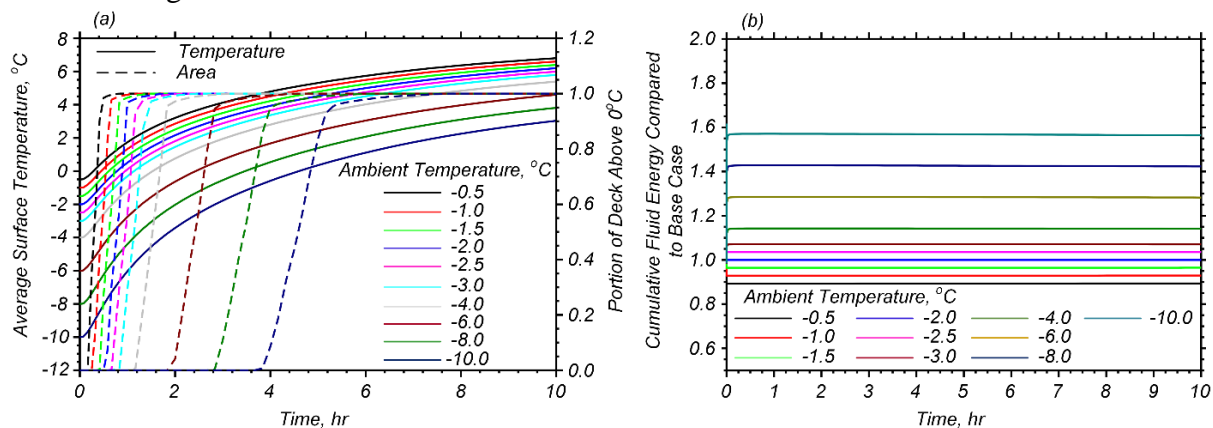


Figure 65. (a) Average deck surface temperature and area of deck surface above 0°C (32°F) for different ambient temperatures (b) Distribution of injected energy to the deck and lost energy for different air temperatures (Bowers Jr, 2016)

Bowers Jr (2016) studied the effect of wind speed on the performance of a bridge deck deicing system. The average deck surface temperature and area of deck surface above 0°C (32°F) for different wind speeds ranging from 2 m/s (6.6 ft/s) to 20 m/s (65.6 ft/s) are shown in Figure 66(a). At higher wind speeds, the average surface temperature decreased and it took longer for the deck to heat the surface above 0°C (32°F). Distribution of added energy used to heat the deck and the amount of energy lost to the environment for different wind speeds are shown in Figure 66(b). The higher the wind speed, the greater the amount of energy lost to the environment. At a wind speed of 20 m/s (65.6 ft/s), more than 75 % of the energy is lost to the environment, which is 50% less than the energy lost at a wind speed of 2 m/s (6.6 ft/s). At wind speeds higher than 15 m/s (49 ft/s), over 90% of the energy was lost due to convection rather than radiation, while for a wind speed as low as 2 m/s (6.6 ft/s), over 70% of the energy lost was from convection.

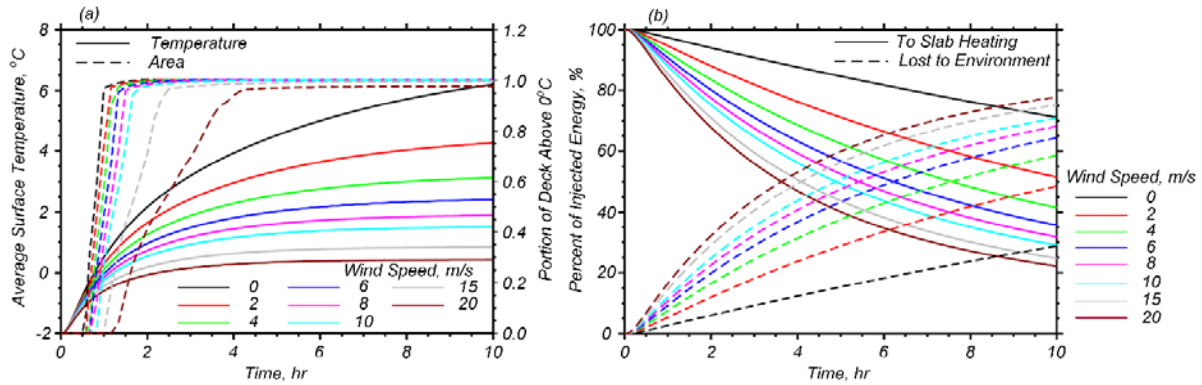


Figure 66. (a) Average deck surface temperature and area of deck surface above 0°C (32°F) for different wind speeds (b) Distribution of injected energy to the deck and lost energy for different wind speeds (Bowers Jr, 2016)

Yu et al. (2017) studied the effect of wind speed on the bridge deck heating process. The wind speeds varied between 1 m/s (3.3 ft/s) to 6 m/s (20 ft/s). The effect of wind speed on the average surface temperature and the time required to reach above 0°C (32°F) at the bridge deck surface are shown in Figure 67(a) and (b), respectively. The results indicated that the average surface temperature decreased as the wind speed increased. In contrast, the time required for the deck surface to reach above 0°C (32°F) increased with the wind speed. The effect of wind speed on the average surface temperature was found to be more significant when the wind speed exceeded 2 m/s (6.6 ft/s), while it was negligible at wind speeds lower than 2 m/s (6.6 ft/s). At a wind speed of 4 m/s (13.1 ft/s) or higher, the effect of wind speed on the average surface temperature was less significant.

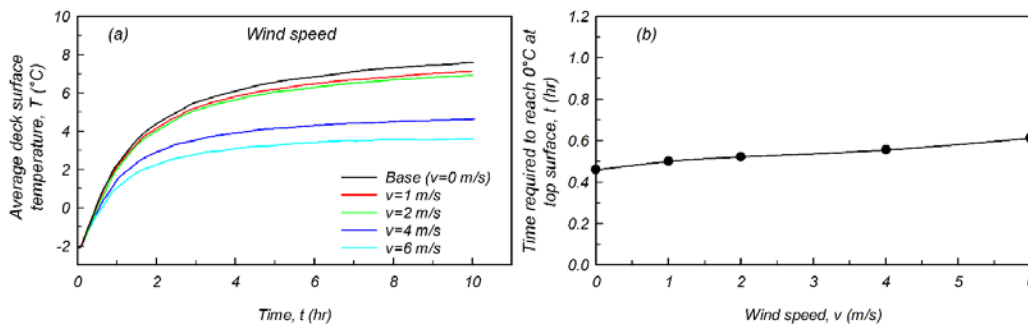


Figure 67. (a) Average deck surface temperature (b) time required to reach above-freezing point at bridge deck surface (Yu et al., 2017)

Bowers Jr (2016) studied the performance of a bridge deck deicing system at three different snowfall rates of 2 cm/hr (0.79 inch/hr) (mild condition), 5 cm/hr (1.97 inch/hr) (moderate condition), and 10 cm/hr (3.94 inch/hr) (severe condition). Figure 68(a) displays the average deck surface temperature for different snowfall rates. The results indicated that the rate of surface temperature decrease during a snowfall depended on the snowfall rate. The higher the snowfall rate, the more the surface temperature decreased. As shown in Figure 57 (a), after an initial decrease, the surface temperature increased. The deck heating flux per surface area for different snowfall rates is compared in Figure 68(b). Deck heating flux is defined as the rate at which energy

was transferred to the deck per unit surface area. As shown in Figure 68(b), higher rates of snowfall demanded higher deck heating fluxes.

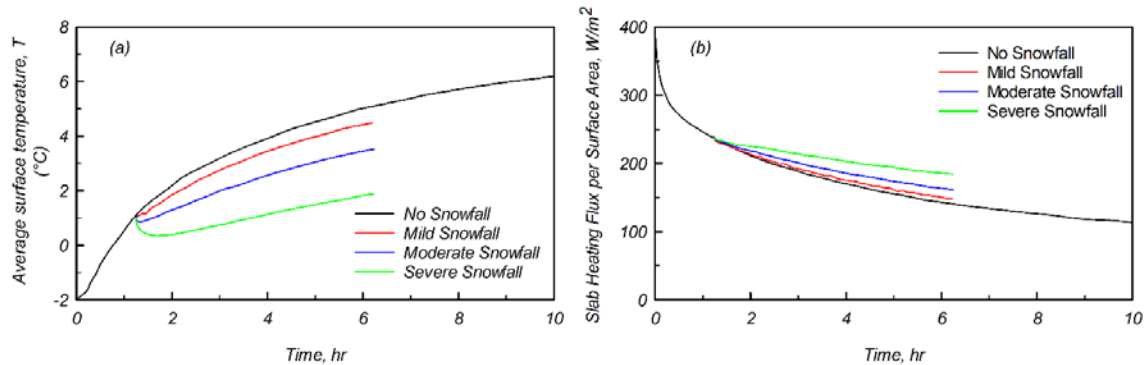


Figure 68. (a) Average deck surface temperature with different snowfall rate (b) deck heating flux per surface area for different snowfall rates (Bowers Jr, 2016)

Liu et al. (2019) performed a sensitivity analysis and investigated the impact of snowfall rate on the optimum design of a hydronic snow melting system. In this study, the length, width, and thickness of the deck model were 4 m (13 ft), 7 m (23 ft), and 0.2 m (8 inch), respectively. The horizontal pipe spacing was 5 cm (2 inch) and the pipes were placed 20 cm (8 inch) below the surface. Figure 69(a) shows the 3D numerical model configuration. Inlet fluid temperature and flow rate were selected using the Nelder-Mead algorithm to minimize the energy employed for snow melting. The flow rate of the circulating fluid was 1 m/s (3.3 ft/s) and the hourly inlet temperature corresponding to the optimum design was selected. The bottom and side boundaries of the model were insulated (no heat flow), and a complete energy balance was used for the calculation of the required heat flux. Considering that the energy balance at the deck surface depended on different climate related factors including snowfall rate, ambient temperature, and wind speed, two different snowfall rates were considered in this study: 1) a base case with a snowfall rate of 0.3 cm/h (0.12 inch/h) and 2) a case with a snowfall rate of 0.39 cm/h (0.15 inch/h) (30% increase from base case). Figure 69(b) shows a comparison of accumulated energy consumption for two snowfall rates. The results indicated that a 30% increase in snowfall rate from 0.3 cm/h (0.12 inch/h) to 0.39 cm/h (0.15 inch/h) resulted in an increase in energy consumption of 35%. The results imply that the heat energy that snow required during a phase change was considerably higher in the snow melting system. Therefore, the snowfall rate is a key factor in designing a hydronic heating system for snow melting purposes.

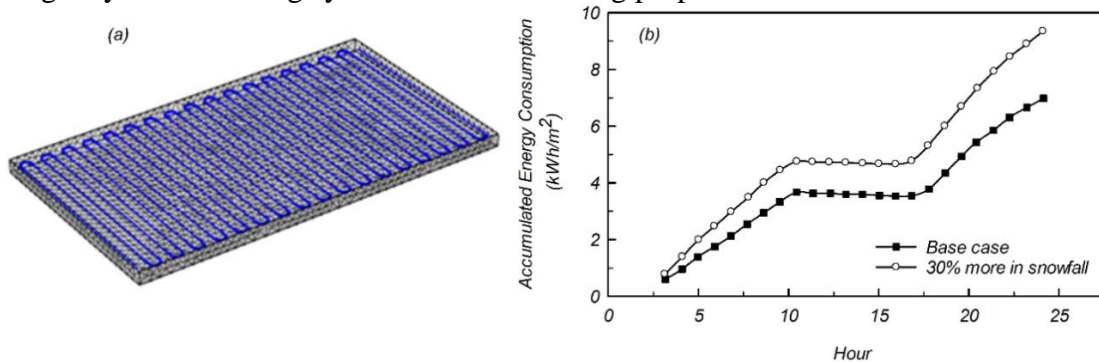


Figure 69. (a) Mesh of bridge deck model and snow melting system (b) accumulated energy consumption with various snowfall rate (Liu et al., 2019)

Ghasemi-Fare and Basu (2016) used finite difference analysis to investigate the thermal performance of geothermal piles with a single U-shaped circulation pipe. Figure 70 shows the effects of key parameters on the efficiency of geothermal piles after 12 hours and 60 days of operation. Based on their analyses, the capacity of a hydronic heated system to melt snow and ice depended on: 1) the initial temperature difference, θ ($\theta = T_{\text{inlet}} - T_{\text{initial}}$), 2) the thermal properties of soil, k_s , and concrete, k_c , and 3) design parameters of the circulation system (e.g., radius of circulation pipe, r_t , pipe depth, and pipe spacing). Their study showed that the efficiency of the de-ice bridge system increases as fluid temperature and concrete thermal conductivity increase. Greater pipe embedded depth and wider pipe spacing are not desirable for the efficiency of system (Ghasemi-Fare & Basu, 2016). As shown in Figure 70, the long-term thermal efficiency of a heat exchanger pile was most sensitive to soil thermal properties, while the short-term efficiency was most sensitive to the radius of the circulation pipe. It was also concluded that ambient air temperature, the temperature difference between the ground and fluid circulated to the ground, and groundwater level highly affected the efficiency of GSHP systems. For some areas in Montana where the groundwater level is close to the surface, the GSHP system is expected to be more efficient.

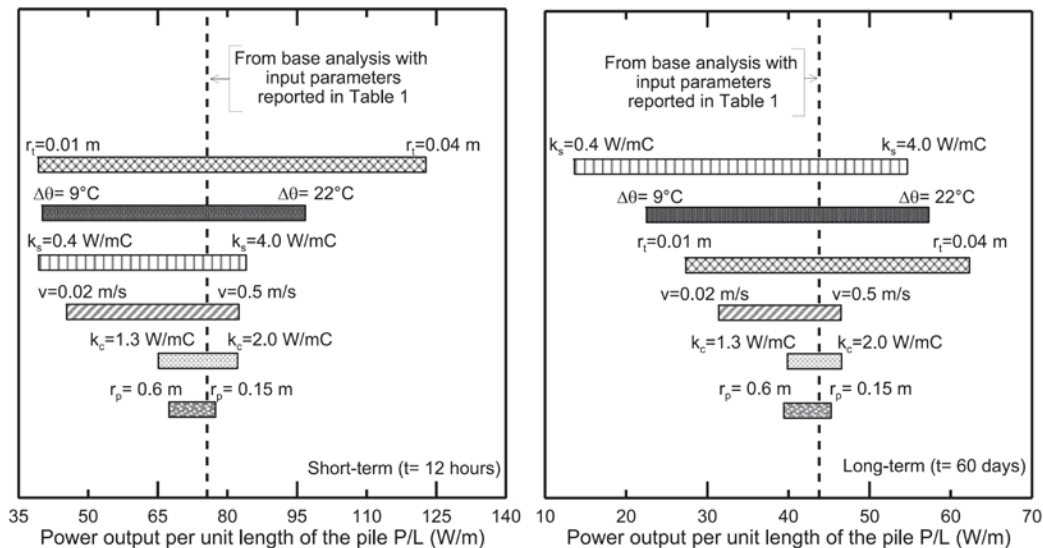


Figure 70. Effects of key parameters on the efficiency of a geothermal piles after 12 hrs and 60 days of operation (Ghasemi-Fare & Basu, 2016)

Optimization of Heat Extraction/Injection in Primary Unit

One of the main challenges in the design and operation of GSHP systems is the change of ground temperature over its lifetime due to heat extraction and injection from and to the ground. The configuration of the heat injection/extraction system can influence the in-situ ground temperature over time and thus the system performance. Several studies have investigated selective utilization of energy piles and wells within a typical grid to minimize the amount of energy lost to the ground and maximize heat pump performance. The findings from previous studies are evaluated in this section to understand the thermal impact of geometric arrangement and operation mode on GSHP systems with multiple energy piles or wells.

Optimization of energy extraction has been studied by de Paly et al. (2012), Beck et al. (2013), and Bowers Jr and Olgun (2020). Bowers Jr and Olgun (2020) developed a numerical model using COMSOL Multiphysics™ of vertical heat exchangers to investigate different heat injection and extraction scenarios and the effects on shallow geothermal energy (SGE) system efficiency. The model was based on the approach developed and calibrated by Ozudogru et al. (2015). The model included the entire borehole-soil system and utilized several components including: fluid circulation pipes, a 1-dimensional line element through the middle of the fluid circulation pipes, the thermal grout, and the soil surrounding the energy pile. To decrease the computational time, they utilized two main simplifications for modeling fluid flow, symmetry, and domain discretization. A 6×6 grid of energy piles with a diameter of 15 cm (5.9 inch) and a center-to-center distance of 8 m (26 ft) was modeled. Figure 71(a) shows the numerical model geometry. Quadrilateral symmetry with zero heat flux at the symmetry boundaries was used in the model to reduce computational effort. A constant temperature equal to the initial ground temperature was assigned to the outer boundaries of the model. A single U-shaped heat exchanger pipe with an inner diameter of 3.4 cm (1.34 inch) and a wall thickness of 3.8 mm (0.15 inch) was modeled inside each energy pile. The meshed area around the geothermal boreholes is shown in Figure 71(b).

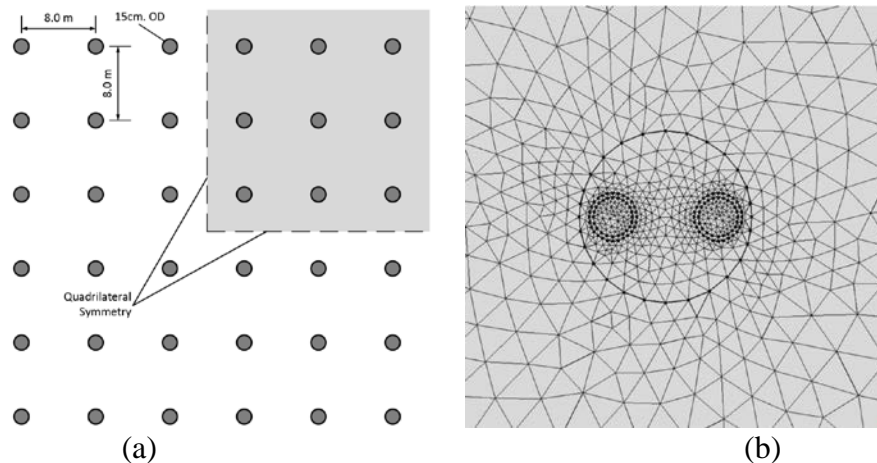


Figure 71. (a) Grid arrangement of boreholes (b) the Meshing of the pile and heat exchanger pipes (Bowers Jr & Olgun, 2020)

The results of this study suggested the arrangement of the geothermal piles affects the amount of energy lost within the system and, thus, the long-term efficiency of the system. As shown in Figure 72, the energy piles in the grid were divided into the three groups (inner, middle, and outer) and different heat extraction and injection scenarios were studied. In the first scenario, the “Base” scenario, all three groups of energy piles were modeled for a duration of five months with an extraction rate of 20 W/m (6 W/ft) per energy piles. In the second scenario, the “Outside-Inside” scenario, for the first 75 days, only the outer energy piles were used for heat extraction with an extraction rate of 36 W/m (11 W/ft); then, the inner and middle energy piles were used for the remaining 75 days with an extraction rate of 45 W/m (14 W/ft). In the last scenario, the “Different Rates” scenario, different rates for heat extraction were set. In this case, all the energy piles were in operation for the entire five months, but the extraction rates of the outer group, middle group, and inner group were 25 W/m (7.6 W/ft), 16 W/m (5 W/ft), and 7 W/m (2.1 W/ft), respectively.

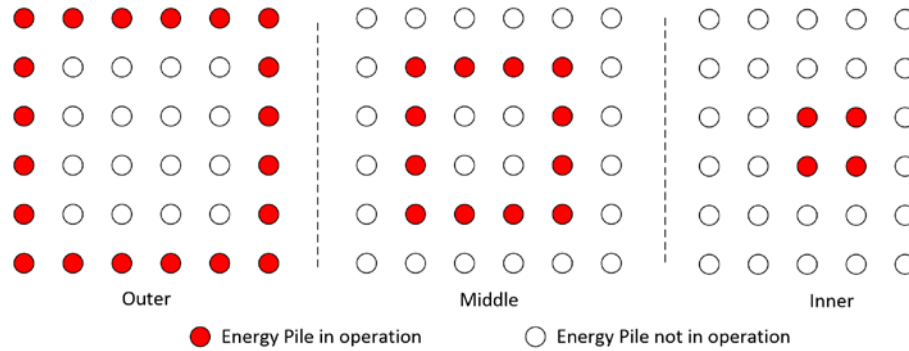


Figure 72. Different extraction strategies (Bowers Jr & Olgun, 2020)

Several metrics have been employed to evaluate each scenario, including temperatures at select locations and the net change of energy within the geothermal footprint area (Bowers, 2016). The net change of energy changes with volumetric heat capacity of the soil and the change in average air temperature. Figure 73 presents the net change in energy within a grid of energy piles at the end of the operation period of five months (end of extraction) and one year were compared. At the end of extraction, none of the scenarios experienced a net positive amount of energy (Figure 73). The results indicated that the third scenario, with different extraction rates, resulted in a positive change in energy (8 MJ) at the end of one operational year compared to the other cases (-13 MJ in the second scenario, and -17 MJ in the base case). It was found that extracting energy from the outer group either first or at a higher rate retained more energy within the geothermal footprint area. Among the three different scenarios, scenario two and scenario three were more efficient in maintaining energy within the geothermal footprint compared to the base case. They also concluded that a larger difference in the extraction rate in case three makes this technique more efficient.

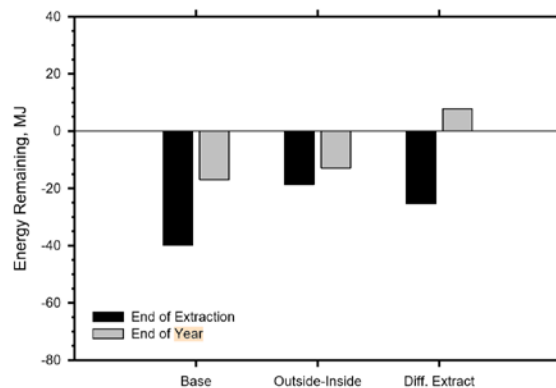


Figure 73. Comparison of the net energy remaining within the energy pile grids at the end of extraction and end of operational year for three scenarios (Bowers Jr & Olgun, 2020)

de Paly et al. (2012) developed an algorithm utilizing linear programming to optimize the energy extraction for a borehole heat exchanger (BHE) system. Because there is a linear relationship between the individual loads of the boreholes and the temperature change of the ground, they were able to formulate a linear optimization program. The objective of this study was to minimize the temperature decrease in the ground by changing the heat extraction rates at each borehole. They considered 30 years of operation and utilized an analytical line heat source equation to represent each borehole. The superposition principle was then applied to estimate the temperature change in the ground induced by multiple boreholes with different time-variable energy loads. The model

geometry shown in Figure 74 consisted of a 5×5 grid of 100 m (328 ft) long boreholes spaced 10 m (32.8 ft) center-to-center. The optimized model was compared with the non-optimized case with equal energy extracted for all boreholes.

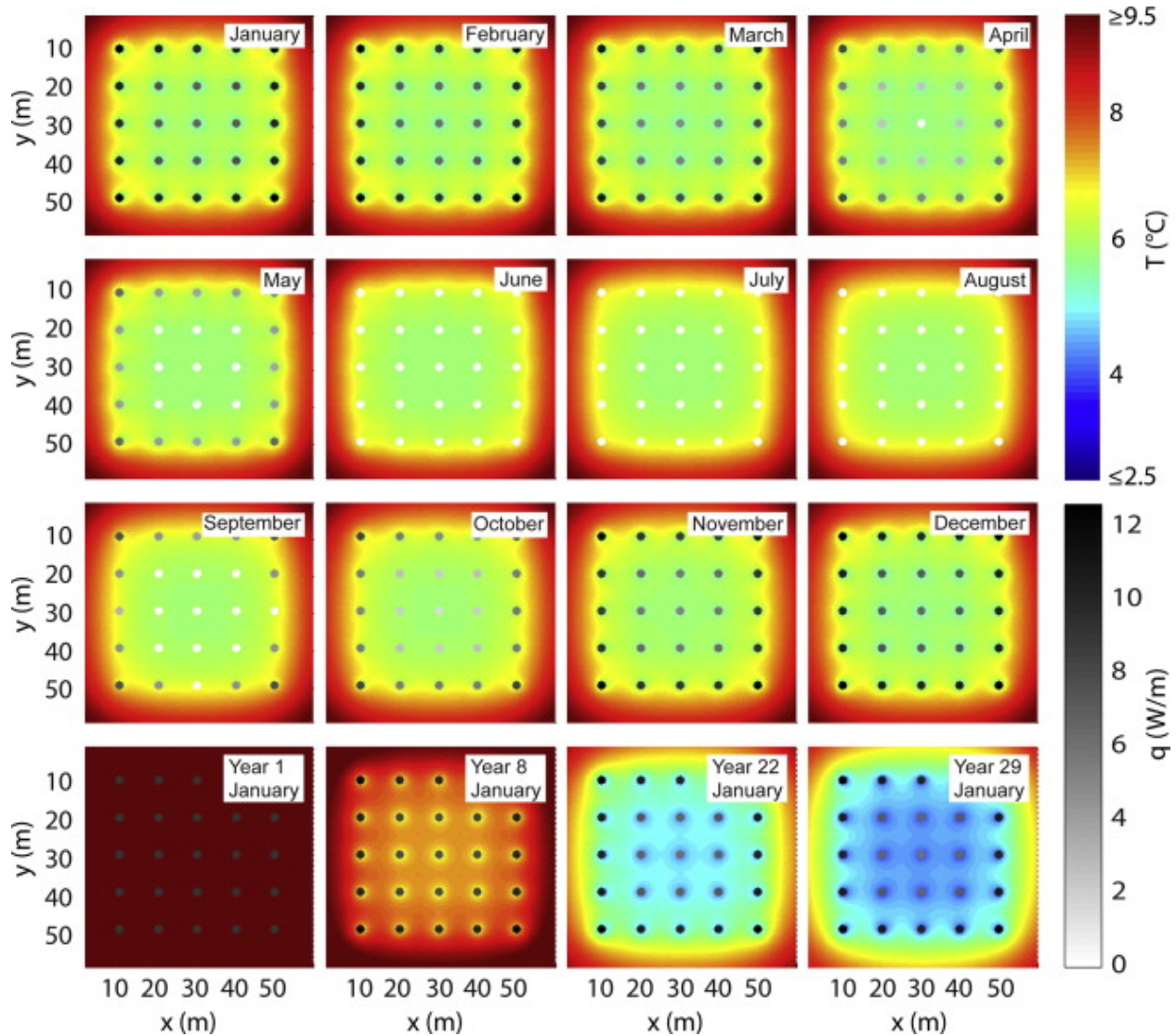


Figure 74. Temperature distribution and BHE workloads for the optimized case. Each circle represents a BHE with its corresponding load in grayscale. Darker color shades illustrate higher BHE loads. The subsurface temperature distribution at a depth of 50 m (164 ft) is shown by colors, where high absolute temperatures appear in red and lower temperatures in blue (de Paly et al., 2012).

Figure 74 shows the temperature distribution and BHE workloads for an optimized case. During winter, with higher energy demand, heat extraction reactivation started from boreholes at the outer edge of the field, going toward those at the center. The results revealed that inner boreholes in the field are insulated by the outer boreholes, which prevented sufficient conductive energy supply from the ambient ground. For the same amount of energy extracted per year over 30 years of operation, the temperature reduction in the subsurface decreased by 18%. Finally, it was concluded that the optimization scheme leads to more balanced ground temperature and higher energy extraction rate without increasing environmental impact. However, implementation of this system

requires an advanced control system that constantly monitors and adjusts the heat extraction rate for each borehole.

Beck et al. (2013) used a similar model to optimize a BHE system. This was accomplished by optimizing the geometric arrangement within the field and energy extraction for each borehole to minimize the drop in the surface temperature. Like the study by de Paly et al. (2012), boreholes were represented using an analytical line source model. The optimization scenarios were performed over a 50 m (164 ft) × 50 m (164 ft) field with 36 boreholes of 100 m (328 ft) depth and a center-to-center distance of 10 m (32.8 ft). The authors investigated the optimum borehole arrangement and different optimization scenarios including a base case with equal energy extraction for all boreholes and other variations of heat extraction rate, as shown in Figure 75.

Figure 75 shows the temperature distribution at a depth of 50 m (164 ft) after 30 years of simulation for both optimized and base cases. The results showed higher temperature changes in the system with the optimized case (Figure 75(g)). However, the authors concluded that if seasonally variable heat demand was incorporated in the optimization technique for geometric arrangements, the maximum temperature in the ground was diminished by up to 10-15%. The results of borehole geometric arrangement optimization showed that it is beneficial to place boreholes away from the central square. This arrangement allowed the system to maximize the conductive heat transfer towards the field from the ambient ground. It was also concluded that energy extraction schemes could compensate for a less than ideal arrangement of boreholes. If the geometric arrangement is optimized, load optimization is not required since little difference was observed between the optimized and base cases.

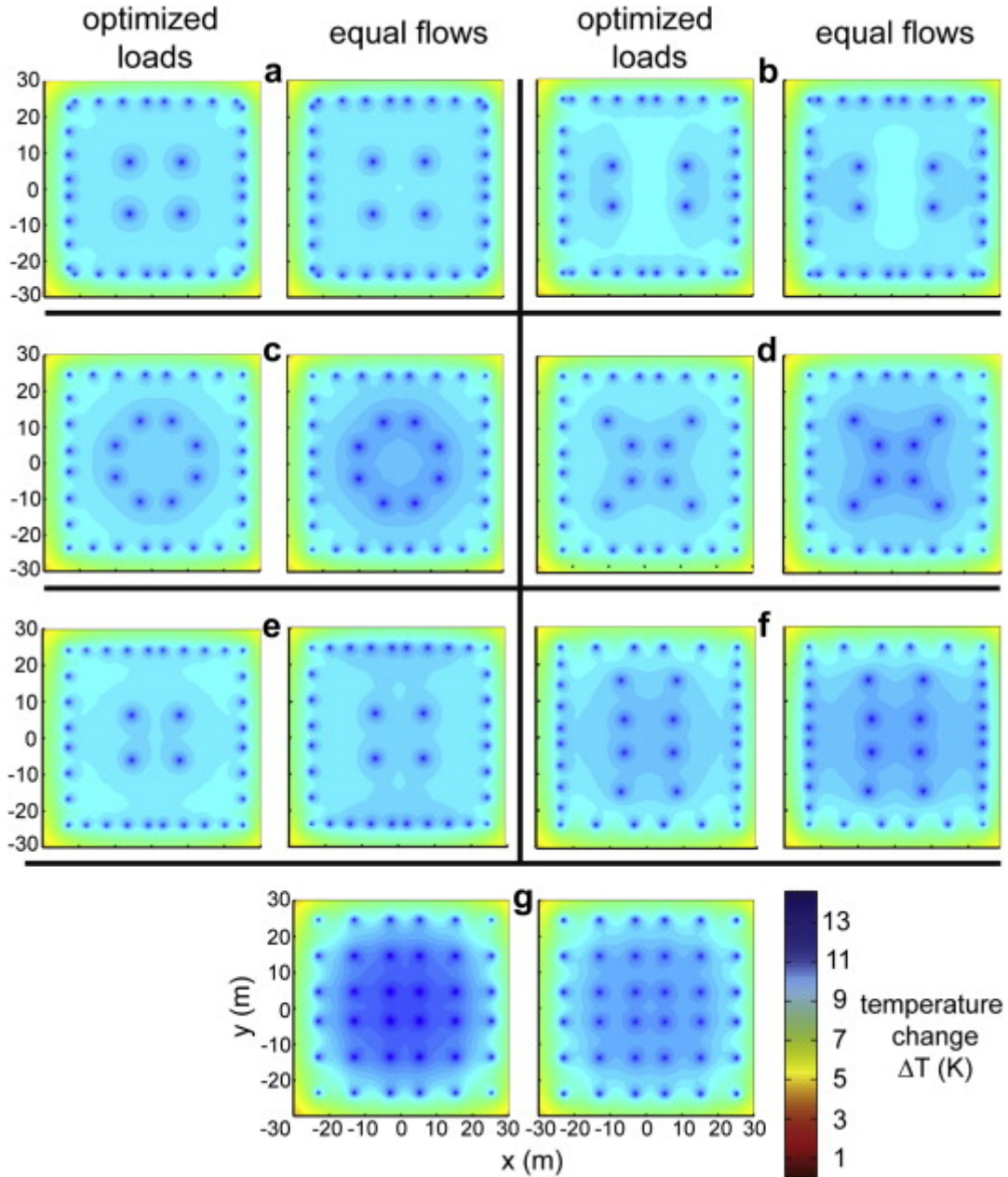


Figure 75. The subsurface temperature distribution at depth of 50 m for the optimized case and the equal heat extraction case (Beck et al., 2013)

CONCLUSION

This report provides an overview of the application of geothermal energy for bridge decks and culvert deicing. Case studies, model scale lab experiments, and numerical modeling of shallow geothermal foundations are summarized to evaluate recent advances in GSHP systems. Also, a survey was conducted to capture MDT's perceptions and preferences about deicing and anti-icing measures, summarize pertinent Montana winter weather conditions, and statewide car crash data.

The results of the survey identified the fundamental strategies of MDT for winter road maintenance operations. Before a cold-weather event, MDT may use an anti-icing strategy. When the pavement surface is covered with ice and compacted snow, MDT typically employs a deicing approach. The most common deicing/anti-icing materials for bridge decks in Montana are Sodium Chloride, Magnesium Chloride, and Potassium Acetate. In addition, abrasives, such as crushed stone, are being used to increase surface friction. The survey also identified that after a cold weather event, the typical strategy of MDT for culvert maintenance is mechanical removal.

According to the survey results, on average, 5,430 car crashes occur annually due to slippery road conditions (ice/frost, slush, and snow), 8% of which can be expected to occur on Montana bridges. The results indicated that 10% of car crashes are due to slushy road conditions while 90% are due to other slippery road surface conditions (ice and snow). Therefore, changing snow and ice to plowable slush can increase driving safety.

The weather data collected from 73 RWIS stations over the period of 2015 to 2020 showed that, spatially, the temperature was relatively consistent across the state. Wind speed, however, was more spatially variable and was higher in the northern and eastern regions of the state. The lowest average daily ambient temperature of -35°C (-31°F) was recorded in Northern Montana during February 2019, while the highest average daily ambient temperature of 38°C (100.4°F) was recorded in Southern Montana during July 2018. The average relative humidity was found to be higher during the colder times of the year.

The feasibility and applicability of GSHP systems have been demonstrated in several field, lab, and numerical modeling studies describing the implementation of this system for deicing or snow melting on bridge decks. The efficiency of the primary unit in a GSHP system was shown to rely on many factors, including heat exchanger pipe arrangement, construction techniques, circulating fluid type, and grouting material. The results of previous studies suggested that GSHP systems can be successfully utilized for accelerating the snow melting process and keeping the deck surface above 0°C (32°F) in an ambient temperature as low as -23°C (-9.4°F) if the snow melting heat demand for the bridge deck was satisfied. The results from lab experiments and numerical simulations indicated that several factors including pipe spacing, pipe embedded depth, inlet fluid temperature, and fluid flow rate affected the efficiency of secondary unit of a bridge deck deicing system. The most important factors were pipe spacing and inlet fluid temperature, and the least important factor was fluid flow rate. Ambient temperature, snowfall rate, and wind speed were also found to be important variables in designing a snow melting system. We plan to use the experimental data available in the literature and summarized in this report to develop preliminary numerical simulations. For example, data from Bowers (2016), "*Ground-Source Bridge Deck Deicing and Integrated Shallow Geothermal Energy Harvesting Systems*", will be used to calibrate early numerical models while laboratory experiments are being conducted. Once the lab and

model-scale experiments are performed, we will further calibrate and refine our numerical model with those results.

The literature review and MDT survey suggested that two power sources could be coupled with a GSHP system to increase the efficiency of the system. A solar-assisted heat pump system is a promising approach to provide higher efficiency by generating electric power and reducing the thermal load of ground heat exchangers. It was found that solar thermal collectors may optimize the number and depth of boreholes in a GSHP system through reducing the thermal load of boreholes. In addition, the weather data collected in the MDT survey suggested that wind energy could also be hybridized with geothermal energy to generate the electrical power required for a GSHP system. The daily average wind speed varied from 9.0 km/hr (5.6 mph) in Western Montana (Missoula) to 54.3 km/hr (33.7 mph) in the northern region (Havre).

Previous studies indicated that the thermal efficiency of a heat exchanger pile (in both long-term and short-term operations) was sensitive to the thermal properties of the surrounding soil. Heat transfer in the soil varies with grain size, composition, density, and water content of the soil layer. Other important structural factors influencing the thermal properties of soil are the number and nature of the contacts between the soil particles. If the soil particles are connected by bio-cementation, the thermal contact is significantly improved due to precipitation of calcite crystals in the contact areas between the soil particles, and formation of ‘thermal bridges’ (Venuleo et al., 2016). MICP treatment of sand could lead to a significant increase in soil thermal conductivity by up to 250% (Venuleo et al., 2016), and therefore, could increase the efficiency of the GSHP system.

The results of previous studies have demonstrated that GSHP systems can be successfully utilized for deicing or snow melting on bridge decks, however, the possible application of geothermal energy for culvert deicing and anti-icing has not been published to date. The proposed research program will investigate the feasibility of the use of a GSHP system as an alternative for deicing bridges and culverts through model-scale experiments and numerical modeling simulations. The results from experiments and numerical simulations together with the information gathered in the survey (e.g. weather data and car crashes) will be used to: 1) perform an economic feasibility study and compare deicing and anti-icing systems using geothermal energy with the current methods being used by MDT, and 2) design a geothermal bridge deck/culvert heating system for future field pilot studies. Finally, the use of bio-mediated soil improvement, such as MICP to improve the efficiency of GSHP systems will be investigated.

REFERENCES

- Abbasy, F. (2009). Thermal conductivity of mine backfill [*Doctoral dissertation, Concordia University*].
- Adam, D., & Markiewicz, R. (2009). Energy from earth-coupled structures, foundations, tunnels and sewers. *Géotechnique*, 59(3), 229-236.
- Agent, K. R., & Deen, R. C. (1976). Highway accidents at bridges. *Journal of the Transportation Research Board, Transportation Research Record* (601).
- Akrouch, G. A., Sánchez, M., & Briaud, J.-L. (2014). Thermo-mechanical behavior of energy piles in high plasticity clays. *Acta Geotechnica*, 9(3), 399-412.
- Al-Kaisy, A., & Ewan, L. (2017). Prioritization scheme for proposed road weather information system sites: Montana case study. *Frontiers in built environment*, 3, 45.
- Allan, M., & Philippacopoulos, A. (1999). Ground water protection issues with geothermal heat pumps. (No. BNL-66666; EF4001). *Brookhaven National Lab.*, Upton, NY (US).
- Alrtimi, A., Rouainia, M., & Haigh, S. (2016). Thermal conductivity of a sandy soil. *Applied Thermal Engineering*, 106, 551-560.
- ASHRAE, B. A. I., & Design, E. (2011). ASHRAE Handbook-HVAC Applications (SI). *American Society of Heating, Refrigerating and Air-Conditioning Engineers, Inc., Atlanta, USA*.
- Atalay, F. (2019). Engineered transition zone systems for enhanced heat transfer in thermo-active foundations [*Doctoral dissertation, Georgia Institute of Technology*].
- ATSDR, A. (1997). Agency for toxic substances and disease registry. *Case Studies in environmental medicine*. <http://www.atsdr.cdc.gov/HEC/CSEM/csem.html>.
- Baboiian, R. (1992). Synergistic effects of acid deposition and road salts on corrosion. In *Corrosion forms and control for infrastructure* (pp. 17-29). ASTM International.
- Bach, B., Werling, J., Ommen, T., Münster, M., Morales, J. M., & Elmegaard, B. (2016). Integration of large-scale heat pumps in the district heating systems of Greater Copenhagen. *Energy*, 107, 321-334.
- Bakker, M., Zondag, H., Elswijk, M., Strootman, K., & Jong, M. (2005). Performance and costs of a roof-sized PV/thermal array combined with a ground coupled heat pump. *Solar energy*, 78(2), 331-339.
- Balbay, A., & Esen, M. (2010). Experimental investigation of using ground source heat pump system for snow melting on pavements and bridge decks. *Scientific Research and Essays*, 5(24), 3955-3966.
- Balbay, A., & Esen, M. (2013). Temperature distributions in pavement and bridge slabs heated by using vertical ground-source heat pump systems. *Acta Scientiarum. Technology*, 35(4), 677-685.
- Beck, M., Bayer, P., de Paly, M., Hecht-Méndez, J., & Zell, A. (2013). Geometric arrangement and operation mode adjustment in low-enthalpy geothermal borehole fields for heating. *Energy*, 49, 434-443.
- Beran, D., & Wilfong, T. (1998). US wind profilers: a review. *Office of the Federal Coordinator for Meteorological Services and Supporting Research (OFCM) Rep.*
- Bernier, M., & Shirazi, A. S. (2007). Solar heat injection into boreholes: a preliminary analysis, *Canadian Solar Buildings Conference, Calgary*, June 10-13, 2007. paper T1-1-1.
- Bloomquist, R. G. (2000). Geothermal heat pumps five plus decades of experience in the United States. *Proceedings World Geothermal Congress 2000*.

- Bowers, J., G Allen, & Olgun, C. G. (2014). Ground-source bridge deck deicing systems using energy foundations. *Geo-Congress 2014: Geo-characterization and Modeling for Sustainability*.
- Bowers Jr, G. A. (2016). Ground-source bridge deck deicing and integrated shallow geothermal energy harvesting systems [Doctoral dissertation, Virginia Tech].
- Bowers Jr, G. A., & Olgun, C. G. (2020). Optimization of Energy Pile Grids during Unbalanced Heating and Cooling Operations. *Geo-Congress 2020: Geo-Systems, Sustainability, Geoenvironmental Engineering, and Unsaturated Soil Mechanics, Geoenvironmental Engineering, and Unsaturated Soil Mechanics* (pp. 70-79). Reston, VA: American Society of Civil Engineers.
- Boyd, T. L. (2003). New snow melt projects in Klamath Falls, OR. *Geo-Heat Center Quarterly Bulletin*, 24(3), 12-15.
- Bozis, D., Papakostas, K., & Kyriakis, N. (2011). On the evaluation of design parameters effects on the heat transfer efficiency of energy piles. *Energy and buildings*, 43(4), 1020-1029.
- Brandl, H. (2006). Energy foundations and other thermo-active ground structures. *Géotechnique*, 56(2), 81-122.
- Carey, K. L. (1984). Solving problems of ice-blocked drainage. US Army Corps of Engineers, *Cold Regions Research & Engineering Laboratory*, (No. 84).
- Chen, X., Kong, G., Liu, H., Yang, T., & Zhu, X. (2020). Experimental on thermal performance of bridge deck with hydronic heating system. *Cold regions science and technology*, 178, 103130.
- Chou, C.-W., Seagren, E. A., Aydilek, A. H., & Lai, M. (2011). Biocalcification of sand through ureolysis. *Journal of Geotechnical and Geoenvironmental Engineering*, 137(12), 1179-1189.
- Chowdhury, M. (2019). Analytical and numerical modeling of externally heated geothermal bridge deck [Doctoral dissertation, University of Texa].
- Cuthbert, M. O., McMillan, L. A., Handley-Sidhu, S., Riley, M. S., Tobler, D. J., & Phoenix, V. R. (2013). A field and modeling study of fractured rock permeability reduction using microbially induced calcite precipitation. *Environmental science & technology*, 47(23), 13637-13643.
- Dawoud, B., Amer, E. H., & Gross, D. M. (2007). Experimental investigation of an adsorptive thermal energy storage. *International Journal of Energy Research*, 31(2), 135-147.
- De Moel, M., Bach, P. M., Bouazza, A., Singh, R. M., & Sun, J. O. (2010). Technological advances and applications of geothermal energy pile foundations and their feasibility in Australia. *Renewable and Sustainable Energy Reviews*, 14(9), 2683-2696.
- de Paly, M., Hecht-Méndez, J., Beck, M., Blum, P., Zell, A., & Bayer, P. (2012). Optimization of energy extraction for closed shallow geothermal systems using linear programming. *Geothermics*, 43, 57-65.
- DeJong, J. T., Fritzges, M. B., & Nüsslein, K. (2006). Microbially induced cementation to control sand response to undrained shear. *Journal of Geotechnical and Geoenvironmental Engineering*, 132(11), 1381-1392.
- DeJong, J. T., Mortensen, B. M., Martinez, B. C., & Nelson, D. C. (2010). Bio-mediated soil improvement. *Ecological Engineering*, 36(2), 197-210.
- Duffie, J. A., Beckman, W. A., & Blair, N. (2020). Solar engineering of thermal processes, photovoltaics and wind. *John Wiley & Sons*.

- Ebigbo, A., Phillips, A., Gerlach, R., Helmig, R., Cunningham, A. B., Class, H., & Spangler, L. H. (2012). Darcy-scale modeling of microbially induced carbonate mineral precipitation in sand columns. *Water Resources Research*, 48(7).
- Eugster, W. J. (2007). Road and bridge heating using geothermal energy. overview and examples. *Proceedings European geothermal congress*, (Vol. 2007).
- Faizal, M., Bouazza, A., McCartney, J. S., & Haberfield, C. (2019). Effects of cyclic temperature variations on thermal response of an energy pile under a residential building. *Journal of Geotechnical and Geoenvironmental Engineering*, 145(10), 04019066.
- Faizal, M., Bouazza, A., & Singh, R. M. (2016). Heat transfer enhancement of geothermal energy piles. *Renewable and Sustainable Energy Reviews*, 57, 16-33.
- Farouki, O. T. (1981). The thermal properties of soils in cold regions. *Cold regions science and technology*, 5(1), 67-75.
- Feng, J., & Yin, G. (2019). Thermal Analyses and Responses of Bridge Deck Hydronic Snow Melting System. *Advances in Civil Engineering*, 2019.
- Feng, K., & Montoya, B. (2015). Drained shear strength of MICP sand at varying cementation levels. In *IFCEE 2015* (pp. 2242-2251).
- FHWA. (2013). Highway statistics 2013. (FHWA, *Office of Highway Policy Information, Highway Statistics Series*, Table DL-22–Highway Statistics 2013). <http://www.fhwa.dot.gov/policyinformation/statistics/2013/dl22.cfm>
- Fischel, M. (2001). Evaluation of selected deicers based on a review of the literature. *CDOT-DTD-R-2001-15*, 160. (Colorado Department of Transportation).
- Fliegel, J., Flyer, J., Katz, M., Le, A., Ngo, T., Roberts, K., Santoro, A., Sun, C., & Weyforth, T. (2010). Design and evaluation of a retrofitable electric snow melting system for pavements [Doctoral dissertation, University of Maryland].
- Frederickson, W., Grothaus, J., & Schaefer, K. (2005). Minnesota Snow and Ice Control Field Handbook.
- Gao, J., Zhang, X., Liu, J., Li, K. S., & Yang, J. (2008). Thermal performance and ground temperature of vertical pile-foundation heat exchangers: A case study. *Applied Thermal Engineering*, 28(17-18), 2295-2304.
- Ghasemi-Fare, O., & Basu, P. (2016). Predictive assessment of heat exchange performance of geothermal piles. *Renewable Energy*, 86, 1178-1196.
- Ghasemi-Fare, O., Bowers, G. A., Kramer, C. A., Ozudogru, T. Y., Basu, P., Olgun, C. G., Bulbul, T., & Sutman, M. (2015). *A feasibility study of bridge deck deicing using geothermal energy*.
- Goodwin, L. C., & Pisano, P. (2003). Best practices for road weather management. *Road Weather, FHWA-OP-03-081*, 131.
- Granata, R., & Hartt, W. H. (2009). Integrity of infrastructure materials and structures. *U.S.D.o.T. FHWA, ed., FHWA, U.S. Department of Transportation, United States*, 90p.
- Habibzadeh-Bigdarvish, O., Yu, X., Lei, G., Li, T., & Puppala, A. J. (2019). Life-Cycle cost-benefit analysis of Bridge deck de-icing using geothermal heat pump system: A case study of North Texas. *Sustainable cities and society*, 47, 101492.
- Hamada, Y., Saitoh, H., Nakamura, M., Kubota, H., & Ochifuji, K. (2007). Field performance of an energy pile system for space heating. *Energy and buildings*, 39(5), 517-524.

- Han, C., & Yu, X. B. (2017). Feasibility of geothermal heat exchanger pile-based bridge deck snow melting system: A simulation based analysis. *Renewable Energy*, *101*, 214-224.
- Heinonen, E., Tapscott, R., Wilden, M., & Bell, A. (1996). Assessment of Anti-Freeze Solutions for Ground Source Heat Pumps. *New Mexico Engineering Research Institute NMERI 96/15/32580*, 156 p.
- Hiller, C. (2000). Grouting for Vertical Geothermal Heat Pump Systems: Engineering Design and Field Procedures Manual. *International Ground Source Heat Pump Association*.
- Ho, I.-H., & Dickson, M. (2017). Numerical modeling of heat production using geothermal energy for a snow-melting system. *Geomechanics for Energy and the Environment*, *10*, 42-51.
- Ho, I.-H., Li, S., & Abudureyimu, S. (2019). Alternative hydronic pavement heating system using deep direct use of geothermal hot water. *Cold regions science and technology*, *160*, 194-208.
- Hommel, J., Lauchnor, E., Phillips, A., Gerlach, R., Cunningham, A. B., Helmig, R., Ebigbo, A., & Class, H. (2015). A revised model for microbially induced calcite precipitation: Improvements and new insights based on recent experiments. *Water Resources Research*, *51*(5), 3695-3715.
- Ismail, A. F., Hassan, A. R., & Cheer, N. B. (2002). Effect of shear rate on the performance of nanofiltration membrane for water desalination. *Songklanakarin J. Sci. Technol*, *24*, 879-889.
- Johnston, I., Narsilio, G., & Colls, S. (2011). Emerging geothermal energy technologies. *KSCE Journal of Civil Engineering*, *15*(4), 643-653.
- Kelting, D. L., & Laxon, C. L. (2010). Review of effects and costs of road de-icing with recommendations for winter road management in the Adirondack Park. *Adirondack Watershed Institute*.
- Kim, T., Olek, J., & Jeong, H. (2015). Alkali-silica reaction: kinetics of chemistry of pore solution and calcium hydroxide content in cementitious system. *Cement and Concrete Research*, *71*, 36-45.
- Koch, G. H., Brongers, M. P., Thompson, N. G., Virmani, Y. P., & Payer, J. H. (2002). Corrosion cost and preventive strategies in the United States. *FHWA, U.S. Department of Transportation, United States*, 790p.
- Kong, G., Wu, D., Liu, H., Laloui, L., Cheng, X., & Zhu, X. (2019). Performance of a geothermal energy deicing system for bridge deck using a pile heat exchanger. *International Journal of Energy Research*, *43*(1), 596-603.
- Kuishan, L., Xu, Z., Jun, G., & Jun, L. (2007). Research of Heat transfer performance of Pile-foundation groundcoupled heat pump and soil temperature rise. Hangzhou: *the 2007 academic conference of the Chinese association of refrigeration-innovation and development*, 54-59.
- Kusuda, T., & Achenbach, P. R. (1965). Earth temperature and thermal diffusivity at selected stations in the United States, *National Bureau of Standards Gaithersburg MD (No. NBS-8972)*.
- Lee, C., & Lam, H. (2013). A simplified model of energy pile for ground-source heat pump systems. *Energy*, *55*, 838-845.
- Lee, C., Lee, K., Choi, H., & Choi, H.-P. (2010). Characteristics of thermally-enhanced bentonite grouts for geothermal heat exchanger in South Korea. *Science in China Series E: Technological Sciences*, *53*(1), 123-128.
- Leenders, F., Schaap, A., van der Ree, B., & Van der Helden, W. v. (2000). Technology review on PV/Thermal concepts. edited by H. Scheer et al. James and James, *Proceedings of the 16th European Photovoltaic solar energy conference. Glasgow*.
- Likos, W. J. (2015). Pore-scale model for thermal conductivity of unsaturated sand. *Geotechnical and Geological Engineering*, *33*(2), 179-192.

- Lin, H., Suleiman, M. T., Brown, D. G., & Kavazanjian Jr, E. (2016). Mechanical behavior of sands treated by microbially induced carbonate precipitation. *Journal of Geotechnical and Geoenvironmental Engineering*, 142(2), 04015066.
- Liu, H., Maghoul, P., & Holländer, H. M. (2019). Sensitivity analysis and optimum design of a hydronic snow melting system during snowfall. *Physics and Chemistry of the Earth, Parts A/B/C*, 113, 31-42.
- Liu, X. (2005). Development and experimental validation of simulation of hydronic snow melting systems for bridges [Doctoral dissertation, Oklahoma State University].
- Liu, X., Rees, S. J., & Spitler, J. D. (2007). Modeling snow melting on heated pavement surfaces. Part I: Model development. *Applied Thermal Engineering*, 27(5-6), 1115-1124.
- Loveridge, F. (2012). The thermal performance of foundation piles used as heat exchangers in ground energy systems [Doctoral dissertation, University of Southampton].
- Loveridge, F., McCartney, J. S., Narsilio, G. A., & Sanchez, M. (2020). Energy geostructures: a review of analysis approaches, in situ testing and model scale experiments. *Geomechanics for Energy and the Environment*, 22, 100173.
- Lund, J., & Boyd, T. (2016). Direct utilization of geothermal energy 2015 Worldwide review. *Geothermics*, 60, pp. 66-93.
- Lund, J. W., & Toth, A. N. (2020). Direct Utilization of geothermal energy 2020 Worldwide review. *Geothermics*, 101915.
- Martinez, A., Huang, L., & Gomez, M. (2019). Thermal conductivity of MICP-treated sands at varying degrees of saturation. *Géotechnique Letters*, 9(1), 15-21.
- McCartney, J. S., Sánchez, M., & Tomac, I. (2016). Energy geotechnics: Advances in subsurface energy recovery, storage, exchange, and waste management. *Computers and Geotechnics*, 75, 244-256.
- Midttomme, K., & Roaldset, E. (1998). The effect of grain size on thermal conductivity of quartz sands and silts. *Petroleum Geoscience*, 4(2), 165-172.
- Mimouni, T. (2014). Thermomechanical characterization of energy geostructures with emphasis on energy piles [Doctoral dissertation, EPFL].
- Minsk, L. D. (1999). Heated Bridge Technology-Report on ISTE A Sec. 6005 Program.
- Mitchell, A. C., Phillips, A., Schultz, L., Parks, S., Spangler, L., Cunningham, A. B., & Gerlach, R. (2013). Microbial CaCO₃ mineral formation and stability in an experimentally simulated high pressure saline aquifer with supercritical CO₂. *International Journal of Greenhouse Gas Control*, 15, 86-96.
- Montoya, B., & DeJong, J. (2015). Stress-strain behavior of sands cemented by microbially induced calcite precipitation. *Journal of Geotechnical and Geoenvironmental Engineering*, 141(6), 04015019.
- Nagai, N., Miyamoto, S., Tsuda, T., & Yamahata, S. (2009). Experimental demonstrations and optimal design conditions of snow-melting system using geothermal and solar energy. *Heat Transfer Summer Conference*, 43581, 767-771.
- Ozudogru, T. Y., Ghasemi-Fare, O., Olgun, C. G., & Basu, P. (2015). Numerical modeling of vertical geothermal heat exchangers using finite difference and finite element techniques. *Geotechnical and Geological Engineering*, 33(2), 291-306.
- Pahud, D. (2013). A case study: the Dock Midfield of zurich Airport. *Energy Geostructures: Innovation in Underground Engineering*, 281-296.

- Park, H., Lee, S.-R., Yoon, S., & Choi, J.-C. (2013). Evaluation of thermal response and performance of PHC energy pile: Field experiments and numerical simulation. *Applied Energy*, *103*, 12-24.
- Park, H., Lee, S.-R., Yoon, S., Shin, H., & Lee, D.-S. (2012). Case study of heat transfer behavior of helical ground heat exchanger. *Energy and buildings*, *53*, 137-144.
- Phillips, A. J., Cunningham, A. B., Gerlach, R., Hiebert, R., Hwang, C., Lomans, B. P., Westrich, J., Mantilla, C., Kirksey, J., & Esposito, R. (2016). Fracture sealing with microbially-induced calcium carbonate precipitation: A field study. *Environmental science & technology*, *50*(7), 4111-4117.
- Phillips, A. J., Gerlach, R., Lauchnor, E., Mitchell, A. C., Cunningham, A. B., & Spangler, L. (2013). Engineered applications of ureolytic biomineralization: a review. *Biofouling*, *29*(6), 715-733.
- Preene, M., & Powrie, W. (2009). Ground energy systems: from analysis to geotechnical design. *Géotechnique*, *59*(3), 261-271.
- Rafferty, K. D. (2009). Commercial open loop heat pump systems. *Ashrae Journal*, *51*(3), 52-59.
- Rawlings, R., & Sykulski, J. (1999). Ground source heat pumps: a technology review. *Building Services Engineering Research and Technology*, *20*(3), 119-129.
- Sani, A. K., Singh, R. M., Amis, T., & Cavarretta, I. (2019). A review on the performance of geothermal energy pile foundation, its design process and applications. *Renewable and Sustainable Energy Reviews*, *106*, 54-78.
- Sanner, B., & Knoblich, K. (1991). Advances in drilling and installation for vertical ground heat exchangers. *Proc. Workshop Ground Source Heat Pumps, Montreal, IEA Heat Pump Center, Report HPC-WR-8*.
- Sarbu, I., & Sebarchievici, C. (2014). General review of ground-source heat pump systems for heating and cooling of buildings. *Energy and buildings*, *70*, 441-454.
- Shahed, A. M., & Harrison, S. J. (2009). Preliminary review of geothermal solar assisted heat pumps. *Proc. 4th Canadian Solar Buildings Conference*, 104p.
- Shi, X., Du, S., & Fay, L. (2018). Environmental Risks of Snow and Ice Control Materials. *Sustainable Winter Road Operations*, 180-210.
- Sinyak, Y. (1994). Global climate and energy systems. *Science of the total environment*, *143*(1), 31-51.
- Tagliabue, L. C., Maistrello, M., & Del Pero, C. (2012). Solar heating and air-conditioning by GSHP coupled to PV system for a cost effective high energy performance building. *Energy Procedia*, *30*, 683-692.
- Thompson III, W. H. (2013). Numerical analysis of thermal behavior and fluid flow in geothermal energy piles [Doctoral dissertation, Virginia Tech].
- Trillat-Berdal, V., Souyri, B., & Fraisse, G. (2006). Experimental study of a ground-coupled heat pump combined with thermal solar collectors. *Energy and buildings*, *38*(12), 1477-1484.
- van Paassen, L. A., Ghose, R., van der Linden, T. J., van der Star, W. R., & van Loosdrecht, M. C. (2010). Quantifying biomediated ground improvement by ureolysis: large-scale biogROUT experiment. *Journal of Geotechnical and Geoenvironmental Engineering*, *136*(12), 1721-1728.
- Venuleo, S., Laloui, L., Terzis, D., Hueckel, T., & Hassan, M. (2016). Microbially induced calcite precipitation effect on soil thermal conductivity. *Géotechnique Letters*, *6*(1), 39-44.
- Virmani, Y., Clear, K., Pasko Jr, T., Jones, W., & Jones, D. (1983). Time-to-corrosion of reinforcing steel in concrete slabs. Volume 5: Calcium nitrite admixture or epoxy-coated reinforcing bars as corrosion protection systems. *STIN*, *84*, 32578.

- Virmani, Y. P., Jones, W. R., & Jones, D. H. (1984). pH at Corrosion Sites. *Public Roads*, 48(3), 96-102.
- Wang, Z., Zhang, N., Lin, F., Ding, J., & Yang, H. (2019). Thermal conductivity of dry sands treated with microbial-induced calcium carbonate precipitation. *Advances in Materials Science and Engineering*, 2019.
- Whiffin, V. S., Van Paassen, L. A., & Harkes, M. P. (2007). Microbial carbonate precipitation as a soil improvement technique. *Geomicrobiology Journal*, 24(5), 417-423.
- White, D., Sritharan, S., Suleiman, M. T., & Chetlur, S. (2005). Identification of the best practices for design, construction, and repair of bridge approaches. *Final Report*, Iowa DOT TR-481, CTRE Report 02-118.
- Wood, C. J., Liu, H., & Riffat, S. B. (2012). Comparative performance of ‘U-tube’ and ‘coaxial’ loop designs for use with a ground source heat pump. *Applied Thermal Engineering*, 37, 190-195.
- Yoshitake, I., Yasumura, N., Syobuzako, M., & Scanlon, A. (2011). Pipe heating system with underground water tank for snow thawing and ice prevention on roads and bridge decks. *Journal of Cold Regions Engineering*, 25(2), 71-86.
- You, S., Cheng, X., Guo, H., & Yao, Z. (2016). Experimental study on structural response of CFG energy piles. *Applied Thermal Engineering*, 96, 640-651.
- Yu, X., Hurley, M. T., Li, T., Lei, G., Pedarla, A., & Puppala, A. J. (2020). Experimental feasibility study of a new attached hydronic loop design for geothermal heating of bridge decks. *Applied Thermal Engineering*, 164, 114507.
- Yu, X., Puppala, A. J., & Zhang, N. (2017). Use of geothermal energy for deicing approach pavement slabs and bridge decks, phase 1. *Texas. Dept. of Transportation. Research and Technology Implementation Office*, No. FHWA/TX-18/0-6872-1.
- Yunovich, M., Thompson, N., & Virmani, Y. P. (2003). Life cycle cost analysis for reinforced concrete bridge decks. *CORROSION 2003, San Diego, California*, 03309.
- Zarrella, A., De Carli, M., & Galgaro, A. (2013). Thermal performance of two types of energy foundation pile: helical pipe and triple U-tube. *Applied Thermal Engineering*, 61(2), 301-310.

APPENDIX A: SURVEY OF ROAD MAINTENANCE ACTIVITIES WITHIN MONTANA STATE

The purpose of this study is to investigate the feasibility of the use of a ground-coupled system that utilizes heat energy harvested from the ground as an alternative for deicing/anti-icing bridges and culverts. This study is being conducted through Montana State University. This questionnaire asks about the typical road/bridge maintenance activities in Montana. Your response will be anonymous, and your participation is entirely voluntary. If there are items you do not feel comfortable answering, please skip them. Thank you for cooperation.

- 1- Based on the pavement condition (e.g. low, medium, and high), what are the fundamental strategies of MDT for road maintenance operation in winter?

<i>Strategies and Tactics</i>	<i>Pavement Condition**</i>			<i>Pavement Condition**</i>		
	<i>Within-winter weather event</i>			<i>After/end-of-winter weather event</i>		
	<i>Low¹</i>	<i>Medium²</i>	<i>High³</i>	<i>Low¹</i>	<i>Medium²</i>	<i>High³</i>
Anti-icing/Pre-wetting						
Deicing						
Mechanical removal alone						
Mechanical removal and abrasive*						
Mechanical removal and anti-icing						
Mechanical removal and deicing						
Combination of tactics (Please describe them here)						

* Abrasive materials are listed in item 9

** Pavement Condition Categories

<i>Pavement Condition</i>	<i>Pavement Snow and Ice Conditions</i>
¹ Low	Conditions 5 and 6
² Medium	Conditions 3 and 4
³ High	Conditions 1 and 2

Condition 1: Dry/wet pavement conditions.

Condition 2: Snow accumulation occurs occasionally. There are patches of ice or packed snow.

Condition 3: Snow accumulation occurs regularly. Loose snow or slush ranging up to 5 cm (2 inches) are accumulated on the pavement surface.

Condition 4: Snow accumulation occurs regularly. Ice or packed snow with only bare wheel tracks.

Condition 5: Pavement surface is covered with ice and compacted snow.

Condition 6: Pavement surface is covered with significant amounts of snow. Unpassable.

- 2- What chemicals are being used by MDT for deicing/anti-icing bridge decks? In what form?

<i>Chemical</i>	<i>Solid</i>	<i>Temperature Range</i>	<i>Liquid</i>	<i>Temperature Range</i>
Sodium chloride (NaCl)				
Calcium chloride (CaCl ₂)				
Magnesium Chloride (MgCl ₂)				
Calcium Magnesium Acetate (CMA)				
Potassium Acetate (KAc)				
Blended Products				
Other (Please describe them here)				

3- Please provide an estimate of the average annual cost of each product used (per gallon or per ton).

4- Does MDT use any of the following bridge deck deicing/anti-icing technologies?

<i>Bridge deck deicing/anti-icing technology</i>	<i>Yes</i>	<i>No</i>
Pre-wetting of solid chemical- in the stockpile		
Pre-wetting of solid chemical- in the spreader		
Pre-wetting of solid chemical- at the point of discharge		
Liquid application directly on the pavement		
Other (Please list them here)		

5- Please provide an estimate of the average annual cost of each technology used.

6- Please provide an estimate of the average annual maintenance and repair cost due to corrosion.

7- How important are the following aspects associated with using chemicals?

	<i>Very Important</i>	<i>Somewhat Important</i>	<i>Not Important</i>
Cost of material			
Environmental impacts			
Increased corrosion			
Pavement deterioration			
Improved Safety			
Public feedback			
Other (Please list them here)			

8- What factors aid in the decision about which chemicals are used?

Cost	
Ease of apply	
Effectiveness	
Availability	
Reduced environmental impacts	
Decreased Corrosion	
Public feedback	
Other (Please list them here)	

9- What abrasives materials are being used by MDT?

Crushed Stone	
Sand	
Metallurgical Slag	
Bottom Ash	
Natural River Sand	
Others (Please list them here)	

10- Does MDT have an abrasive clean-up plan in place?

11- How important is entry of abrasives into waterways as a negative aspect of using abrasive?

12- Does MDT have access to the following weather information systems to aid in winter road maintenance activities? At what level?

RWIS ¹	
Weather Channel (Cable)	
NWS ² /NOAA ³	
DTN ⁴	
Other special weather information service (Please list them here)	

¹ RWIS: Road Weather Information System

² NWS: National Weather System

³ NOAA: National Oceanic and Atmospheric Administration

⁴ DTN: Data Transmission Network

APPENDIX B: SURVEY OF CULVERT MAINTENANCE ACTIVITIES WITHIN MONTANA STATE

The purpose of this study is to investigate the feasibility of the use of a ground-coupled system that utilizes heat energy harvested from the ground as an alternative for deicing/anti-icing bridges and culverts. This study is being conducted through Montana State University. This questionnaire asks about the typical road culvert maintenance activities in Montana. Your response will be anonymous, and your participation is entirely voluntary. If there are items you do not feel comfortable answering, please skip them. Thank you for cooperation.

1- What are the fundamental strategies of MDT for culvert maintenance operations in winter?

<i>Strategies and Tactics</i>	<i>Within-winter weather event</i>		<i>After-winter weather event</i>	
	<i>Before Ice Jam</i>	<i>After Ice Jam</i>	<i>Before Ice Jam</i>	<i>After Ice Jam</i>
Anti-icing				
Deicing				
Mechanical removal alone				
Mechanical removal and anti-icing				
Mechanical and removal deicing				
Using electric heat cables				
Combination of tactics (Please describe them here)				

2- Please provide an estimate of the average annual cost of each technology used.

3- Does MDT use any of the following chemicals for anti-icing/deicing of road culverts? In what form?

<i>Chemical</i>	<i>Solid</i>	<i>Temperature Range</i>	<i>Liquid</i>	<i>Temperature Range</i>
Sodium chloride (NaCl)				
Calcium chloride (CaCl ₂)				
Magnesium Chloride (MgCl ₂)				
Calcium Magnesium Acetate (CMA)				
Potassium Acetate (KAc)				
Blended Products				
Other (Please describe them here)				

4- Please provide an estimate of the average annual cost of each product used (per gallon or per ton).

5- How important are the following aspects associated with using chemicals?

	<i>Very Important</i>	<i>Somewhat Important</i>	<i>Not Important</i>
Cost of material			
Environmental impacts			
Increased corrosion			
Pavement deterioration			
Improved Safety			
Public feedback			
Other (Please list them here)			

6- What factors aid in the decision about which chemicals are used?

Cost	
Ease of apply	
Effectiveness	
Availability	
Reduced environmental impacts	
Decreased Corrosion	
Public feedback	
Other (Please list them here)	

7- What factors are considered in the maintenance of culverts?

Water PH	
Abrasion and erosion	
Freeze-thaw	
Inlet fluid temperature	
Crown corrosion due to seepage of ground water that contains road salts	
Other (Please describe them here)	

8- Please provide an estimate of the average annual maintenance and repair cost due to corrosion.

APPENDIX C: REQUIRED INFORMATION

The purpose of this study is to investigate the feasibility of the use of a ground-coupled system that utilizes heat energy harvested from the ground as an alternative for deicing/anti-icing bridges and culverts. This study is being conducted through Montana State University. This questionnaire asks about: 1) the most common type of bridges and culverts in the state of Montana, 2) the availability of time histories of the weather information for 73 stations of Road Weather Information System, RWIS, and 3) Montana statewide car crashes with snow or ice as a contributing factor. Your response will be anonymous, and your participation is entirely voluntary. If there are items you do not feel comfortable answering, please skip them. Thank you for cooperation.

- 1- Typical **bridge culvert** dimensions (Critical culvert size) in sites where icing and maintenance are known to be a problem.
 - Bridge Culverts: Structures exceeding 6.1 meters measured along centerline of roadway

<i>Geometry</i>	<i>Steel Culvert</i>		<i>Concrete Culvert</i>
	<i>With Concrete Base</i>	<i>Without Concrete Base</i>	
Cover height			
Cross-dimensional Shape			
Thickness of culvert			
Length of Culvert			
Width of Culvert			
Culvert coating			

- 2- Typical **road culvert** dimensions (Critical culvert size) in sites where icing and maintenance are known to be a problem.

<i>Geometry</i>	<i>Steel Culvert</i>		<i>Concrete Culvert</i>
	<i>With Concrete Base</i>	<i>Without Concrete Base</i>	
Cover height			
Cross-dimensional Shape			
Thickness of culvert			
Length of Culvert			
Width of Culvert			
Culvert coating			

- 3- Typical dimensions of cast-in-place concrete type of bridges in Montana.

<i>Geometry</i>	
Length of span	Varies widely. Most are between 50 and 300 ft.
Width of span	Varies. Most are between 28 and 40 ft.
Deck Thickness	Most common are between 6.5 and 8 inches.
Reinforcement cover	Varies between 0.5 and 2.5 inches

4- Representative mix design for cast-in-place concrete which is approved over the past few years.

Type of Aggregate	
Type of Cement	
Cement-aggregate- water ratio	
Type of additives	
Type of reinforcement	Mostly uncoated rebar < 1980's, mostly epoxy-coated rebar in decks since.
Type of wearing surface	Mostly bare concrete, some PMS overlay or thin epoxy, etc.
Type of protection	

5- Time histories of the following weather information from 73 stations of RWIS?

<i>Weather Information</i>	<i>Duration</i>		
	<i>5 Year</i>	<i>10 Year</i>	<i>30 Year</i>
Average snowfall accumulation			
Average temperature			
Wind Speed			
Pavement surface temperature			
Pavement Temperature (2 to 10 cm below the pavement surface)			

6- How many of Montana statewide car crashes had snow or ice as a contributing factor between 2010-2020??

<i>Year</i>	<i>Ice</i>		<i>Slush</i>		<i>Snow</i>	
	<i>Road</i>	<i>Bridge</i>	<i>Road</i>	<i>Bridge</i>	<i>Road</i>	<i>Bridge</i>
2010						
2011						
2012						
2013						
2014						
2015						
2016						
2017						
2018						
2019						
2020						